Cui *et al. Molecular Cancer* (2024) 23:86
https://doi.org/10.1186/s12943-024-01996-y

Molecular Cancer

RESEARCH Open Access

Deubiquitination of CDC6 by OTUD6A promotes tumour progression and chemoresistance

Jianfeng Cui[1,2†], Xiaochen Liu[2,3†], Qinghong Shang[4], Shuna Sun[5], Shouzhen Chen[1], Jianping Dong[6], Yaofeng Zhu[1], Lei Liu[1], Yangyang Xia[1], Yong Wang[1], Lu Xiang[2], Bowen Fan[2], Jiafeng Zhan[2], Yadi Zhou[2], Pengxiang Chen[7], Renchang Zhao[8], Xiaofei Liu[9], Nianzeng Xing[10*], Dalei Wu[4*], Benkang Shi[1*] and Yongxin Zou[2*]

Abstract

Background CDC6 is an oncogenic protein whose expression level fluctuates during the cell cycle. Although several E3 ubiquitin ligases responsible for the ubiquitin-mediated proteolysis of CDC6 have been identified, the deubiquitination pathway for CDC6 has not been investigated.

Methods The proteome-wide deubiquitinase (DUB) screening was used to identify the potential regulator of CDC6. Immunofluorescence, protein half-life and deubiquitination assays were performed to determine the protein stability of CDC6. Gain- and loss-of-function experiments were implemented to analyse the impacts of OUTD6A-CDC6 axis on tumour growth and chemosensitivity in vitro. N-butyl-N-(4-hydroxybutyl) nitrosamine (BBN)-induced conditional *Otud6a* knockout (CKO) mouse model and tumour xenograft model were performed to analyse the role of OTUD6A-CDC6 axis in vivo. Tissue specimens were used to determine the association between OTUD6A and CDC6.

Results OTUD6A interacts with, depolyubiquitinates and stabilizes CDC6 by removing K6-, K33-, and K48-linked polyubiquitination. Moreover, OTUD6A promotes cell proliferation and decreases sensitivity to chemotherapy by upregulating CDC6. CKO mice are less prone to BCa tumorigenesis induced by BBN, and knockdown of OTUD6A inhibits tumour progression in vivo. Furthermore, OTUD6A protein level has a positive correlation with CDC6 protein level, and high protein levels of OTUD6A and CDC6 are associated with poor prognosis in patients with bladder cancer.

†Jianfeng Cui and Xiaochen Liu contributed equally to this work.

*Correspondence:
Nianzeng Xing
xingnianzeng@126.com
Dalei Wu
dlwu@sdu.edu.cn
Benkang Shi
bkang68@sdu.edu.cn
Yongxin Zou
zouyongxin@sdu.edu.cn

Full list of author information is available at the end of the article

Conclusions We reveal an important yet missing piece of novel DUB governing CDC6 stability. In addition, our findings propose a model for the OTUD6A-CDC6 axis that provides novel insights into cell cycle and chemosensitivity regulation, which may become a potential biomarker and promising drug target for cancer treatment.

Keywords CDC6, OTUD6A, Deubiquitinating enzyme, Tumorigenesis

Background

Genomic DNA needs to be replicated no more than once per cell cycle [1]. In addition, the genome is vulnerable to endogenous and exogenous damaging insults, and the persistent replicative stress caused by stalled and collapsed replication forks leads to induction of the DNA damage response (DDR) [2]. Therefore, complex mechanisms are needed to monitor and regulate DNA replication to preserve cellular genomic stability [3]. Dysregulation of DNA replication and the DDR are associated with various diseases, including tumorigenesis, and potentially underlie the process of aging [4]. In eukaryotes, replication origins of DNA are directly recognized and bound by the origin recognition complex (ORC). Subsequently, cell division cycle 6 (CDC6) and chromatin licensing and DNA replication factor 1 (CDT1) are recruited, and the minichromosome maintenance protein (MCM) 2–7 complex is subsequently loaded onto the replication origin to form the pre-replicative complex (pre-RC) [5]. As CDC6 is one of the core proteins of the pre-RC, its mutation or absence prevents pre-RC assembly and origin licensing [6]. In addition to its function in pre-RC formation, CDC6 localizes to the centrosome and is required for proper centrosome assembly and duplication [7]. Moreover, CDC6 is required for ataxia telangiectasia and Rad3-related protein (ATR)-dependent activation of the DDR induced by replication stress [8]. Inhibition of CDC6 expression together with a Chk1/2 inhibitor, could reduce TopBP1 protein levels and ATR S428 and Cdc25C S216 phosphorylation, which results in inhibiting ATR-Chk1 signalling and synergistically increasing treatment efficacy in prostate cancer [9]. Due to its integral role in cell cycle progression, aberrations in CDC6 lead to various physiological and pathological changes. Recessive mutation of CDC6 is associated with Meier-Gorlin syndrome (MGS), a rare congenital anomaly syndrome characterized by impaired pre- and postnatal growth, short stature, microcephaly, microtia and absent or small patellae [10]. Aberrant upregulation of CDC6 has been found in a broad range of human cancers, including lung cancer, colon cancer, and breast cancer, and correlates with poor prognosis [9, 11, 12].

The expression of CDC6 needs to be tightly controlled during the cell cycle. CDC6 is transcriptionally regulated by early region 2 binding factor (E2F) transcription factors, the androgen receptor (AR) and forkhead box M1 (FOXM1) [13–15]. However, it is noteworthy that the protein levels of CDC6 are not consistent with the trends in its mRNA levels throughout the cell cycle. The CDC6 mRNA level is relatively high in G1/S phase, when its protein level is low, suggesting that posttranslational regulation may participate in controlling the CDC6 protein level [16]. The ubiquitin–proteasome system (UPS) is one of the major pathways regulating gene expression at the posttranscriptional level. Dysregulation of ubiquitination plays an important role in various pathological processes, including cancer and the DDR [17, 18]. CDC6 is regulated by several E3 ubiquitin ligase complexes under different conditions [16, 19–21]. CDC6 is targeted for ubiquitin-mediated degradation in early G1 phase by APC/C-CDH1 [16], SCF-CDC4 targets Cdc6 for proteolysis in late G1 and early S phase [19], CRL4-Cdt2 ubiquitinates CDC6 at the G1-S transition [20], and SCF-Cyclin F modulates the CDC6 level in the mitosis phase [21]. Protein ubiquitination is a reversible reaction and can be reversed by catalytically active deubiquitinases (DUBs). In the human proteome, there are almost 100 DUBs, consisting of six families [22]. However, whether CDC6 is also directly regulated by DUBs is unknown.

We herein performed a proteome-wide DUB screening to identify the regulator of CDC6 and identified OTU domain-containing 6 A (OTUD6A) as the first potent DUB for CDC6 depolyubiquitination. We found that OTUD6A can directly interact with CDC6 and reverse its ubiquitination. We further characterized the pivotal role of OTUD6A in tumour progression and chemoresistance via upregulation of CDC6. Together, these results reveal an important yet missing piece comprising a novel DUB that controls CDC6 stability and demonstrate the regulatory function of OTUD6A under both physiological and pathological conditions.

Methods

Cell culture and reagents

HEK293T, HEK293, UMUC3 and U2OS cells were obtained from the American Type Culture Collection (ATCC) and cultured in DMEM (Gibco, 11,995,065). HeLa, T24, 5637, 786-O, H1299, and KYSE150 cells were obtained from ATCC and cultured in RPMI-1640 medium (Gibco, 11,875,093). SV-HUC-1 cells were obtained from ATCC and cultured in F12K medium (Macgene, CM10025). RT4 cells were obtained from ATCC and cultured in McCoy's 5 A medium (Sigma-Aldrich, M4892). The medium was supplemented with 10% fetal bovine serum (Gibco, 10,099,141 C). The cells were maintained at 37 ℃ in an incubator with 5% CO_2.

MG132 (HY-13,259), cycloheximide (HY-12,320), hydroxyurea (HU, HY-B0313), gemcitabine (HY-17,026), methotrexate (HY-14,519), chloroquine (HY-17,589 A), CVT-313 (HY-15,339), VE-821 (HY-14,731) and GDC-0575 (HY-112,167) were purchased from MedChemExpress. Thymidine (T1895) and nocodazole (M1404) were purchased from Sigma–Aldrich. N-butyl-N-(4-hydroxybutyl) nitrosamine (BBN, B0938) was purchased from TCI.

Plasmids

The human DUB plasmid library and the HA-Ub WT, K11R, K27R, K29R, K33R, K48R and K63R plasmids were provided by Pro. CJ Gao [23]. The pCGN.CSH.FL42 plasmid encoding HA-tagged CDC6 was a gift from Pro. L. Drury (Clare Hall Laboratories, Cancer Research UK, London, England). The plasmids encoding Flag-YFP-N terminus (Flag-YN), HA-YFP-C terminus (HA-YC), Flag-YFP-N terminus-OTUD6A (YN-OTUD6A) or HA-YFP-C terminus-CDC6 (YC-CDC6) were purchase from GeneChem Inc. (Shanghai, China). The plasmids encoding Flag-tagged OTUD6A-N-terminal (1-145 aa) and OTUD6A-C-terminal (129–288 aa) and the plasmids encoding GST-tagged full-length OTUD6A, OTUD6A-N-terminal (1-145 aa) and OTUD6A-C-terminal (129–288 aa) were gifts from Pro. LY Huang [24]. The plasmids encoding the HA-tagged CDC6 AAA (S54A, S74A and S106A) and CDC6 DDD (S54D, S74D and S106D) mutants were gifts from Pro. JF Diffley [25]. The Myc-CDC6, Myc-CDH1 and Myc-Cyclin F plasmids were purchased from GeneCopoeia (Guangzhou, China). The OTUD6A catalytic site mutation (C152A) was generated by site-directed mutagenesis (QuickMutation™ Site-Directed Mutagenesis Kit, Beyotime) according to the manufacturer's protocol. The primers used for the construction of mutant vectors are shown in Supplementary Table 1.

Total RNA extraction, reverse transcription PCR and qPCR

Extraction of total RNA, reverse transcription PCR, and qRT-PCR (qPCR) were performed as described previously [26]. Briefly, total RNA was isolated using TRIzol reagent (Invitrogen, 15,596,026) according to the manufacturer's protocol. One microgram of RNA was reverse transcribed into cDNA using the PrimeScript RT Reagent Kit (Accurate Biotechnology, AG11706). qPCR was performed using the LightCycler 480 system (Roche, Mannheim, Germany). The qPCR primers used to detect the indicated gene products were purchased from Sangon Biotech and are described in Supplementary Table 2.

Western blot analysis

Western blotting was performed as described previously [26]. In brief, proteins in samples were separated on SDS polyacrylamide gels by electrophoresis and transferred to PVDF membranes (Millipore, IPVH00010). Then, the membranes were blocked with 5% skim milk for 1 h and incubated with the indicated primary antibodies at 4 ℃ overnight. The membranes were incubated with HRP-conjugated secondary antibodies and visualized in an Amersham™ ImageQuant™ 800 instrument (GE Healthcare, Fairfield, USA) with an ECL kit (Beyotime, P0018FM). The primary antibodies are listed in Supplementary Table 3. Band intensities were quantified with ImageJ software (version 1.6.0.32, National Institutes of Health, USA). The original WB figures were shown in Supplementary Figs. 14–19.

Immunofluorescence

Cellular immunofluorescence staining was performed as described previously [27]. Briefly, cells were grown on cover slips and harvested at the indicated times. The cover slips were washed with PBS three times and fixed with 4% paraformaldehyde for 20 min. The cells were permeabilized with 0.2% Triton X-100 in PBS for 20 min and blocked with 5% goat serum in PBS for 1 h at room temperature. The cover slips were incubated with the appropriate primary antibodies overnight. The cover slips were incubated with secondary antibodies conjugated to Alexa Fluor 488 (Abcam, ab150113) or 594 (Abcam, ab150080). The cells were further stained with DAPI (Sigma-Aldrich, F6057) and imaged with a fluorescence microscope (BX51, Olympus Life Science, Tokyo, Japan). To avoid bleed-through effects in double-staining experiments, each dye was analysed independently in multi-tracking mode, and images were merged with ImageJ. To analyse the colocalization status of OTUD6A and CDC6, we used the Coloc2 plugin function of calculating the M1 and M2 Manders' coefficients and Pearson's coefficients by ImageJ. M1 represents the proportion of overlapping pixel intensity of CDC6 and OTUD6A in CDC6 pixel intensity. M2 represents the proportion of overlapping pixel intensity of CDC6 and OTUD6A in OTUD6A pixel intensity.

For immunofluorescence staining of embryos, paraffin sections were baked for 1 h at 65 ℃, dewaxed in dimethylbenzene, and hydrated in a decreasing ethanol series. Sections were immersed in Tris-EDTA antigen retrieval buffer (Proteintech, PR30002), boiled in a microwave at 95–100 ℃ for 17 min, and cooled naturally to room temperature. Tissues were blocked in 5% bovine serum albumin (BSA) for 1 h before incubation with the primary antibody overnight at 4 ℃. Then, the tissues were incubated with the indicated secondary antibody at room temperature for 1 h and stained with DAPI. The tissues were imaged with a fluorescence microscope (VS120, Olympus Life Science, Tokyo, Japan).

Immunoprecipitation

Immunoprecipitation (IP) was performed by using a Catch and Release® v2.0 Reversible Immunoprecipitation System Kit (Millipore, 17–500) following the manufacturer's protocol. In brief, cell lysates were prepared by incubating cells in Western and IP buffer (Beyotime, P0013) with protease inhibitors (NCM Biotech, P001) on ice for 20 min, followed by sonication (5 s, 15 cycles). This was followed by centrifugation at 15,000 rpm for 15 min at 4 ℃. Two thousand micrograms of protein was added to the affinity column along with 1 μg of the indicated antibody and 10 μL of antibody capture affinity ligand (total 500 μL) and incubated on a rotary shaker at 4 ℃ overnight. The column was centrifuged and washed 3 times, and proteins were then eluted with 70 μL of elution buffer. The eluates were boiled with SDS-PAGE loading buffer at 99 ℃ for 7 min and analysed by Western blotting.

Haematoxylin and eosin (H&E) staining and immunohistochemistry

H&E staining and immunohistochemistry were performed as described previously [28]. In brief, paraffin sections were dewaxed and hydrated, and the tissues were stained with haematoxylin solution for 1 min and rinsed in diluted water for 3 min. Then, the tissues were stained with eosin solution for 2 min and rinsed in diluted water for 3 min prior to dehydration with an increasing ethanol series and clearing in dimethylbenzene. The sections were sealed with Neutral Balsam. IHC staining was performed using a PV-9001 kit (ZSGB-BIO) following the manufacturer's protocol. The sections were imaged with a microscope (BX51, Olympus Life Science, Tokyo, Japan). The staining intensity was defined as follows: 0 (negative), 1 (weak), 2 (moderate), and 3 (strong). The IHC-profiler with ImageJ was used to digitally scoring the positive staining percentage of tumour cells for each intensity according to the previous study [29]. The protein expression was quantified using the H-score, The H-score is calculated as follows: (1 × percentage of weak staining) + (2 × percentage of moderate staining) + (3 × percentage of strong staining), ranging from 0 to 300. In order to evaluate the accuracy of the computer-assisted measurement, the computerized images and the computer-assisted measurements were verified with two pathologist-based scoring results. The receiver operating curve (ROC) analysis was used to determine the probable cutoff value level, and the BCa patients were divided into high and low expression groups according to the optimal cutoff value of OTUD6A (H-score: 177) and CDC6 (H-score: 132).

Mouse models

The *Otud6a*$^{flox/flox}$ mouse (C57BL/6 N) model was established by CRISPR/Cas-mediated genome engineering by Cyagen Biosciences (Suzhou, China). *Dppa3*$^{em1(IRES-Cre)}$ mice (C57BL/6J) were purchased from Shanghai Model Organism Center, Inc. (Shanghai, China). To generate *Otud6a* knockout mice, exons 1 of the *Otud6a* were flanked with CRISPR/Cas9 mediated insertion of LoxP sites (Supplementary Fig. 1o), which the frameshift caused by deletion of exon 1 eliminated the gene product prematurely, and the deletion region contained no other known gene. Then *Otud6a*$^{flox/flox}$ mice were crossed with *Dppa3-Cre* (Dppa3-Cre can exert efficient Cre recombination enzyme activity during the early stage of embryonic development and in germ cell line [30]) mice to obtain *Dppa3-Cre; Otud6a*$^{null/Y}$ and *Dppa3-Cre; Otud6a*$^{null/null}$ mice, designated as *Otud6a*-CKO mice in the study. *Otud6a*$^{flox/flox}$ mice and CKO mice were identified by PCR analysis of tail tip genomic DNA. Amplification of DNA from the *Otud6a*-targeted and wild-type mice resulted in PCR products of 203 bp and 123 bp, respectively, and amplification of DNA from CKO mice produced a PCR product of 187 bp. The PCR primers for genotyping are listed in Supplementary Table 4.

The tumour xenograft model was established as previously described [26]. In brief, four-week-old female BALB/c (nu/nu) mice were purchased from Vital River Laboratory Animal Technology Co. Ltd (Beijing, China). The indicated cells were subcutaneously implanted into the dorsal flank of each mouse. Tumour volumes were calculated every 4 days after a 7-day adaptation period, and mice were sacrificed 31 days after implantation. For gemcitabine treatment assays, fourteen days after tumour inoculation, the mice were randomly divided into two groups. The mice were injected intraperitoneally with gemcitabine (50 mg/kg in DMSO) or DMSO once every 7 days, and the mice were sacrificed 4 weeks post implantation. Tumours were measured with a Vernier calliper, and tumour volumes were calculated with the following formula: $V = (a \times b^2) / 2$, where a and b represent the longest and shortest diameters, respectively. The tumours were harvested, weighed, and embedded in paraffin for IHC staining, and protein and RNA were extracted for Western blotting and qPCR, respectively.

For the BBN-induced mouse model of BCa, eight-week-old indicated male mice were provided with unrestricted access to drinking sterile tap water containing 0.05% BBN for 12 weeks and then were replaced with sterile tap water until the end of the experiment. The control group of mice was given sterile tap water. To analyse the progress of bladder tumorigenesis induced by BBN and the protein levels of OTUD6A and CDC6 during the progress, randomly selected mice were sacrificed at the indicated time. For analysing the role of OTUD6A

in regulating bladder tumorigenesis, all mice were sacrificed at week 20 after BBN treatment. The urinary bladder was removed and embedded in paraffin for H&E and IHC staining. All experiments were approved by the Shandong University Animal Care Committee, and all procedures were performed in compliance with the institutional guidelines.

Statistical analysis

All data were statistically analysed using GraphPad Prism (version 8.0.2, GraphPad Software, CA, USA). The data are presented as the mean±standard deviation (SD) values as indicated in the figure legends. Two-tailed unpaired Student's *t* test was used to compare two groups of data. Two-tailed paired Student's *t* test was used to compare data for matched BCa tissues. The chi-square test was used for comparison of categorical data, and Spearman correlation analysis was used for comparison of continuous variables. Survival curves were generated using Kaplan-Meier estimates, and differences between the survival curves were compared using the log-rank test. P values < 0.05 were considered to be statistically significant.

See supplementary materials for additional methods.

Results

Identification of OTUD6A as a positive regulator of CDC6

To systematically identify the potential DUBs responsible for CDC6 regulation, we performed a proteome-wide DUB screening by transiently transfecting 66 DUB-encoding plasmids into HEK293 (293) cells individually and measuring endogenous CDC6 protein levels. Among the DUBs tested, OTUD6A emerged as the DUB with the strongest upregulating effect on the CDC6 protein level (Fig. 1a and Supplementary Fig. 1a). Ectopic expression of OTUD6A resulted in an elevation of the endogenous CDC6 protein but not mRNA level in a dose-dependent manner (Fig. 1b, c). Immunofluorescence (IF) staining further confirmed that overexpression of the OTUD6A upregulated the endogenous CDC6 protein level, compared to those transfected with empty Flag vector and Flag-OTUD6A untransfected cells (Fig. 1d), and transient transfection with empty Flag vector or Flag-OTUD6A plasmid didn't change the cell cycle distribution (Supplementary Fig. 1b). Consistent with the results of transient transfection, stable overexpression of OTUD6A in 293 and HeLa cells also increased the protein level but not the mRNA level of CDC6 (Fig. 1e and Supplementary Fig. 1c-e). In contrast, stable knockdown of OTUD6A in 293, HeLa and U2OS cells using short hairpin RNAs (shRNAs) markedly decreased the CDC6 protein level but had no effect on the CDC6 mRNA level (Fig. 1f and Supplementary Fig. 1f-j). The upregulation of CDC6 by OTUD6A was not due to changes in the cell cycle as neither stable overexpression nor knockdown of OTUD6A influenced the cell cycle distribution in asynchronous cells (Supplementary Fig. 1k, l).

The subcellular location of CDC6 protein changes in a cell cycle-dependent manner which is important for its function [7, 31–33]. Thus we fractionated cell lysates into cytoplasmic, soluble and chromatin-bound fractions, and found that overexpression of OTUD6A increased while knockdown of OTUD6A decreased the CDC6 protein level in all three fractions (Fig. 1g and Supplementary Fig. 1m, n). Moreover, knockdown of OTUD6A was accompanied by decreased loading of MCM2, a subunit of pre-RC, onto chromatin (Fig. 1h), suggesting that knockdown of OTUD6A prevents pre-RC assembly.

To confirm the role of OTUD6A in CDC6 regulation in vivo, we crossed *Otud6a*$^{flox/flox}$ mice with *Dppa3-Cre* (which exert efficient Cre recombination enzyme activity during the early stage of embryonic development and in germ cell line [30]) mice to generate conditional *Otud6a* knockout (CKO) mice (Supplementary Fig. 1o, p). The abrogation of OTUD6A expression was confirmed by Western blot analyses (Supplementary Fig. 1q). *Otud6a* CKO mice were born at the expected Mendelian ratio (Supplementary Fig. 1r), and the body weight showed no significant difference between CKO and WT newborn mice (Supplementary Fig. 1s, t), suggesting OTUD6A deficiency did not result in growth abnormalities during embryogenesis or fetal development. However, the postnatal growth curves of wild-type and CKO mice started to diverge significantly 18 days after birth (Fig. 1i and Supplementary Fig. 1u). The decrease in body size is also reflected in the weight and size of most of organs examined at adult stage (Fig. 1j and Supplementary Fig. 1v). The decreased body and organ weight in CKO mice were not due to less food intake, which was comparable to control mice (Supplementary Fig. 1w). To investigate whether the growth retardation of *Otud6a* CKO mice reflected a defect in cellular proliferation, we examined the growth properties of *Otud6a* knockout mouse embryonic fibroblasts (MEFs), and the results showed that the cell proliferation of *Otud6a* knockout MEFs was considerably slower than that of wild-type MEFs (Fig. 1k, l and Supplementary Fig. 1x). Together, these results indicate that *Otud6a* knockout resulted in a general growth deficit.

We then determine the effect of OTUD6A knockout on CDC6 expression in vivo. Most of the tissues from CKO mice with successful deletion of OTUD6A exhibited lower expression of the CDC6 protein (Supplementary Fig. 1q, y). Similar results were observed in mouse embryos (Fig. 1m). Moreover, the CDC6 protein level but not mRNA level was reduced in CKO mouse MEFs (Fig. 1n and Supplementary Fig. 1z). Collectively, these

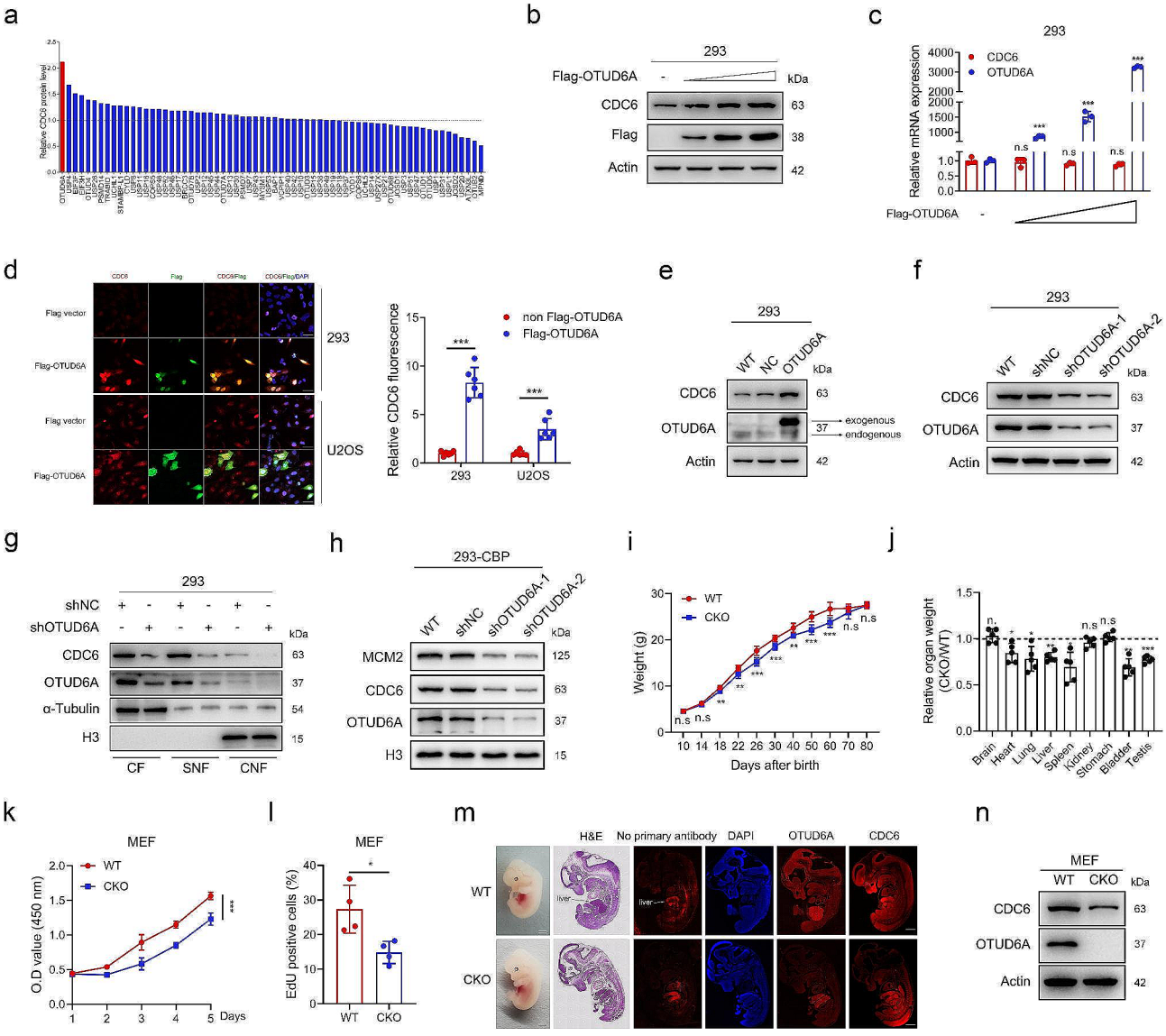

Fig. 1 OTUD6A upregulates CDC6 protein level. **a**, Quantitative analysis of CDC6 protein levels shown in Supplementary Fig. 1a. **b**, **c**, Increasing amounts of Flag-OTUD6A plasmids were transfected into HEK293 (293) cells, and the protein levels of endogenous CDC6 and exogenous OTUD6A were determined by Western blotting (**b**). The mRNA levels of CDC6 and OTUD6A were determined by qPCR (**c**), and the levels in empty Flag vector cells were set as 1. **d**, 293 and U2OS cells were transfected with the empty Flag vector or Flag-OTUD6A plasmid. An additional 24 h later, the cells were fixed and incubated with the Flag and CDC6 antibodies. Representative immunofluorescence images are shown (left). Scale bars, 20 μm. Quantification of the relative fluorescence intensity of CDC6 is shown (right), and the fluorescence intensity of CDC6 in Flag-OTUD6A untransfected or empty Flag vector-transfected cells was set as 1.**e, f**, CDC6 and OTUD6A expression levels were measured in the indicated 293 cells by Western blotting. **g**, Cytoplasmic, soluble nuclear and chromatin-bound nuclear fractions were extracted from the indicated cells using subcellular fractionation assay and detected by Western blotting. CF, cytoplasmic fractions; SNF, soluble nuclear fractions; CNF, chromatin-bound nuclear fractions. **h**, Chromatin-bound proteins (CBP) were extracted from the indicated 293 cells and analysed by Western blotting. **i**, Weight curves of WT and OTUD6A knockout (CKO) mice are shown (WT, $n = 7$; CKO, $n = 7$). **j**, Relative quantification of tissue weights from 8-week-old WT ($n = 5$) and CKO ($n = 5$) mice. **k, l**, The proliferation of the indicated mouse embryonic fibroblasts (MEFs) was measured by CCK8 assays (**k**) and EdU incorporation assays (**l**). **m**, Representative bright-field, H&E and immunofluorescence images of WT and CKO embryos at embryonic day (E) 13.5. The liver tissue is autofluorescent. Scale bar, 1 mm. **n**, CDC6 and OTUD6A expression levels were measured in WT and CKO mouse-derived MEFs by Western blotting. All quantitative analyses were based on three independent experiments. The error bars indicate the SDs. *$P < 0.05$, **$P < 0.01$, ***$P < 0.001$, n.s. not significant, based on two-tailed Student's *t* test

results demonstrate that OTUD6A positively regulates the CDC6 protein level both in vivo and in vitro.

OTUD6A directly interacts with CDC6

We next examined whether OTUD6A physically interacts with CDC6. Immunofluorescence staining revealed that OTUD6A colocalized with CDC6 in the nuclei and cytoplasm (Fig. 2a, b and Supplementary Fig. 2a-d). Coimmunoprecipitation (co-IP) assays confirmed both endogenous and exogenous CDC6 and OTUD6A proteins were coimmunoprecipitated with each other from whole-cell lysates (Fig. 2c, d and Supplementary Fig. 2e, f). Consistently, mass spectrometry analysis also demonstrated that CDC6 was the intracellular binding partner of OTUD6A (Supplementary Fig. 2g). To identify the regions of OTUD6A mediating its interaction with CDC6, a series of vectors encoding Flag-tagged OTUD6A deletion mutants were transfected into 293 cells (Supplementary Fig. 2h). Co-IP assays revealed that the N-terminal region (amino acids 1-145) of OTUD6A mediated its physical interaction with CDC6 (Fig. 2e). Bimolecular fluorescent complimentary (BiFC) assays confirmed that OTUD6A directly interacts with CDC6 (Fig. 2f). GST pulldown and assays confirmed the direct interaction between the N-terminal region of OTUD6A and CDC6 (Fig. 2g).

Given that CDC6 has important functions in cell cycle regulation and that its expression fluctuates periodically during the cell cycle, we sought to determine whether the binding capacity between CDC6 and OTUD6A varies during cell cycle progression. As shown in Fig. 2h and Supplementary Fig. 2i, CDC6 protein level was low in S phase, and it began to increase in late S phase until its maximal level was reached in G2/M phase. Importantly, the interaction between OTUD6A and CDC6 was detected in late S phase and occurred predominantly in G2/M phase, following the same trend as CDC6 protein level (Fig. 2h, i). We then treated cells with the replication-damaging agent hydroxyurea (HU), which inhibits ribonucleotide reductase and leads to replication stress by fork stalling/collapse. HU treatment, which increased CDC6 expression, effectively promoted the interaction between OTUD6A and CDC6, indicating that replication stress enhanced the binding capacity between OTUD6A and CDC6 (Fig. 2j). Phosphorylation by cyclin E-CDK2 has been reported to prevent CDC6 degradation by APC/C and thus increase the stability of CDC6 [25]. However, the interaction between CDC6 and OTUD6A was not changed in cells treated with the CDK2 inhibitor CVT-313 compared with that in control cells (Supplementary Fig. 2j).

OTUD6A depolyubiquitinates CDC6 and maintains CDC6 stability

The finding that OTUD6A increases the CDC6 protein level but does not affect the CDC6 mRNA level suggests that OTUD6A regulates CDC6 expression at the post-transcriptional level. Therefore, we first examined the effect of OTUD6A on CDC6 protein stability. The half-life of the endogenous CDC6 protein was prolonged in OTUD6A-overexpressing cells (Fig. 3a), whereas knockdown or knockout of OTUD6A led to a shortened half-life (Fig. 3b, c and Supplementary Fig. 3a), suggesting that OTUD6A inhibits CDC6 degradation. CDC6 protein stability is known to be associated with its phosphorylation status [25]. To explore whether CDC6 phosphorylation affects the regulation of CDC6 expression by OTUD6A, three CDK-mediated phosphorylation-related residues (S54, S74 and S106) in CDC6 were mutated to alanine (AAA) to mimic the unphosphorylated status or to aspartic acid (DDD) to mimic the phosphorylated status. Consistent with a previous report [25], the DDD mutant was expressed at higher levels but the AAA mutant was expressed at lower levels than WT CDC6 (Supplementary Fig. 3b). Overexpression of OTUD6A upregulated CDC6 protein level and prolonged the half-life of the CDC6 protein, independent of its phosphorylation status (Supplementary Fig. 3c-e). Ubiquitin-proteasome system and the autophagy-lysosome pathway are the two main mechanisms responsible for intracellular protein degradation [34], we next clarified the pathway involved in OTUD6A-mediated CDC6 regulation. The reduced CDC6 protein level caused by OTUD6A knockdown was effectively restored by treatment with the proteasome inhibitor MG132 (Fig. 3d) but not with the lysosome inhibitor chloroquine (Supplementary Fig. 3f), indicating that OTUD6A likely maintains CDC6 protein stability through the proteasomal pathway.

Deubiquitinating enzymes stabilize their substrates by removing ubiquitin chains. Indeed, overexpression of OTUD6A markedly reduced endogenous and exogenous CDC6 polyubiquitination in cells (Fig. 3e and Supplementary Fig. 3g). In vitro deubiquitination assays confirmed that OTUD6A could remove polyubiquitin chains from CDC6 (Fig. 3f). Conversely, knockdown of OTUD6A increased the polyubiquitination of CDC6 (Fig. 3g). Then, the plasmid encoding the deubiquitinase-dead mutant of OTUD6A (C152A mutant, which cysteine 152 was mutated to alanine, cysteine 152 is highly conserved site among species) was constructed. Although mutation of OTUD6A did not affect the interaction between OTUD6A and CDC6 (Supplementary Fig. 3h), the C152A mutant of OTUD6A lost the ability to upregulate CDC6 (Fig. 3h, i and Supplementary Fig. 3i-m). Consistent with this effect, this mutant also failed to prolong the half-life of CDC6 and to decrease the polyubiquitination

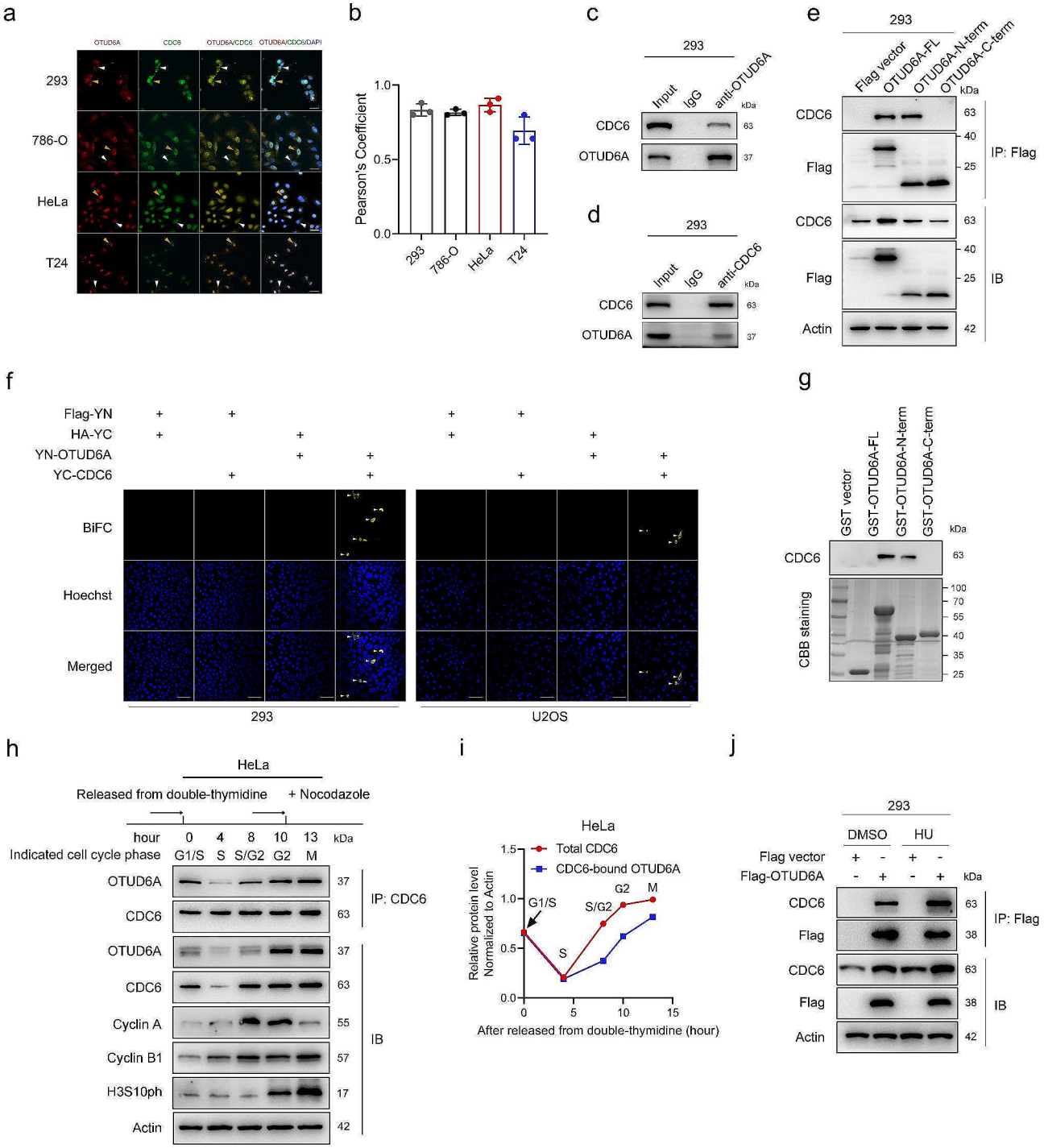

Fig. 2 OTUD6A interacts with CDC6. **a**, Representative immunofluorescence images of endogenous OTUD6A (red) and CDC6 (green) in the indicated cells are shown. Scale bars, 20 μm. **b**, Pearson's coefficient analysis was used to analyse the colocalization of OTUD6A and CDC6. **c**, 293 cell lysates were prepared and subjected to IP with control IgG or an anti-OTUD6A antibody. The immunoprecipitates were analysed by Western blotting. **d**, 293 cell lysates were prepared and subjected to IP with control IgG or an anti-CDC6 antibody. The immunoprecipitates were analysed by Western blotting. **e**, The indicated OTUD6A constructs were cotransfected with HA-CDC6 into 293 cells for 24 h. Whole-cell lysates were prepared and subjected to IP with an anti-Flag antibody. The immunoprecipitates were analysed by Western blotting. **f**, Representative confocal images of bimolecular fluorescent complimentary (BiFC) experiment are shown. White arrows represent that OTUD6A interacts with CDC6. Scale bars, 50 μm. **g**, A GST pull-down assay was performed to indicate the direct interaction between OTUD6A and CDC6. CBB staining, Coomassie brilliant blue staining. **h**, HeLa cells were synchronized at the G1/S boundary using a double-thymidine block. Whole-cell lysates were collected at the indicated time points after release into fresh medium and subjected to IP with an anti-CDC6 antibody. The immunoprecipitates were analysed by Western blotting. **i**, The intensities of the CDC6-bound OTUD6A (IP) and total CDC6 (IB) bands were quantified. **j**, 293 cells transfected with the indicated vectors were treated with HU (2.5 mM) or DMSO for 24 h. Whole-cell lysates were prepared and subjected to IP with an anti-Flag antibody. The immunoprecipitates were analysed by Western blotting

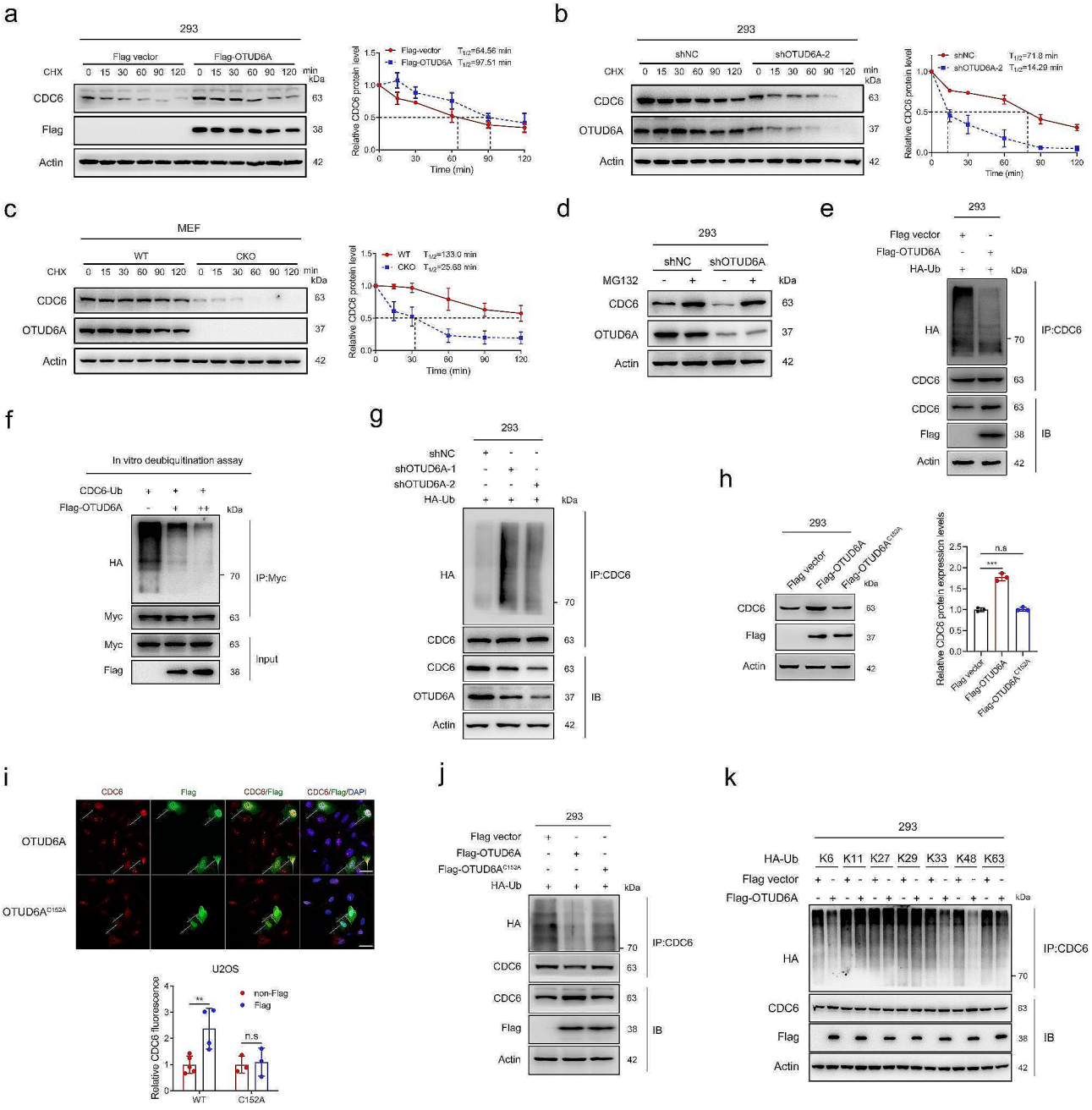

Fig. 3 (See legend on next page.)

of endogenous and exogenous CDC6 (Fig. 3j and Supplementary Fig. 3n, o), indicating that OTUD6A regulates CDC6 in a manner dependent on its DUB activity. We further investigated the role of interaction between CDC6 and OTUD6A in CDC6 protein regulation. Transient transfection with full length but not the C-terminal containing OTUD6A plasmid significantly increased the protein levels of CDC6 (Supplementary Fig. 3p). Consistently, overexpression of OTUD6A-C-terminal did not prolong the half-life of CDC6 (Supplementary Fig. 3q), indicating the direct interaction with CDC6 is required for OTUD6A to exert its function on regulating CDC6.

To extend our findings, a series of ubiquitin mutants were cotransfected with OTUD6A into cells. The results showed that OTUD6A removed K6-, K33-, and K48-linked polyubiquitin chains from CDC6 (Fig. 3k). CDC6 is targeted for proteasomal degradation by the APC/C-CDH1 and SCF-Cyclin F E3 ubiquitin ligase complex [16, 21]. We found that the downregulation and polyubiquitination of CDC6 by APC/C-CDH1 and SCF-Cyclin F could be completely reversed by OTUD6A

(See figure on previous page.)

Fig. 3 OTUD6A deubiquitinates CDC6 and promotes CDC6 stability. **a**, 293 cells transfected with the indicated vectors were treated with CHX (20 μg/mL) and harvested at the indicated time points prior to Western blotting (left). The intensities of the CDC6 bands were quantified from three independent repeated Western blotting analysis (right); the intensity at 0 min was set as 1. **b**, 293 cells with stable OTUD6A knockdown were treated with CHX and harvested at the indicated time points prior to Western blotting (left). The intensities of the CDC6 bands were quantified from three independent repeated Western blotting analysis (right), and the level at 0 min was set as 1. **c**, WT and CKO mouse-derived MEFs were treated with CHX and harvested at the indicated time points prior to Western blotting (left). The intensities of the CDC6 bands were quantified from three independent repeated Western blotting analysis (right), and the level at 0 min was set as 1. **d**, Western blot analysis of cell lysates from the indicated 293 cells treated with MG132 (20 μM) or DMSO for 6 h. **e**, 293 cells transfected with the indicated vectors were treated with MG132 (20 μM) for 6 h. Whole-cell lysates were prepared and subjected to IP with an anti-CDC6 antibody. The immunoprecipitates were analysed by Western blotting. **f**, In vitro deubiquitination assay with Flag-OTUD6A and Myc-CDC6-Ub purified from 293 cells. **g**, 293 cells with stable OTUD6A knockdown and transfected with HA-Ub were treated with MG132 for 6 h. Whole-cell lysates were prepared and subjected to IP with an anti-CDC6 antibody. The immunoprecipitates were analysed by Western blotting. **h**, Western blot analysis of proteins extracted from 293 cells transfected with the indicated vectors (left). The intensities of the CDC6 bands were quantified (right), and the level in empty Flag vector cells was set as 1. **i**, U2OS cells transfected with the indicated vectors were fixed and stained as indicated. Representative immunofluorescence images are shown (top). Scale bars, 20 μm. Quantification of the relative fluorescence intensity of CDC6 is shown (bottom), and the fluorescence intensity of CDC6 in Flag-OTUD6A untransfected cells was set as 1. **j**, 293 cells transfected with the indicated vectors were treated with MG132 for 6 h. Whole-cell lysates were prepared and subjected to IP with an anti-CDC6 antibody. The immunoprecipitates were analysed by Western blotting. **k**, Flag-OTUD6A was cotransfected with wild-type HA-Ub or its lysine residue mutants (for example, K6 indicates that all lysines except for K6 were mutated to arginine) into 293 cells for 24 h. The cells were treated with MG132 for 6 h. Whole-cell lysates were prepared and subjected to IP with an anti-CDC6 antibody. The immunoprecipitates were analysed by Western blotting. All quantitative analyses were based on three independent experiments. The error bars indicate the SDs. $^{**}P < 0.01$, $^{***}P < 0.001$, n.s. not significant, based on two-tailed Student's *t* test

(Supplementary Fig. 3r-u). Taken together, these data demonstrated that OTUD6A maintains CDC6 stability, removes K6-, K33- and K48-linked polyubiquitin chains, and reverses CDC6 degradation caused by APC/C-CDH1 and SCF-Cyclin F.

OTUD6A participates in cell cycle progression by regulating CDC6

We proposed that OTUD6A, like CDC6, might function in cell cycle regulation. 4D label-free quantitative proteomic analysis was performed to explore the function of OTUD6A. A total of 6073 proteins were identified, of which 5050 were quantifiable. Overexpression of OTUD6A resulted in a total of 84 differentially expressed proteins (with a fold change of >1.5), namely, 41 upregulated proteins and 43 downregulated proteins (Supplementary Fig. 4a and Supplementary Table 5). Notably, CDC6 was identified as one of the significantly upregulated proteins in OTUD6A-overexpressing cells (Supplementary Fig. 4a and Supplementary Table 5). By EuKaryotic Orthologous Groups (KOG) and Gene Ontology (GO) analysis of all 41 differentially upregulated proteins, we found that OTUD6A overexpression was closely associated with processes related to cell cycle progression, such as "DNA replication", "mitotic cell cycle", and "cell division" (Supplementary Fig. 4b-e).

We next analysed OTUD6A expression during cell cycle progression. The OTUD6A protein level in U2OS cells fluctuated in a cell cycle-dependent manner, peaking strongly in the G2/M phase and then decreasing during progression to the G1 and S phases (Fig. 4a and Supplementary Fig. 4f, g). Similar results were observed in HeLa cells (Supplementary Fig. 4h-j). Notably, a fairly strong concordance of endogenous protein level of OTUD6A with that of CDC6 was observed during cell cycle progression (Fig. 4a and Supplementary Fig. 4j-l). Immunofluorescence staining confirmed that the OTUD6A abundance was elevated in mitotic cells (Fig. 4b and Supplementary Fig. 4m). Moreover, OTUD6A was localized mainly in nuclei in M- and G1-phase cells and translocated to the cytoplasm in S phase (Fig. 4b and Supplementary Fig. 4m). qPCR analysis also showed that the OTUD6A mRNA level was increased in the mitotic phase and decreased in the S phase (Fig. 4c and Supplementary Fig. 4n). Together, these data demonstrate that OTUD6A is expressed in a cell cycle-dependent manner and that its expression coincides with the CDC6 protein level during the cell cycle.

Next, we evaluated the role of OTUD6A in cell proliferation. Knockdown of OTUD6A inhibited the cell proliferation (Fig. 4d, e). Cell cycle analysis showed that inhibition of OTUD6A resulted in G2/M delay (Fig. 4f, g and Supplementary Fig. 4o, p). Similar results were obtained in CDC6-knockdown cells (Fig. 4f and Supplementary Fig. 4o, q). Importantly, overexpression of CDC6 abrogated the G2/M delay induced by knockdown of OTUD6A (Fig. 4h, i and Supplementary Fig. 4r-t), suggesting that OTUD6A regulates cell cycle progression in a CDC6-dependent manner.

The OTUD6A-CDC6 axis promotes the tumorigenicity of cancer cells

Owing to its role in cell cycle progression and CDC6 regulation, we speculated that OTUD6A may function as an oncogene. To test this possibility, we first examined endogenous OTUD6A expression in the immortalized human uroepithelial cell line SV-HUC-1 and five bladder cancer (BCa) cell lines. The protein levels of OTUD6A in UMUC3, T24, 5637 and 253 J cells were much higher than those in SV-HUC-1 cells (Fig. 5a). We then established stable OTUD6A knockdown cancer cell lines

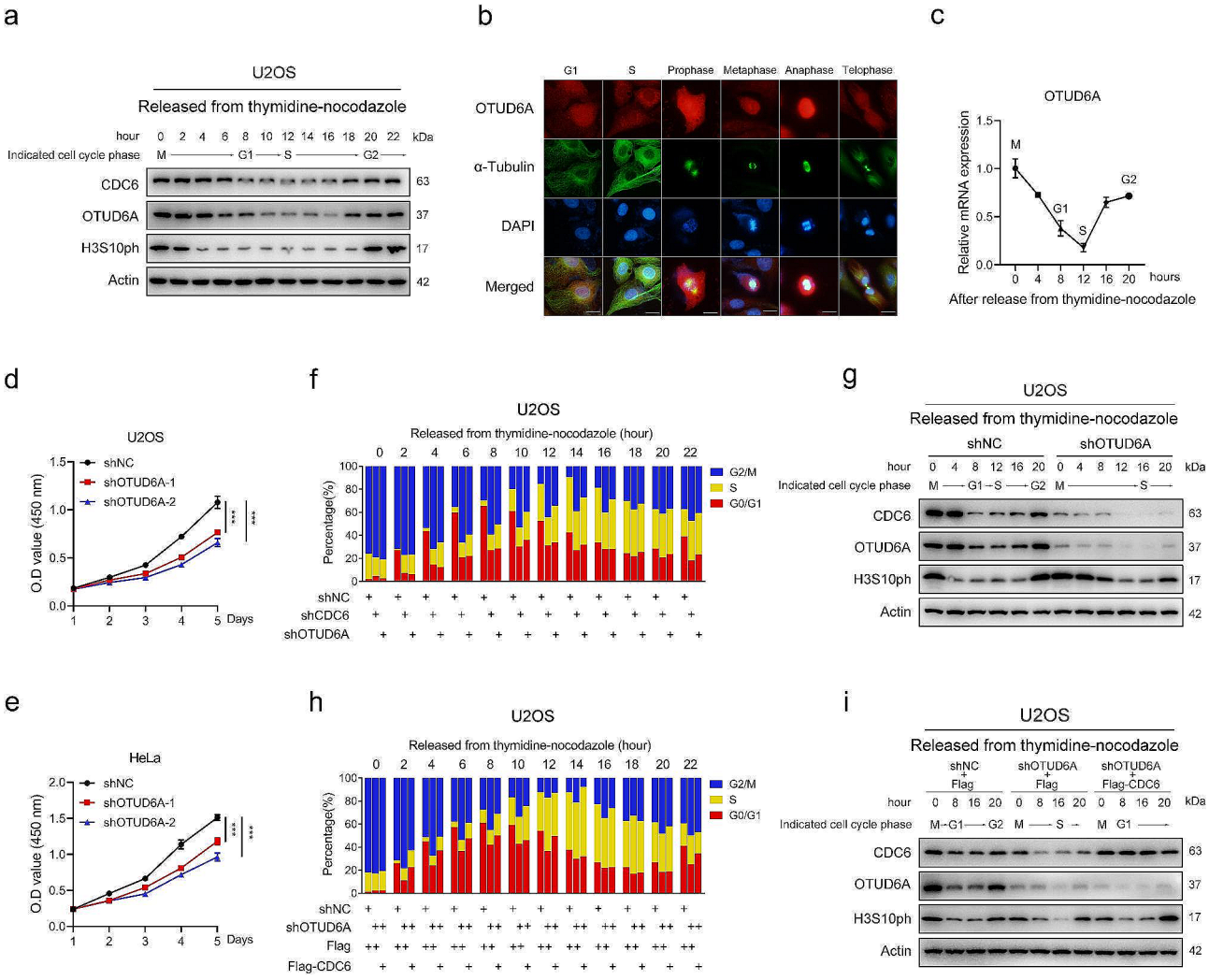

Fig. 4 OTUD6A expression fluctuates during the cell cycle and regulates cell cycle progression. **a**, U2OS cells were synchronized in prometaphase and released into fresh medium. Cells were analysed at the indicated time points by Western blotting. **b**, Representative immunofluorescence images of U2OS cells stained with an anti-OTUD6A antibody (red), α-tubulin antibody (green), and DAPI (blue). Scale bars, 10 μm. **c**, U2OS cells were synchronized in prometaphase and released into fresh medium. mRNA level in cells was analysed at the indicated time points by qPCR. The levels at 0 h were set as 1. **d**, **e**, The proliferation of the indicated U2OS (**d**) and HeLa (**e**) cells was determined by CCK8 assays. **f-i**, U2OS cells transfected with the indicated vectors were synchronized in prometaphase and released into fresh medium. Cells were analysed at the indicated time points by flow cytometry (**f, h**) and Western blotting (**g, i**). The levels at 0 h were set as 1. All quantitative analyses were based on three independent experiments. The error bars indicate the SDs. $^{*}P < 0.05$, $^{***}P < 0.001$, based on two-tailed Student's *t* test

including T24, 5637, 786-O (clear cell renal carcinoma), KYSE150 (oesophageal squamous carcinoma) and H1299 (non-small cell lung cancer). In all cell lines detected, knockdown of OTUD6A decreased the protein level of CDC6, while the mRNA level was not affected (Fig. 5b and Supplementary Fig. 5a-e). We further established stable OTUD6A overexpressed UMUC3 and 786-O cells. Consistent with findings in OTUD6A knockdown cancer cells, overexpression of OTUD6A increased the protein level but not the mRNA level of CDC6 in UMUC3 and 786-O cells (Fig. 5c and Supplementary Fig. 5f, g).

The Cell Counting Kit-8 (CCK8), colony formation and EdU incorporation assays showed that knockdown of OTUD6A inhibited the proliferation of all the cancer cells detected (Fig. 5d, e and Supplementary Fig. 5h-u). Consistent with these findings, overexpression of wild-type OTUD6A increased the cancer cell proliferation (Fig. 5f, g and Supplementary Fig. 6a-h). However, overexpression of OTUD6A-C-terminus, which could not interact with CDC6, lost its ability to promote cell proliferation (Supplementary Fig. 6f-h). To confirm the role of OTUD6A in cancer cell proliferation regulation in vivo, we subsequently utilized subcutaneous xenograft mouse models. Knockdown of OTUD6A in T24 and 786-O cells significantly inhibited tumour growth (Fig. 5h-j and Supplementary Fig. 6i-k). The decrease in tumour growth

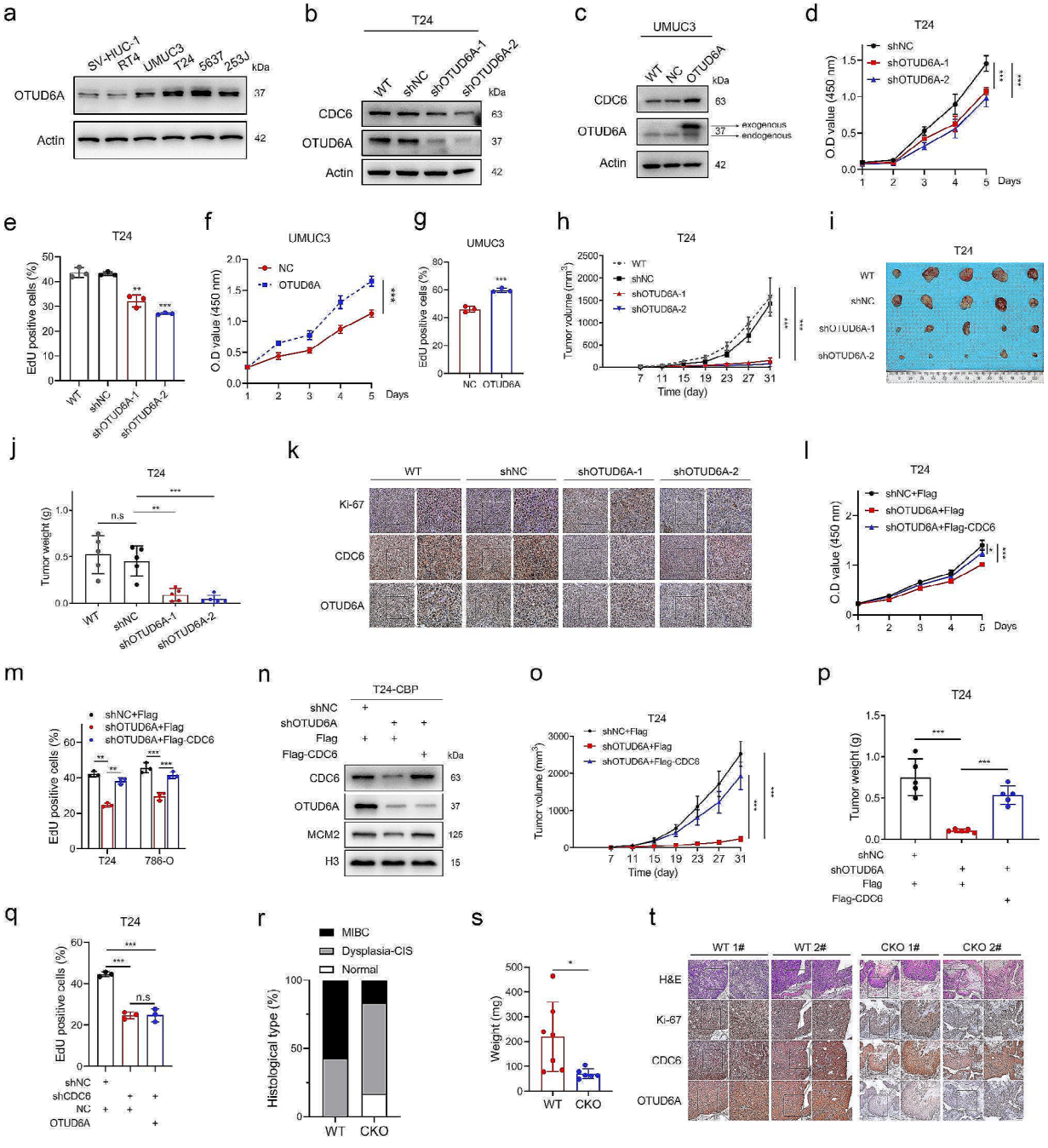

Fig. 5 The OTUD6A-CDC6 axis promotes tumour growth. **a**, The protein expression levels of OTUD6A in BCa cells and uroepithelial SV-HUC-1 cells were determined by Western blotting. **b, c**, CDC6 and OTUD6A expression levels in the indicated T24 (**b**) and UMUC3 (**c**) cells were measured by Western blotting. **d, e**, The proliferation of OTUD6A knockdown and control T24 cells was examined by CCK8 assays (**d**) and EdU incorporation assays (**e**). **f, g**, The effect of OTUD6A overexpression on UMUC3 cell proliferation was examined by CCK8 assays (**f**) and EdU incorporation assays (**g**). **h**, Growth curves of the indicated T24 tumours are shown. Tumours were measured every 4 days. **i**, An image of subcutaneous tumours formed by the indicated T24 cells is shown. **j**, The indicated T24 tumours were weighed. **k**, Representative IHC images indicating Ki-67, CDC6 and OTUD6A expression in the indicated T24 tumours are shown. Scale bars, 50 μm (left) and 20 μm (right). **l, m**, CCK8 assays (**l**) and EdU incorporation assays (**m**) were used to examine the proliferation of the indicated T24 cells. **n**, Chromatin-bound proteins (CBP) were extracted from the indicated T24 cells and analysed by Western blotting. **o**, Growth curves of the indicated T24 tumours are shown. Tumours were measured every 4 days. **p**, The indicated T24 tumours were weighed. **q**, EdU incorporation assays were used to examine the proliferation of the indicated T24 cells. **r**, Different histologic types in the indicated mouse bladders after 20 weeks of BBN treatment are shown (WT mice, $n = 7$; CKO mice, $n = 6$). **s**, The mouse bladders were weighed. **t**, Representative H&E staining images and IHC images indicating Ki-67, CDC6 and OTUD6A expression in the indicated mouse bladders. Scale bars, 100 μm (left) and 50 μm (right). All quantitative analyses were based on three independent experiments. The error bars indicate the SDs. $^{*}P < 0.05$, $^{**}P < 0.01$, $^{***}P < 0.001$, n.s. not significant, based on two-tailed Student's *t* test

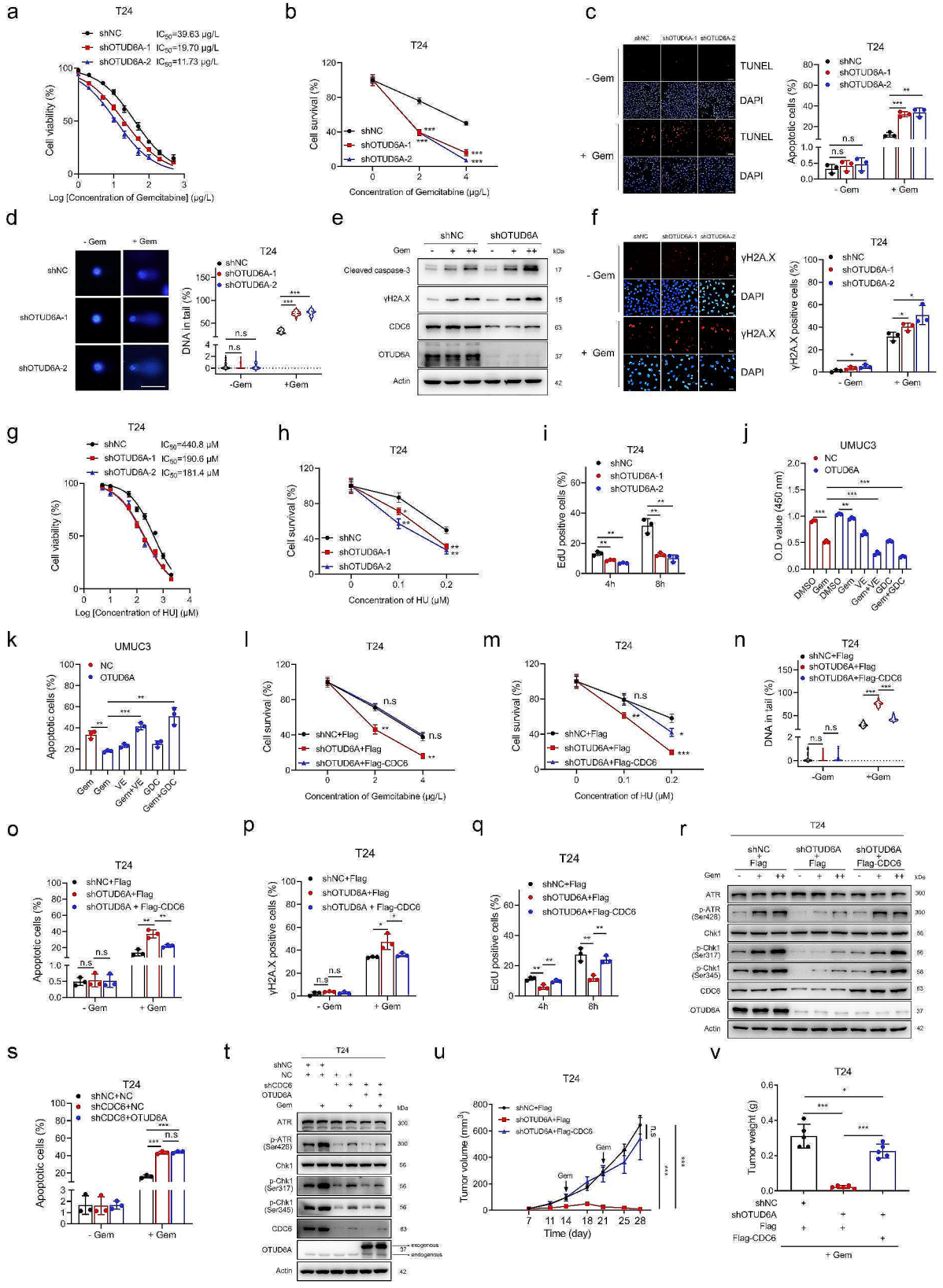

Fig. 6 (See legend on next page.)

(See figure on previous page.)

Fig. 6 OTUD6A decreases sensitivity to chemotherapy via the CDC6-ATR-Chk1 pathway. **a**, The cell viability of the indicated T24 cells was determined after 48 h of continuous exposure to multiple concentrations of gemcitabine. The IC_{50} value was defined as the concentration causing a 50% decrease in cell viability. The IC_{50} values were estimated by nonlinear regression using a variable Hill slope model. **b**, The indicated T24 cells were treated with different concentrations of gemcitabine. Cell survival was determined by colony formation assays. **c**, Apoptosis was measured by TUNEL assays in the indicated T24 cells treated with or without 20 μg/L gemcitabine for 48 h. Representative images are shown (left). Scale bars, 50 μm. **d**, The amount of DNA strand breaks was quantified by alkaline comet assays in the indicated T24 cells treated with or without 20 μg/L gemcitabine for 48 h. Representative images are shown (left). Scale bars, 20 μm. **e**, The indicated T24 cells were treated with different concentrations of gemcitabine. Cleaved caspase-3 and γH2A.X protein levels were determined by Western blotting. **f**, The γH2A.X protein level was measured by immunofluorescence staining in the indicated T24 cells treated with or without 20 μg/L gemcitabine for 48 h. Representative immunofluorescence images are shown (left). Scale bars, 20 μm. **g**, The cell viability of the indicated T24 cells was determined after 48 h of continuous exposure to multiple concentrations of hydroxyurea (HU). **h**, The indicated T24 cells were treated with different concentrations of HU. Cell survival was determined by colony formation assays. **i**, Recovery of DNA replication activity was quantified by replication reinitiation assays. The indicated T24 cells were treated with 2 mM HU for 24 h and released into fresh medium for 4 h and 8 h. **j, k**, The effects of ATR and Chk1 inhibitors (VE-821 and GDC-0575) on regulating the sensitivity of OTUD6A-overexpressing UMUC3 cells to gemcitabine was determined by CCK8 (**j**) and TUNEL (**k**) assays. **l**, **m**, The indicated T24 cells were treated with different concentrations of gemcitabine (**l**) and HU (**m**). Cell survival was determined by colony formation assays. **n**, The amount of DNA strand breaks was quantified by alkaline comet assays in the indicated T24 cells treated with or without 20 μg/L gemcitabine for 48 h. **o**, Apoptosis was measured by TUNEL assays in the indicated T24 cells treated with or without 20 μg/L gemcitabine for 48 h. **p**, The γH2A.X protein level was measured by immunofluorescence staining in the indicated T24 cells treated with or without 20 μg/L gemcitabine for 48 h. **q**, Recovery of DNA replication activity was quantified by replication reinitiation assays. The indicated T24 cells were treated with 2 mM HU for 24 h and released into fresh medium for 4 h and 8 h. **r**, ATR-Chk1 pathway protein levels in the indicated T24 cells treated with 20 μg/L gemcitabine for 6 h were determined by Western blotting. **s**, Apoptosis was measured by TUNEL assays in the indicated T24 cells treated with or without 20 μg/L gemcitabine for 48 h. **t**, ATR-Chk1 pathway protein levels in the indicated T24 cells treated with 20 μg/L gemcitabine for 6 h were determined by Western blotting. **u**, Growth curves of the indicated subcutaneous T24 tumours treated with 50 mg/kg gemcitabine are shown. **v**, The indicated subcutaneous T24 tumours were weighed. All quantitative analyses were based on three independent experiments. The error bars indicate the SDs. $^{*}P < 0.05$, $^{**}P < 0.01$, $^{***}P < 0.001$, n.s. not significant, based on two-tailed Student's *t* test

coincided with a reduction in the protein levels of Ki-67 and CDC6 (Fig. 5k and Supplementary Fig. 6l). Moreover, the protein but not the mRNA level of CDC6 was decreased in OTUD6A-knockdown T24 tumours (Supplementary Fig. 6m, n). Consistent with these findings, overexpression of OTUD6A accelerated tumour growth and upregulated CDC6 level in UMUC3 and 786-O cells in athymic mice (Supplementary Fig. 6o-v).

We next evaluated the role of CDC6 in OTUD6A-regulated tumorigenicity. Similar to the observations in OTUD6A knockdown and overexpressed cancer cells, knockdown of CDC6 inhibited while overexpression of CDC6 promoted cancer cell proliferation (Supplementary Fig. 7a-k). Importantly, ectopic expression of CDC6 effectively reduced the defects in cell proliferation of cancer cells and restored the decreased level of chromatin-bound MCM2 in vitro caused by OTUD6A knockdown (Fig. 5l-n, Supplementary Fig. 7l and Supplementary Fig. 8a-l). Moreover, ectopic expression of CDC6 effectively reversed the OTUD6A knockdown-mediated tumour growth inhibition in vivo (Fig. 5o, p and Supplementary Fig. 8m, n). In contrast, overexpression of OTUD6A has no effect on cell proliferation of CDC6 knockdown cells (Fig. 5q and Supplementary Fig. 8o-x). Collectively, these results indicated that OTUD6A promotes the tumorigenicity of human cancer cells by upregulating CDC6.

To confirm that OTUD6A acts as an oncogene in the process of tumorigenesis, we employed the BBN-induced BCa mouse model, which is the most common approach for exploring the mechanism of BCa tumorigenesis [35]. N-butyl-N-(3-carboxybutyl) nitrosamine (BCPN) is a major oxidative metabolite of chemical carcinogen BBN in the urine which has mutagenic function and induces bladder carcinogenesis [36]. Individual mice were sacrificed at every 1 month until 6 months and examined for urothelial tumours. Similar to the effects observed in a previous study [35], 12 weeks of BBN treatment resulted in the development of carcinoma in situ (CIS), and 20 weeks of BBN treatment resulted in the development of muscle-invasive BCa (Supplementary Fig. 9a-d). Immunohistochemical (IHC) staining showed that the OTUD6A, CDC6 and Ki-67 protein levels increased with prolonged BBN treatment (Supplementary Fig. 9e-g), demonstrating that OTUD6A and CDC6 might play roles in BCa tumorigenesis. Notably, knockout of OTUD6A resulted in less bladder tumorigenesis, lower malignancy and a lower CDC6 protein level upon BBN treatment (Fig. 5r-t), indicating that knockout of OTUD6A inhibited BCa tumorigenesis and CDC6 expression induced by chemical carcinogen.

OTUD6A decreases sensitivity to chemotherapy via the CDC6-ATR-Chk1 pathway

Enhancement of the DDR is one of the most important mechanisms of cellular chemoresistance [37, 38]. CDC6 is reported to be an important factor in promoting DDR activation [39, 40]. Given that OTUD6A stabilizes the CDC6 protein, we next explored whether OTUD6A also functions in the DDR and the response to chemotherapy. Knockdown of OTUD6A caused hypersensitivity to gemcitabine and methotrexate in different cancer cell lines detected (Fig. 6a, b and Supplementary Fig. 10a-d). Moreover, the number of apoptotic cells was increased

in OTUD6A-knockdown T24 cells treated with gemcitabine, not in untreated cells (Fig. 6c). The results of alkaline comet assays showed that the comet tailing was not different between OTUD6A-knockdown and control T24 cells without gemcitabine treatment. However, comet tailing was significantly increased in OTUD6A-knockdown T24 cells after treatment with gemcitabine (Fig. 6d). The level of cleaved caspase-3 and γH2A.X, a marker of DDR activation [41], was also increased in OTUD6A-knockdown T24 cells exposed to gemcitabine (Fig. 6e, f). In contrast, OTUD6A overexpression increased the chemoresistance of UMUC3 cells to gemcitabine and methotrexate (Supplementary Fig. 10e, f). Together, these data indicated that OTUD6A decreases the chemosensitivity of BCa cells.

To confirm the role of OTUD6A in the DDR, we induced DNA damage with HU. Knockdown of OTUD6A increased but overexpression of OTUD6A decreased the sensitivity of BCa cells to HU (Fig. 6g, h and Supplementary Fig. 10g, h). Immunofluorescence staining of γH2A.X also showed that the level of DNA damage was increased in OTUD6A-knockdown T24 cells treated with HU (Supplementary Fig. 10i). We next assessed the role of OTUD6A in DNA replication reinitiation after HU treatment, and the results showed that the DNA replication reinitiation rate was decreased in OTUD6A-knockdown T24 cells after release from HU (Fig. 6i and Supplementary Fig. 10j), suggesting that inhibition of OTUD6A increases DNA damage and reduces DNA repair caused by HU in BCa cells.

The ATR-Chk1 pathway is a key signalling axis driving the DDR [2], and CDC6 has been identified as a critical regulator of ATR-Chk1 activation [2, 8, 9, 42]. We proposed that OTUD6A might regulate the sensitivity of BCa cells to chemotherapy by activating the ATR-Chk1 pathway. Knockdown of OTUD6A decreased the levels of phosphorylated ATR and Chk1 but not Chk2 in T24 cells (Supplementary Fig. 10k), while OTUD6A overexpression increased the levels of phosphorylated ATR and Chk1 in T24 and UMUC3 cells (Supplementary Fig. 10l, m). Moreover, knockdown of OTUD6A inhibited gemcitabine-induced ATR and Chk1 phosphorylation (Supplementary Fig. 10n). Notably, treatment with the ATR inhibitor VE-821 and the Chk1 inhibitor GDC-0575 abrogated the decreased gemcitabine sensitivity induced by overexpression of OTUD6A in UMUC3 cells (Fig. 6j, k and Supplementary Fig. 10o-q). Furthermore, knockdown of ATR results in more apoptotic cells and DNA damage with or without gemcitabine treatment (Supplementary Fig. 10r, s). Knockdown of ATR also reduced Chk1 phosphorylation levels (Supplementary Fig. 10t). And knockdown of ATR and ATR inhibition caused a decrease in ATR and Chk1 activation upon gemcitabine treatment in UMUC3 cells (Supplementary Fig. 10u, v).

We further evaluated whether OTUD6A regulates chemosensitivity through modulation of CDC6. Similar to the results obtained in OTUD6A-knockdown cells, knockdown of CDC6 increased the sensitivity of cancer cells to anticancer chemotherapeutic drugs and HU (Supplementary Fig. 11a-e). Moreover, knockdown of CDC6 resulted in more DNA damage induced by gemcitabine (Supplementary Fig. 11f). Similar to that of OTUD6A overexpression, CDC6 overexpression decreased the chemosensitivity and promoted gemcitabine-induced ATR and Chk1 activation in UMUC3 cells (Supplementary Fig. 11g-k). Notably, ectopic expression of CDC6 rescued the hypersensitivity to gemcitabine, methotrexate and HU caused by OTUD6A knockdown (Fig. 6l, m, Supplementary Fig. 10c, d and Supplementary Fig. 12a-e). The increases in DNA damage and apoptosis induced by OTUD6A knockdown were also significantly ameliorated by CDC6 overexpression in T24 cells treated with gemcitabine and HU (Fig. 6n-p and Supplementary Fig. 12f-i). Moreover, CDC6 overexpression effectively restored the decrease in DNA replication reinitiation and ATR and Chk1 activation in gemcitabine-treated cells caused by OTUD6A knockdown (Fig. 6q, r and Supplementary Fig. 12j). In contrast, ectopic expression of OTUD6A could not ameliorate the increased sensitivity and the decreased ATR and Chk1 activation to HU or gemcitabine treatment caused by CDC6 knockdown (Fig. 6s, t, Supplementary Fig. 11d, e and Supplementary Fig. 12k-o).

Tumour xenograft models were used to further examine the role of the OTUD6A-CDC6 axis in regulating sensitivity to chemotherapy in vivo. Consistent with the in vitro results, enhanced chemosensitivity to gemcitabine and increased DNA damage induced by gemcitabine were observed in OTUD6A-knockdown T24 tumours (Fig. 6u, v and Supplementary Fig. 12p, q). Consistent with the observation from in vitro experiments, overexpression of CDC6 rescued the increased chemosensitivity caused by OTUD6A knockdown in gemcitabine-treated T24 tumours (Fig. 6u, v and Supplementary Fig. 12p, q). Taken together, these data demonstrated that OTUD6A promotes CDC6-ATR-Chk1 signalling pathway activity to confer chemoresistance on tumour cells.

OTUD6A level is correlated with the level of the CDC6 protein in cancer cells

We then determined whether OTUD6A-mediated upregulation of CDC6 is of potential clinical significance. A positive correlation between the OTUD6A and CDC6 protein levels was observed in BCa cell lines, whereas no correlation was found between the CDC6 mRNA level and the OTUD6A protein or mRNA level (Fig. 7a-d). We further examined the expression level of OTUD6A and CDC6 in 20 fresh human BCa tissues and matched

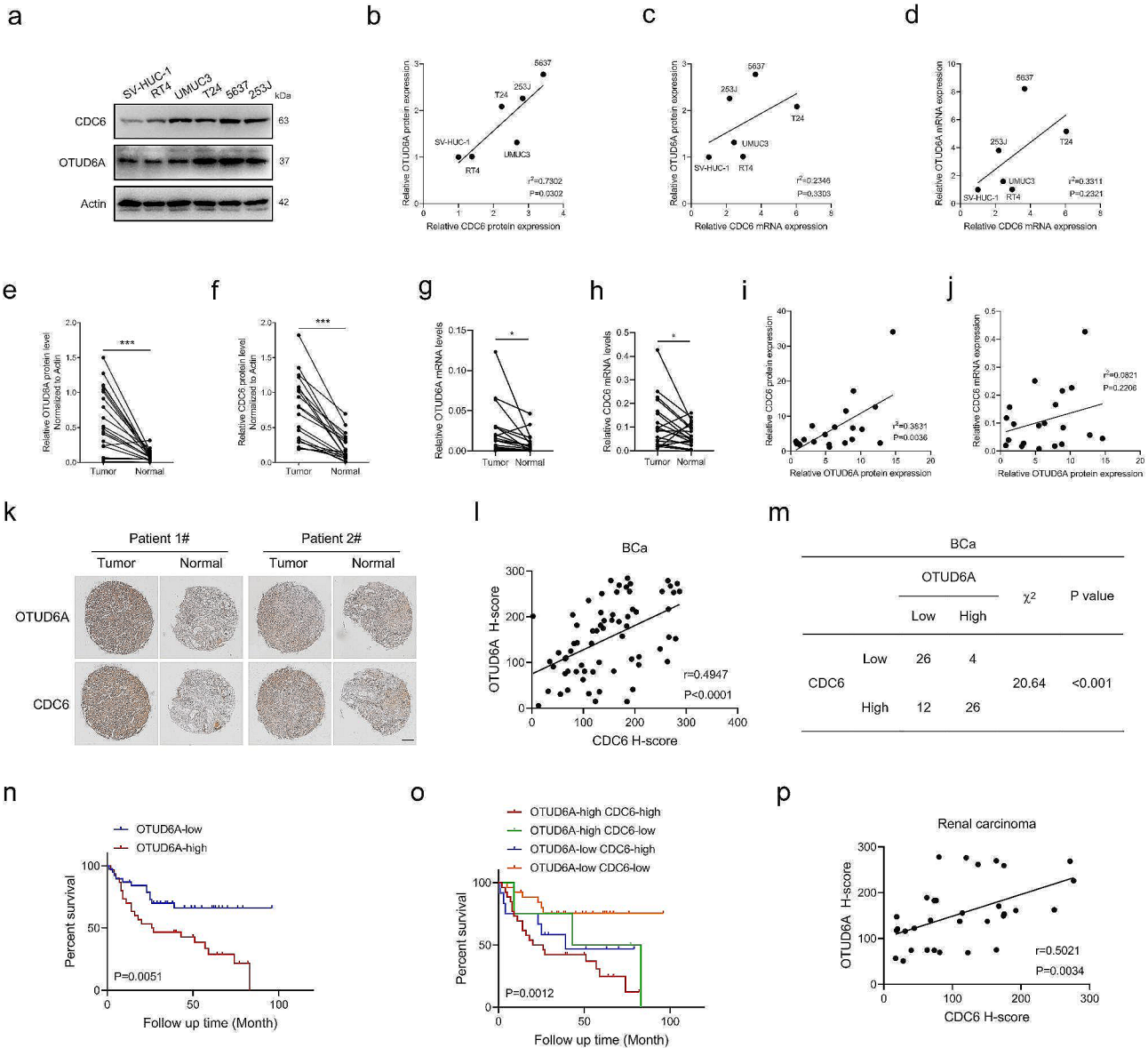

Fig. 7 CDC6 protein level is correlated with the OTUD6A protein level in tumour tissue. **a**, The protein levels of OTUD6A and CDC6 in the indicated cells were determined by Western blotting. **b-d**, The correlation between OTUD6A and CDC6 levels in the indicated cells was assessed by Pearson correlation analysis. OTUD6A and CDC6 protein levels (**b**); OTUD6A protein and CDC6 mRNA levels (**c**); OTUD6A and CDC6 mRNA levels (**d**). **e**, **f**, The intensities of the OTUD6A (**e**) and CDC6 (**f**) bands in BCa tissues were quantified and compared with those in matched normal tissues. Data were analysed using two-tailed paired Student's *t* test. **g**, **h**, Quantitative PCR analysis of OTUD6A (**g**) and CDC6 (**h**) mRNA level in BCa tissues compared with matched normal tissues. Data were analysed using two-tailed paired Student's *t* test. **i**, The correlation between OTUD6A and CDC6 protein levels in BCa tissues was assessed by Pearson correlation analysis. **j**, The correlation between OTUD6A protein and CDC6 mRNA levels in BCa tissues was assessed by Pearson correlation analysis. **k**, Representative IHC images indicating OTUD6A and CDC6 expression in the tissue microarray are shown. Scale bar, 500 μm. **l**, The correlation between OTUD6A and CDC6 protein levels in the BCa tissue microarray was assessed by Pearson correlation analysis. **m**, The correlation between OTUD6A and CDC6 protein levels in the BCa tissue microarray was assessed by the chi-square test. **n**, Kaplan-Meier curves of overall survival for patients with BCa stratified by the OTUD6A expression level in the tissue microarray are shown. Data were analysed using the log-rank test. **o**, Kaplan-Meier curves of overall survival for patients with BCa stratified by OTUD6A and CDC6 expression levels in the tissue microarray are shown (the numbers of patients with high and low OTUD6A and CDC6 expression are shown in Fig. 7m). Data were analysed using the log-rank test. **p**, The correlation between OTUD6A and CDC6 protein levels in the renal carcinoma tissue microarray was assessed by Pearson correlation analysis. All quantitative analyses were based on three independent experiments. The error bars indicate the SDs. **P* < 0.05, ****P* < 0.001

adjacent normal bladder tissues. Both the protein and mRNA levels of OTUD6A and CDC6 were higher in BCa tissues than in the matched normal bladder tissues (Fig. 7e-h and Supplementary Fig. 13a). CDC6 protein levels in BCa tissues were inconsistent with the CDC6 mRNA levels, indicating the important role of posttranscriptional regulation in CDC6 protein level (Supplementary Fig. 13b). Importantly, CDC6 protein level was positively correlated with OTUD6A protein level in BCa tissues (Fig. 7i). However, there was no correlation between the OTUD6A protein and CDC6 mRNA levels in BCa tissues (Fig. 7j). We then performed IHC staining of OTUD6A and CDC6 in a BCa tissue microarray, and the results confirmed that the protein levels of OTUD6A and CDC6 were highly consistent in BCa tissues (Fig. 7k-m and Supplementary Fig. 13c). Patients bearing BCa tumours with relatively high levels of OTUD6A or CDC6 showed poorer overall survival (OS) outcomes (Fig. 7n and Supplementary Fig. 13d). Notably, combined high level of OTUD6A and CDC6 was more strongly correlated with worse outcomes in BCa patients, and patients with high OTUD6A and low CDC6 level had better OS outcomes than patients with low OTUD6A and high CDC6 level (Fig. 7o). However, no discernible difference in OS between patients with high OTUD6A and high CDC6 level and patients with low OTUD6A and high CDC6 level was observed (Fig. 7o). The protein levels of OTUD6A and CDC6 were also consistent in renal carcinoma tissues (Fig. 7p and Supplementary Fig. 13e). Collectively, these data demonstrated that the OTUD6A-CDC6 axis is preferentially activated in BCa and renal carcinoma and that its level is correlated with poor survival in BCa patients. Therefore, OTUD6A and CDC6 may serve as a new set of prognostic biomarkers in BCa patients.

Discussion

Precise regulation of the cell cycle is essential for living organisms. As CDC6 is one of the key factors in the cell cycle, its expression and localization during the cell cycle are regulated by multiple posttranslational regulatory pathways [14, 20, 21, 25, 32, 43]. The CDC6 protein can be degraded by the ubiquitin–proteasome system mediated by the E3 ubiquitin ligases APC/C-CDH1, SCF-CDC4, CRL4-CDT2 and SCF-Cyclin F [16, 19–21, 25]. Ubiquitination can be reversed by DUBs that cleave ubiquitin chains from the substrate protein [22]. Through a screening of DUBs, we found that OTUD6A interacts with CDC6 and increases the CDC6 protein level by promoting the stability of CDC6 through removing polyubiquitin chains, whose attachment was mediated by SCF-Cyclin F and APC/C-CDH1 (Fig. 8).

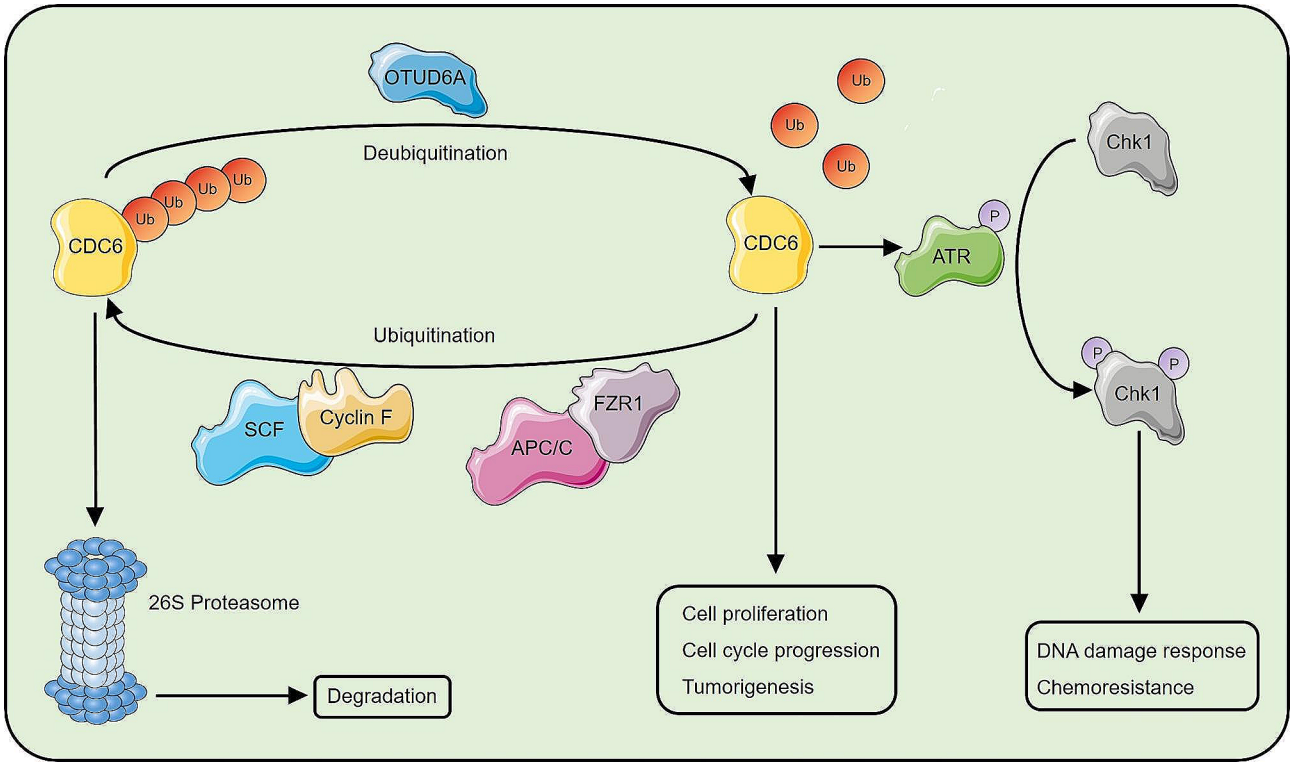

Fig. 8 A schematic model showing the mechanism by which the OTUD6A-CDC6 axis regulates cell proliferation and the DNA damage response. OTUD6A directly binds to and deubiquitinates CDC6, reverses CDC6 degradation mediated by APC/C-CDH1 and SCF-Cyclin F, and consequently promotes cell proliferation and induces chemoresistance

CDC6 expression fluctuates during the cell cycle [32]. Our results confirmed that the changes in the levels of CDC6 protein caused by OTUD6A were not results from changes in the cell cycle. The OTUD6A protein level pattern is similar to that of CDC6 in cell cycle progression. Importantly, the interaction pattern of OTUD6A and CDC6 is in line with the CDC6 protein level during cell cycle progression. Moreover, OTUD6A translocates into the cytoplasm in the S phase, indicating that the cytoplasmic translocation of OTUD6A permits the degradation of CDC6 and prevents the re-replication of DNA. Therefore, OTUD6A cooperates with the ubiquitination system to regulate CDC6 protein level during cell cycle progression.

OTUD6A belongs to the ovarian tumour protease (OTU) family and the OTUD subfamily, which contains OTUD1, OTUD2, OTUD3, OTUD4, OTUD5, OTUD6A, OTUD6B and ALG13. The OTUD subfamily members have emerged as important factors in various human diseases and pathological processes. OTUD1 binds to and deubiquitinates apoptosis-inducing factor (AIF), thereby activating both caspase-independent and caspase-dependent apoptotic signalling [44]. OTUD3 inhibits the activation of the AKT pathway by deubiquitinating PTEN and suppresses tumour progression in breast cancer (BC), colon cancer and cervical cancer [45]. OTUD6B has the highest homology with OTUD6A among the OTUD subfamily members. Two OTUD6B splice isoforms recognize different substrates and have completely opposite effects on non-small cell lung cancer cell proliferation [46]. Mice with homozygous *Otud6b* knockout show embryonic lethality, and biallelic mutations cause human mental retardation syndrome [47]. However, the physiological function of OTUD6A remains to be fully elucidated. Here, we demonstrated that OTUD6A plays a vital role in organism growth. Depletion of OTUD6A results in downregulation of CDC6 protein level and proliferation defects in MEFs. Importantly, similar to Meier-Gorlin syndrome in humans, which can be caused by CDC6 mutation, depletion of OTUD6A in mice causes postnatal growth retardation, suggesting that OTUD6A is required for normal development at least partially through maintenance of CDC6 protein stability.

CDC6 is overexpressed and acts as a proto-oncogene in various cancers [42, 48]. Here, we found that OTUD6A upregulated CDC6 protein level in several types of cancer cells. OTUD6A was previously reported to be an oncogene in colorectal cancer (CRC), PCa and BC, and OTUD6A is overexpressed in CRC, PCa and BC tissues [24, 49–51]. OTUD6A interacts with and deubiquitinates Drp1 to enhance mitochondrial fission [49]. OTUD6A deubiquitinates Brg1 and AR to promote PCa progression, and knockdown of OTUD6A suppresses prostate tumorigenesis by reversing Myc-driven metabolic remodelling [24, 50]. In addition, OTUD6A inhibits TopBP1 ubiquitination by disrupting the interaction between TopBP1 and UBR5 and promotes tumour cell resistance to chemoradiotherapy [51]. Despite several substrates of OTUD6A were identified recently, herein, we identified the first deubiquitinase, OTUD6A, targeting CDC6 for deubiquitination. OTUD6A protein level is upregulated during the progression of BCa and is positively associated with CDC6 level induced by BBN treatment in mice. Depletion of OTUD6A inhibits CDC6 expression as well as BBN-induced BCa tumorigenesis and tumour progression. We further showed that OTUD6A, through upregulation of CDC6, promotes the proliferation of multiple types of human tumour cells in vitro and tumour growth in vivo, suggesting the importance of OTUD6A-CDC6 axis in these cancer cells. Moreover, both the OTUD6A and CDC6 protein levels are increased in BCa and renal carcinoma tumour tissues, and the trend in OTUD6A protein level is consistent with the trend in CDC6 protein level in both BCa and renal carcinoma tissues. In addition, BCa patients with high CDC6 and high OTUD6A protein levels have the worst OS outcomes, and patients with low CDC6 and high OTUD6A protein levels exhibited improved OS compared with patients with high CDC6 and low OTUD6A protein levels, suggesting that OTUD6A exerts its oncogenic effects mainly through upregulation of CDC6 in BCa cells. These findings broaden our understanding of OTUD6A under both physiological and pathological conditions.

Genome instability elicits ongoing DNA damage and DNA replication stress [1, 3]. The DDR is a complex suite of mechanisms that counteract threats to genomic integrity [52]. In response to DNA damage induced by chemotherapeutic drugs and ionizing radiation, the DDR is activated, leading to suppression of DNA damage and promotion of cancer cell survival [53]. DNA damage is first recognized by molecular "sensors", most notably those in the ATR/Chk1- and ATM/Chk2-mediated signalling pathways [54], which are hyperactivated in various cancers and associated with chemoresistance and poor prognosis [54–56]. CDC6 is also involved in the DDR. CDC6 silencing suppresses ATR function and increases genomic instability and DNA damage-induced cell death. In addition, CDC6 promotes the DDR by activating the ATR-Chk1 pathway in PCa and BCa [9, 42]. We showed that DNA damage promotes the binding of OTUD6A to CDC6, subsequently upregulating CDC6 protein level, activating the ATR-Chk1 pathway and resulting in chemoresistance (Fig. 8). Our results confirmed the synergistic effect of ATR/Chk1 inhibitors and gemcitabine in OTUD6A-overexpressing BCa cells, suggesting the possible beneficial effects of targeting ATR/

Chk1 in cancers with high expression of OTUD6A and CDC6.

Conclusions

In conclusion, our study identifies OTUD6A as a novel positive regulator of CDC6, which plays an important role in the cell cycle, cell proliferation, organism growth, tumorigenesis, the DDR and chemosensitivity, providing global insight into the physiological and pathological functions of OTUD6A. Our data suggest that the OTUD6A-CDC6 axis may be exploited as a promising clinical target for cancer therapy. In addition, the combination of ATR/Chk1 inhibitors with chemotherapy can be effective in patients with high OTUD6A expression.

Abbreviations

DDR	DNA damage response
ORC	origin recognition complex
CDC6	cell division cycle 6
CDT1	chromatin licensing and DNA replication factor 1
MCM2	minichromosome maintenance protein 2
pre-RC	pre-replicative complex
ATR	ataxia telangiectasia and Rad3-related protein
MGS	Meier-Gorlin syndrome
E2F	early region 2 binding factor
AR	androgen receptor
FOXM1	forkhead box M1
UPS	ubiquitin–proteasome system
DUB	deubiquitinase
OTUD6A	OTU domain-containing 6 A
IF	Immunofluorescence
shRNA	short hairpin RNA
CKO	conditional *Otud6a* knockout
MEF	mouse embryonic fibroblast
co-IP	Coimmunoprecipitation
HU	hydroxyurea
KOG	EuKaryotic Orthologous Groups
GO	Gene Ontology
BCa	bladder cancer
CCK8	Cell Counting Kit-8
BCPN	N-butyl-N-(3-carboxybutyl) nitrosamine
CIS	carcinoma in situ.
IHC	Immunohistochemical
OS	overall survival
AIF	apoptosis-inducing factor
BC	breast cancer
CRC	colorectal cancer

Supplementary Information

The online version contains supplementary material available at https://doi.org/10.1186/s12943-024-01996-y.

Supplementary Material 1

Acknowledgements

We thank Pro. CJ Gao for providing the human DUB plasmid library, HA-Ub WT, K11R, K27R, K29R, K33R, K48R and K63R plasmids, Pro. L. Drury for providing pCGN.CSH.FL42 plasmid encoding HA-tagged CDC6, Pro. LY Huang for providing pcDNA3.1 plasmids and encoding Flag-tagged OTUD6A-N-terminal (1-145aa) and C-terminal (129-288 aa), and pGEX-4T-1 plasmids encoding GST-tagged full-length OTUD6A, OTUD6A-N-terminal (1-145 aa) and C-terminal (129-288 aa) and. Pro. JF Diffley for providing the plasmids encoding HA-tagged CDC6 AAA (S54A, S74A and S106A) and DDD (S54D, S74D and S106D) mutants. We thank Translational Medicine Core Facility of Shandong University for consultation and instrument availability that supported this work.

Author contributions

Y. Zou, B. Shi, D. Wu and N. Xing conceived and designed the entire project. Y. Zou, B. Shi and D. Wu supervised the research conducted in their laboratories. Q. Shang contributed to the GST-pull down and constructed plasmids. J. Cui, X. Liu, L. Xiang, J. Zhan, Y. Zhou, S. Chen and L. Liu contributed to construct all the stable cells and perform the plasmid transfection and RNA interference, lentivirus packaging, qPCR, Western blot, co-IP, immunofluorescence, subcellular protein fractionation extraction and chromatin fractionation extraction. J. Cui, X. Liu, and Y. Xia performed deubiquitination in vivo and in vitro and protein half-life measurement. X. Liu, B. Fan, P. Chen and R. Zhao prepared all of the samples for proteomic analysis and mass spectrometry. J. Cui and Y. Wang performed cell cycle synchronization and flow cytometry. J. Cui, X. Liu, J. Dong, L. Xiang and B. Fan performed CCK8, EdU incorporation, colony formation, replication re-initiation/restart, H&E, IHC, TUNEL, alkaline comet and tissue specimen collection. J. Cui, X. Liu, J. Zhan and Y. Zhou performed mouse experiments. J. Cui, X. Liu, S. Sun, Y. Zhu and X. Liu conducted all of the data analyses. J. Cui and X. Liu wrote the manuscript and all authors commented on the manuscript.

Funding

This work was supported by the National Key R&D Program of China (Grant No. 2023YFC2507000 to B. Shi), the National Natural Science Foundation of China (grants 32070712 and 31671427 to Y. Zou, grants 81970661 and 82370767 to B. Shi, grants 82303098 to J. Cui, grant 81804104 to L. Liu), the Natural Science Foundation of Shandong Province (grant ZR2021MH318 to Y. Zhu, grant ZR2021JQ30 to D. Wu, grant ZR2023QH455 to J. Cui, grant ZR2023QH263 to X. Liu and grant ZR2020MH356 to X. Liu), China Postdoctoral Science Foundation (2023M732096 to J. Cui and 2022M721969 to X. Liu), Postdoctoral Innovation Talents Support Program of Shandong Province (SDBX2022009 to J. Cui) and the Taishan Scholars Project of Shandong (tsqn201909004 to D. Wu).

Data availability

The proteomics data are uploaded on PRIDE database (https://www.ebi.ac.uk/pride/). Data are available via ProteomeXchange with identifier PXD042935. All data needed to evaluate the conclusions in the paper are present in the main text and the supplementary materials.

Declarations

Competing interests

The authors declare no competing interests.

Ethical approval and consent to participate

This study was approved by the Medical Ethics Committee, Shandong University of Clinical Medicine and Shandong University Animal Care Committee.

Consent for publication

Not applicable.

Author details

[1]Department of Urology, Qilu Hospital, Department of Molecular Medicine and Genetics, School of Basic Medical Sciences, Shandong University, Jinan, Shandong 250012, China
[2]The Key Laboratory of Experimental Teratology, Ministry of Education and Department of Molecular Medicine and Genetics, School of Basic Medical Sciences, Qilu Hospital, Shandong University, Jinan, Shandong 250012, China
[3]Department of Clinical laboratory, Qilu Hospital, Shandong University, Jinan, Shandong 250012, China
[4]Helmholtz International Lab, State Key Laboratory of Microbial Technology, Shandong University, Qingdao, Shandong 266237, China
[5]Department of Dermatology, The Affiliated Hospital of Shandong University of Traditional Chinese Medicine, Shandong Provincial Hospital of Traditional Chinese Medicine, Jinan, Shandong 250011, China
[6]Department of Urology, Shouguang People's Hospital, Weifang, Shandong 262750, China

[7]Department of Radiation Oncology, Qilu Hospital, Shandong University, Jinan, Shandong 250012, China
[8]Department of Thoracic Surgery, Qilu Hospital, Shandong University, Jinan, Shandong 250012, China
[9]Departement of Breast and Thyroid Surgery, The Affiliated Hospital of Shandong University of Traditional Chinese Medicine, Shandong Provincial Hospital of Traditional Chinese Medicine, Jinan, Shandong 250011, China
[10]Department of Urology, National Cancer Center/National Clinical Research Center for Cancer/Cancer Hospital, Chinese Academy of Medical Sciences and Peking Union Medical College, Beijing 100021, China

Received: 4 December 2023 / Accepted: 5 April 2024
Published online: 29 April 2024

References

1. Abbas T, Keaton MA, Dutta A. Genomic instability in cancer. Cold Spring Harb Perspect Biol. 2013;5(3):a012914. https://doi.org/10.1101/cshperspect.a012914.
2. Macheret M, Halazonetis TD. DNA replication stress as a hallmark of cancer. Annu Rev Pathol. 2015;10:425–48. https://doi.org/10.1146/annurev-pathol-012414-040424.
3. Hernández-Pérez S, Cabrera E, Amoedo H, Rodríguez-Acebes S, Koundrioukoff S, Debatisse M, et al. USP37 deubiquitinates Cdt1 and contributes to regulate DNA replication. Mol Oncol. 2016;10(8):1196–206. https://doi.org/10.1016/j.molonc.2016.05.008.
4. Hernández-Pérez S, Cabrera E, Salido E, Lim M, Reid L, Lakhani SR, et al. DUB3 and USP7 de-ubiquitinating enzymes control replication inhibitor geminin: molecular characterization and associations with breast cancer. Oncogene. 2017;36(33):4802–9. https://doi.org/10.1038/onc.2017.21.
5. Fragkos M, Ganier O, Coulombe P, Méchali M. DNA replication origin activation in space and time. Nat Rev Mol Cell Biol. 2015;16(6):360–74. https://doi.org/10.1038/nrm4002.
6. Oehlmann M, Score AJ, Blow JJ. The role of Cdc6 in ensuring complete genome licensing and S phase checkpoint activation. J Cell Biol. 2004;165(2):181–90. https://doi.org/10.1083/jcb.200311044.
7. Xu X, Huang S, Zhang B, Huang F, Chi W, Fu J, et al. DNA replication licensing factor Cdc6 and Plk4 kinase antagonistically regulate centrosome duplication via Sas-6. Nat Commun. 2017;8:15164. https://doi.org/10.1038/ncomms15164.
8. Yoshida K, Sugimoto N, Iwahori S, Yugawa T, Narisawa-Saito M, Kiyono T, et al. CDC6 interaction with ATR regulates activation of a replication checkpoint in higher eukaryotic cells. J Cell Sci. 2010;123(Pt 2):225–35. https://doi.org/10.1242/jcs.058693.
9. Karanika S, Karantanos T, Li L, Wang J, Park S, Yang G, et al. Targeting DNA damage response in prostate Cancer by inhibiting androgen Receptor-CDC6-ATR-Chk1 signaling. Cell Rep. 2017;18(8):1970–81. https://doi.org/10.1016/j.celrep.2017.01.072.
10. de Munnik SA, Otten BJ, Schoots J, Bicknell LS, Aftimos S, Al-Aama JY, et al. Meier-Gorlin syndrome: growth and secondary sexual development of a microcephalic primordial dwarfism disorder. Am J Med Genet Part A. 2012;158a(11):2733–42. https://doi.org/10.1002/ajmg.a.35681.
11. Karakaidos P, Taraviras S, Vassiliou LV, Zacharatos P, Kastrinakis NG, Kougiou D, et al. Overexpression of the replication licensing regulators hCdt1 and hCdc6 characterizes a subset of non-small-cell lung carcinomas: synergistic effect with mutant p53 on tumor growth and chromosomal instability–evidence of E2F-1 transcriptional control over hCdt1. Am J Pathol. 2004;165(4):1351–65. https://doi.org/10.1016/s0002-9440(10)63393-7.
12. Mahadevappa R, Neves H, Yuen SM, Bai Y, McCrudden CM, Yuen HF, et al. The prognostic significance of Cdc6 and Cdt1 in breast cancer. Sci Rep. 2017;7(1):985. https://doi.org/10.1038/s41598-017-00998-9.
13. Yan Z, DeGregori J, Shohet R, Leone G, Stillman B, Nevins JR, et al. Cdc6 is regulated by E2F and is essential for DNA replication in mammalian cells. Proc Natl Acad Sci USA. 1998;95(7):3603–8. https://doi.org/10.1073/pnas.95.7.3603.
14. Mallik I, Davila M, Tapia T, Schanen B, Chakrabarti R. Androgen regulates Cdc6 transcription through interactions between androgen receptor and E2F transcription factor in prostate cancer cells. Biochim Biophys Acta. 2008;1783(10):1737–44. https://doi.org/10.1016/j.bbamcr.2008.05.006.
15. Liu Y, Gong Z, Sun L, Li X. FOXM1 and androgen receptor co-regulate CDC6 gene transcription and DNA replication in prostate cancer cells. Biochim Biophys Acta. 2014;1839(4):297–305. https://doi.org/10.1016/j.bbagrm.2014.02.016.
16. Petersen BO, Wagener C, Marinoni F, Kramer ER, Melixetian M, Lazzerini Denchi E, et al. Cell cycle- and cell growth-regulated proteolysis of mammalian CDC6 is dependent on APC-CDH1. Genes Dev. 2000;14(18):2330–43. https://doi.org/10.1101/gad.832500.
17. Sulkshane P, Ram J, Thakur A, Reis N, Kleifeld O, Glickman MH. Ubiquitination and receptor-mediated mitophagy converge to eliminate oxidation-damaged mitochondria during hypoxia. Redox Biol. 2021;45:102047. https://doi.org/10.1016/j.redox.2021.102047.
18. Abbas R, Larisch S. Killing by degradation: regulation of apoptosis by the ubiquitin-proteasome-system. Cells. 2021;10(12). https://doi.org/10.3390/cells10123465.
19. Perkins G, Drury LS, Diffley JF. Separate. SCF(CDC4) recognition elements target Cdc6 for proteolysis in S phase and mitosis. EMBO J. 2001;20(17):4836–45. https://doi.org/10.1093/emboj/20.17.4836.
20. Clijsters L, Wolthuis R. PIP-box-mediated degradation prohibits re-accumulation of Cdc6 during S phase. J Cell Sci. 2014;127(Pt 6):1336–45. https://doi.org/10.1242/jcs.145862.
21. Walter D, Hoffmann S, Komseli ES, Rappsilber J, Gorgoulis V, Sørensen CS. SCF(cyclin F)-dependent degradation of CDC6 suppresses DNA re-replication. Nat Commun. 2016;7:10530. https://doi.org/10.1038/ncomms10530.
22. Mevissen TET, Komander D. Mechanisms of Deubiquitinase specificity and regulation. Annu Rev Biochem. 2017;86:159–92. https://doi.org/10.1146/annurev-biochem-061516-044916.
23. Guo Y, Jiang F, Kong L, Wu H, Zhang H, Chen X, et al. OTUD5 promotes innate antiviral and antitumor immunity through deubiquitinating and stabilizing STING. Cell Mol Immunol. 2021;18(8):1945–55. https://doi.org/10.1038/s41423-020-00531-5.
24. Fu X, Zhao J, Yu G, Zhang X, Sun J, Li L, et al. OTUD6A promotes prostate tumorigenesis via deubiquitinating Brg1 and AR. Commun Biology. 2022;5(1):182. https://doi.org/10.1038/s42003-022-03133-1.
25. Mailand N, Diffley JF. CDKs promote DNA replication origin licensing in human cells by protecting Cdc6 from APC/C-dependent proteolysis. Cell. 2005;122(6):915–26. https://doi.org/10.1016/j.cell.2005.08.013.
26. Liu L, Cui J, Zhao Y, Liu X, Chen L, Xia Y, et al. KDM6A-ARHGDIB axis blocks metastasis of bladder cancer by inhibiting Rac1. Mol Cancer. 2021;20(1):77. https://doi.org/10.1186/s12943-021-01369-9.
27. Zou Y, Mi J, Cui J, Lu D, Zhang X, Guo C, et al. Characterization of nuclear localization signal in the N terminus of CUL4B and its essential role in cyclin E degradation and cell cycle progression. J Biol Chem. 2009;284(48):33320–32. https://doi.org/10.1074/jbc.M109.050427.
28. Liu X, Cui J, Gong L, Tian F, Shen Y, Chen L, et al. The CUL4B-miR-372/373-PIK3CA-AKT axis regulates metastasis in bladder cancer. Oncogene. 2020;39(17):3588–603. https://doi.org/10.1038/s41388-020-1236-1.
29. Varghese F, Bukhari AB, Malhotra R, De A. IHC profiler: an open source plugin for the quantitative evaluation and automated scoring of immunohistochemistry images of human tissue samples. PLoS ONE. 2014;9(5):e96801. https://doi.org/10.1371/journal.pone.0096801.
30. Meng W, Sjöholm LK, Kononenko O, Tay N, Zhang D, Sarkisyan D, et al. Genotype-dependent epigenetic regulation of DLGAP2 in alcohol use and dependence. Mol Psychiatry. 2021;26(8):4367–82. https://doi.org/10.1038/s41380-019-0588-9.
31. Lee I, Kim GS, Bae JS, Kim J, Rhee K, Hwang DS. The DNA replication protein Cdc6 inhibits the microtubule-organizing activity of the centrosome. J Biol Chem. 2017;292(39):16267–76. https://doi.org/10.1074/jbc.M116.763680.
32. Lim N, Townsend PA. Cdc6 as a novel target in cancer: oncogenic potential, senescence and subcellular localisation. Int J Cancer. 2020;147(6):1528–34. https://doi.org/10.1002/ijc.32900.
33. Kim GS, Lee I, Kim JH, Hwang DS. The replication protein Cdc6 suppresses centrosome over-duplication in a Manner Independent of its ATPase activity. Mol Cells. 2017;40(12):925–34. https://doi.org/10.14348/molcells.2017.0191.
34. Liu H, Zhao WL, Wang JP, Xin BM, Shao RG. EBP50 suppresses the proliferation of MCF-7 human breast cancer cells via promoting Beclin-1/p62-mediated lysosomal degradation of c-Myc. Acta Pharmacol Sin. 2018;39(8):1347–58. https://doi.org/10.1038/aps.2017.171.
35. Degoricija M, Korac-Prlic J, Vilovic K, Ivanisevic T, Haupt B, Palada V, et al. The dynamics of the inflammatory response during BBN-induced bladder carcinogenesis in mice. J Translational Med. 2019;17(1):394. https://doi.org/10.1186/s12967-019-02146-5.
36. Tratnjek L, Jeruc J, Romih R, Zupančič D. Vitamin A and retinoids in bladder Cancer chemoprevention and treatment: a narrative review of current

evidence, challenges and Future prospects. Int J Mol Sci. 2021;22(7). https://doi.org/10.3390/ijms22073510.
37. Bradbury A, Hall S, Curtin N, Drew Y. Targeting ATR as Cancer Therapy: a new era for synthetic lethality and synergistic combinations? Pharmacol Ther. 2020;207:107450. https://doi.org/10.1016/j.pharmthera.2019.107450.
38. Gralewska P, Gajek A, Marczak A, Rogalska A. Participation of the ATR/CHK1 pathway in replicative stress targeted therapy of high-grade ovarian cancer. J Hematol Oncol. 2020;13(1):39. https://doi.org/10.1186/s13045-020-00874-6.
39. Sun M, Feng X, Liu Z, Han W, Liang YX, She Q. An Orc1/Cdc6 ortholog functions as a key regulator in the DNA damage response in Archaea. Nucleic Acids Res. 2018;46(13):6697–711. https://doi.org/10.1093/nar/gky487.
40. Hall JR, Lee HO, Bunker BD, Dorn ES, Rogers GC, Duronio RJ, et al. Cdt1 and Cdc6 are destabilized by rereplication-induced DNA damage. J Biol Chem. 2008;283(37):25356–63. https://doi.org/10.1074/jbc.M802667200.
41. Piquet S, Le Parc F, Bai SK, Chevallier O, Adam S, Polo SE. The histone chaperone FACT coordinates H2A.X-Dependent signaling and repair of DNA damage. Mol Cell. 2018;72(5):888–e901887. https://doi.org/10.1016/j.molcel.2018.09.010.
42. Chen S, Chen X, Xie G, He Y, Yan D, Zheng D, et al. Cdc6 contributes to cisplatin-resistance by activation of ATR-Chk1 pathway in bladder cancer cells. Oncotarget. 2016;7(26):40362–76. https://doi.org/10.18632/oncotarget.9616.
43. Alexandrow MG, Hamlin JL. Cdc6 chromatin affinity is unaffected by serine-54 phosphorylation, S-phase progression, and overexpression of cyclin A. Mol Cell Biol. 2004;24(4):1614–27. https://doi.org/10.1128/mcb.24.4.1614-1627.2004.
44. Luo Q, Wu X, Zhao P, Nan Y, Chang W, Zhu X, et al. OTUD1 activates caspase-independent and caspase-dependent apoptosis by promoting AIF Nuclear translocation and MCL1 degradation. Adv Sci (Weinheim Baden-Wurttemberg Germany). 2021;8(8):2002874. https://doi.org/10.1002/advs.202002874.
45. Yuan L, Lv Y, Li H, Gao H, Song S, Zhang Y, et al. Deubiquitylase OTUD3 regulates PTEN stability and suppresses tumorigenesis. Nat Cell Biol. 2015;17(9):1169–81. https://doi.org/10.1038/ncb3218.
46. Sobol A, Askonas C, Alani S, Weber MJ, Ananthanarayanan V, Osipo C, et al. Deubiquitinase OTUD6B isoforms are important regulators of growth and proliferation. Mol cancer Research: MCR. 2017;15(2):117–27. https://doi.org/10.1158/1541-7786.Mcr-16-0281-t.
47. Santiago-Sim T, Burrage LC, Ebstein F, Tokita MJ, Miller M, Bi W, et al. Biallelic variants in OTUD6B cause an intellectual disability Syndrome Associated with seizures and dysmorphic features. Am J Hum Genet. 2017;100(4):676–88. https://doi.org/10.1016/j.ajhg.2017.03.001.
48. Zhang L, Huo Q, Ge C, Zhao F, Zhou Q, Chen X, et al. ZNF143-Mediated H3K9 trimethylation upregulates CDC6 by activating MDIG in Hepatocellular Carcinoma. Cancer Res. 2020;80(12):2599–611. https://doi.org/10.1158/0008-5472.Can-19-3226.
49. Shi L, Liu J, Peng Y, Zhang J, Dai X, Zhang S, et al. Deubiquitinase OTUD6A promotes proliferation of cancer cells via regulating Drp1 stability and mitochondrial fission. Mol Oncol. 2020;14(12):3169–83. https://doi.org/10.1002/1878-0261.12825.
50. Peng Y, Liu J, Wang Z, Cui C, Zhang T, Zhang S, et al. Prostate-specific oncogene OTUD6A promotes prostatic tumorigenesis via deubiquitinating and stabilizing c-Myc. Cell Death Differ. 2022;29(9):1730–43. https://doi.org/10.1038/s41418-022-00960-x.
51. Zhao Y, Huang X, Zhu D, Wei M, Luo J, Yu S, et al. Deubiquitinase OTUD6A promotes breast cancer progression by increasing TopBP1 stability and rendering tumor cells resistant to DNA-damaging therapy. Cell Death Differ. 2022. https://doi.org/10.1038/s41418-022-01036-6.
52. Lord CJ, Ashworth A. The DNA damage response and cancer therapy. Nature. 2012;481(7381):287–94. https://doi.org/10.1038/nature10760.
53. Huang R, Zhou PK. DNA damage repair: historical perspectives, mechanistic pathways and clinical translation for targeted cancer therapy. Signal Transduct Target Therapy. 2021;6(1):254. https://doi.org/10.1038/s41392-021-00648-7.
54. Kiss RC, Xia F, Acklin S. Targeting DNA damage response and repair to Enhance Therapeutic Index in Cisplatin-Based Cancer Treatment. Int J Mol Sci. 2021;22(15). https://doi.org/10.3390/ijms22158199.
55. Hong J, Hu K, Yuan Y, Sang Y, Bu Q, Chen G, et al. CHK1 targets spleen tyrosine kinase (L) for proteolysis in hepatocellular carcinoma. J Clin Investig. 2012;122(6):2165–75. https://doi.org/10.1172/jci61380.
56. Hayes M, Lan C, Yan J, Xie Y, Gray T, Amirkhan RH, et al. ERCC1 expression and outcomes in head and neck cancer treated with concurrent cisplatin and radiation. Anticancer Res. 2011;31(12):4135–9.

Publisher's Note

Supplementary materials

Methods

Plasmid DNA transfection and RNA interference

Cells at 70% confluence were transfected with the indicated plasmid DNA using Lipofectamine™ 3000 transfection reagent (Invitrogen, L3000015) according to the manufacturer's protocol. siRNA duplex oligomers of ATR and the negative control siRNA were synthesized by Shandong Gene&Bio Co. Ltd (Shandong, China) . Cells at 30-40% confluence were transfected with X-tremeGENE siRNA Transfection Reagent (Roche, 4476093001) following the manufacturer's protocol.

Lentiviral packaging and infection

To generate lentiviral shRNA constructs targeting human CDC6, lentiviral vectors carrying a shRNA targeting human CDC6 were purchased from GeneChem Inc. (Shanghai, China). The CDC6 shRNA/negative control shRNA (shNC) and the pMD2.G and psPAX2 plasmids were cotransfected into HEK293T cells for 48 h, and the viral supernatant was filtered through a 0.45 μm filter (Millipore).

For the construction of cells with stable OTUD6A- and CDC6-knockdown/overexpression cells were infected with lentivirus as indicated. OTUD6A knockdown/overexpression and CDC6 overexpression lentiviruses were purchased from Genechem Inc. (Shanghai, China). Lentiviruses containing empty plasmids (NC) and shNC were used as controls.

Viruses were used to infect cells in the presence of polybrene for 48 h, and the cells

were cultured in medium containing puromycin (1 mg/mL) for 5 days. Stably transduced cells resistant to puromycin were identified and verified by qRT-PCR and Western blot analysis.

Subcellular fractionation

Subcellular fractionation was performed using a Subcellular Protein Fractionation Kit (Thermo Fisher Scientific, 78840) following the manufacturer's instructions. Briefly, cells were harvested, CEB buffer was added for 10 min, and the supernatant was taken as the cytoplasmic protein fraction after centrifugation. Soluble nuclear proteins were collected after adding NEB buffer. The remaining sample was treated with micrococcal nuclease, which released chromatin-bound nuclear proteins into the supernatant. The supernatant was boiled with SDS-PAGE loading buffer at 99 ℃ for 10 min and analysed by Western blotting.

Chromatin fractionation

Chromatin-bound protein was extracted using the Chromatin Extraction Kit (Abcam ab117152) according to the manufacturer's instructions. Briefly, treated cells were harvested in working lysis buffer on ice for 10 min and centrifuged at 5,000 rpm for 5 min. Then, the supernatant was removed, and working extraction buffer was added on ice for another 10 min, followed by sonication (10 s, 20 cycles). The samples were centrifuged at 12,000 rpm for 10 min at 4 ℃. The samples were boiled with SDS-PAGE loading buffer at 99 ℃ for 10 min and analyzed by Western blotting.

Proteomic analysis

The Flag-OTUD6A or Flag vector was transfected into 293 cells for 24 h. No less than 10 million cells were harvested using a cell scraper and were sent to PTM BIO company for 4D label-free quantitative proteomic analysis (Hangzhou, China). Data are uploaded on PRIDE database (https://www.ebi.ac.uk/pride/) and available via ProteomeXchange with identifier PXD042935. Differentially expressed proteins were subjected to further Gene Ontology (GO) and EuKaryotic Orthologous Groups (KOG) analysis.

Mass spectrometry

HEK293 cells were transfected with the Flag-OTUD6A or Flag vector, and cell lysates were subjected to IP with an anti-Flag antibody. The immunoprecipitates were separated on 10% gels, which were then stained with Coomassie Brilliant Blue solution (Beyotime, P0017F). The gels were cut into small pieces, destained with 100 mM NH_4HCO_3/30% ACN and dried in a vacuum centrifuge. The in-gel proteins were incubated with dithiothreitol (10 mM DTT/100 mM NH_4HCO_3) at 56 ℃ for 30 min and were then rinsed in iodoacetamide (200 mM IAA/100 mM NH_4HCO_3) in the dark at room temperature for 20 min. The gels were washed sequentially with 100 mM NH_4HCO_3 and ACN. The gels were digested with 5 ng/μL trypsin (Promega) at 4 ℃ for 1 h and incubated with 50 mM NH_4HCO_3 at 37 ℃ for 18 h. Peptides were extracted three times with 60% ACN/0.1% TFA by ultrasonic shearing. The extracts were pooled and dried completely in a vacuum centrifuge. Peptides were recovered by solid-phase

extraction using C18 ZipTips (Millipore) and resuspended in 0.1% TFA/50% ACN for analysis by LC-MS/MS (Orbitrap Elite, Thermo Scientific). All raw files were processed using proteinDiscover (version 1.4, Thermo Scientific) for database searching. MS/MS spectra were searched against the UniProtKB/SwissProt human database (downloaded on December 29, 2017).

Bimolecular fluorescent complimentary (BiFC) assay

293 and U2OS cells were transfected with Flag-YFP-N terminus (Flag-YN), HA-YFP-C terminus (HA-YC), Flag-YFP-N terminus-OTUD6A (YN-OTUD6A) or HA-YFP-C terminus-CDC6 (YC-CDC6) plasmids. An additional 24 h later, the cells were stained with Hoechst 33342 and imaged with a confocal microscope (LSM880 NLO, Zeiss, Germany). YFP and Hoechst 33342 were excited by a 514 nm Argon and 405 nm diode laser respectively, and their fluorescence was detected at 527 nm and 461 nm, respectively.

GST pull-down assay

The GST-tagged full-length OTUD6A, OTUD6A-N-terminal (1-145 aa) and OTUD6A-C-terminal (129-288 aa) constructs were transfected into *E. coli* BL21 (DE3), and protein expression was induced with 200 μM isopropyl β-D-1-thiogalactopyranoside (IPTG) at 20 ℃ overnight. The bacteria were collected and lysed in lysis buffer (PBS + 0.1 μM PMSF + 0.1 μM DTT) under sonication for 20 min at 4 ℃. The lysate was centrifuged at 15,000 rpm for 15 min at 4 ℃, and the supernatant

was incubated with 200 μL of glutathione-sepharose (Cytiva, 17513201) for 2 h at 4 ℃. Then, the beads were washed with lysis buffer four times and incubated with total protein lysate from HEK293 cells for 2 h at 4 ℃. Then, the beads were washed with Western and IP buffer four times, followed by Western blotting.

Protein half-life assay

Cells were transfected with the indicated plasmids for 24 h in individual experiments. Then, the cells were treated with cycloheximide (CHX, 20 μg/mL) for the indicated durations before harvesting. Stable OTUD6A-knockdown cells were treated only with CHX (20 μg/mL) for the indicated durations before harvesting.

***In vivo* deubiquitination assay**

The indicated plasmids were transfected into HEK293 cells for 24 h. After incubation with 20 μM MG132 for 6 h, the cells were harvested and lysed in Western and IP buffer with protease inhibitors. Then, an IP assay was used to assess ubiquitination levels by immunoblotting with the indicated antibodies.

***In vitro* deubiquitination assay**

HEK293 cells were transfected together with the Myc-CDC6 and HA-Ub expression plasmids for 48 h. The cells were treated with MG132 for 6 h and lysed. The lysate was purified with an anti-Myc affinity gel, eluted with Myc peptide and subjected to HA affinity gel purification to enrich HA-Ub-conjugated CDC6 (Ub-CDC6). HEK293 cells

were transfected with Flag-OTUD6A, and the cell lysates were incubated with anti-Flag affinity gel for 2 h. The beads were then washed five times with lysis buffer. Recombinant OTUD6A proteins were subsequently incubated with Ub-CDC6 in deubiquitination reaction buffer (50 mM Tris-HCl (pH 8.0), 50 mM NaCl, 1 mM EDTA, 10 mM DTT, 5% glycerol) at 37 ℃ for 30 min. The ubiquitination status of CDC6 was analysed by Western blotting.

Cell cycle synchronization assay

U2OS cells were treated with 2 mM thymidine for 24 h, washed twice with PBS, and released for 4 h in fresh medium before being treated with 100 ng/mL nocodazole in DMEM for 16 h to obtain a prometaphase population by a “shake-off” procedure. For synchronization in G1/S phase, HeLa cells were cultured in the presence of 2.5 mM thymidine for 16 h, washed two times with PBS, and released in fresh medium without thymidine for 8 h. After another 16 h of culture in medium containing thymidine, the cells were washed two times with PBS and released in fresh RPMI-1640 medium.

Flow cytometry

Cells were fixed with 70% ethanol and stained with propidium iodide (PI) using standard methods. In brief, cells were harvested using trypsin, centrifuged at 3,000 rpm for 3 min, and washed once with cold PBS. The cells were fixed with cold 70% ethanol at -20 ℃ overnight. The fixed cells were washed with PBS once and then incubated with 500 μL of PBS containing 100 μg/mL RNase A (Solarbio, R1030) and 50 μg/mL

PI (Solarbio, P8080) at room temperature in the dark for 30 minutes. The cell cycle distribution was analysed by using a BD Biosciences FACScan II cytometer (Becton Dickinson, San Jose, CA, USA).

CCK8, colony formation and EdU incorporation assays

CCK8, colony formation, and EdU incorporation assays were performed as previously described. Briefly, for the CCK-8 assay, 10 μL of CCK-8 (NCM Biotech, C6005) was added to each well for 1 h. The optical density (OD) values were determined at 450 nm. For half-maximal inhibitory concentration (IC_{50}) measurement, cells were plated in 96-well dishes and treated with multiple concentrations of various drugs for 48 h. Then, a CCK8 assay was used, and the OD was determined at 450 nm. GraphPad Prism (version 8.0.2, GraphPad Software, CA, USA) software was used to calculate cell viability. The cell viability (%) is calculated as follows: [OD value (drug treatment)-OD value (blank)/OD value (average control)-OD value (blank)]×100).

For the colony formation assay, eight hundred cells per well were seeded in 6-well plates and cultured for 7-14 days. The cell colonies were fixed with 4% paraformaldehyde, stained with crystal violet and counted.

The EdU (5-ethynyl-2′-deoxyuridine) incorporation assay was performed using the Cell-Light™ EdU Apollo 567 In Vitro Kit (Ribobio, C10310-1, Guangzhou, China) according to the manufacturer's instructions. Briefly, cells were cultured on coverslips overnight, EdU was added to the medium for 30 min, and the cells were fixed with 4% paraformaldehyde. After fixation, the cells were incubated with EdU staining solution

for 1 h and subsequently stained with DAPI. The EdU-labelled cells were imaged with a fluorescence microscope (BX51, Olympus Life Science, Tokyo, Japan).

Replication reinitiation assays

Cells were treated with HU (2 mM) for 24 h to arrest at S phase which lost the ability to undergo DNA replication. Subsequently, the cells were released in fresh medium for 0 h, 4 h and 8 h. EdU was added for 30 minutes before harvesting. Then the EdU incorporation assay was performed as described above. The EdU positive cells represent the DNA replication reinitiation cells.

Tissue specimens

A total of 20 paired human fresh BCa tumour and matched adjacent normal tissues were obtained at Hospital. All samples were surgical specimens collected from patients with no neoadjuvant chemotherapy or radiotherapy. Informed consent was obtained from all patients or their relatives before surgery. This study was approved by the Medical Ethics Committee, Shandong University of Clinical Medicine. Bladder tissue microarrays containing 68 BCa tissues and 40 normal bladder tissues were obtained from Shanghai Outdo Biotech (Cat No. HBlaU108Su01, Shanghai, China). Renal tissue microarrays containing 32 renal carcinoma tissues and 15 normal renal tissues were obtained from Shanghai Outdo Biotech (Cat No. HKidCRC030PG01 and HKidE030PG02, Shanghai, China).

Terminal deoxynucleotidyl transferase-mediated dUTP-fluorescein nick end labelling (TUNEL) assay

The TUNEL assay was performed using a one-step TUNEL Apoptosis Assay Kit (Beyotime, C1089) according to the manufacturer's instructions. Cells were cultured on coverslips and exposed to gemcitabine for 48 h. The cells were fixed with 4% paraformaldehyde for 30 min, incubated with TUNEL mixture for 1 h and subsequently stained with DAPI. The TUNEL-labelled cells were imaged with a fluorescence microscope (BX51, Olympus Life Science, Tokyo, Japan).

Alkaline comet assay

The alkaline comet assay was performed using the Single Cell Gel Electrophoresis Assay Kit (Trevigen, 4250-050-K) according to the manufacturer's protocol. Briefly, cells were treated with gemcitabine for 48 h, harvested and suspended in ice-cold PBS (Ca^{2+} and Mg^{2+} free). Then, molten LMAgarose (at 37 °C) was combined with the cells at a ratio of 1:10 (v/v), and 50 μL was immediately pipetted onto a CometSlide™. The slides were incubated at 4 °C in the dark for 10 min. Then, the slides were immersed in lysis solution overnight at 4 °C prior to incubation in Alkaline Unwinding Solution for 60 min at 4 °C. Alkaline single-cell gel electrophoresis was performed, and the slides were stained with DAPI and imaged with a fluorescence microscope (BX51, Olympus Life Science, Tokyo, Japan). % DNA in tail was used to quantify the extent of DNA damage using CometScore software (version 1.5).

MEF cell isolation

The indicated mice were killed at 13.5-14.5 days of gestation. Mouse embryos were dissected, and the embryonic internal organs, head, tail, and limbs were removed. The carcasses were cut into small pieces. The tissues were incubated in 0.15% trypsin/EDTA solution for 15 min at 37 °C and vortexed every 5 min prior to centrifugation at 1500 rpm for 5 min. The supernatant was removed, and the cells were resuspended and cultured in RPMI-1640 medium. Primary MEFs were used for a maximum of five passages.

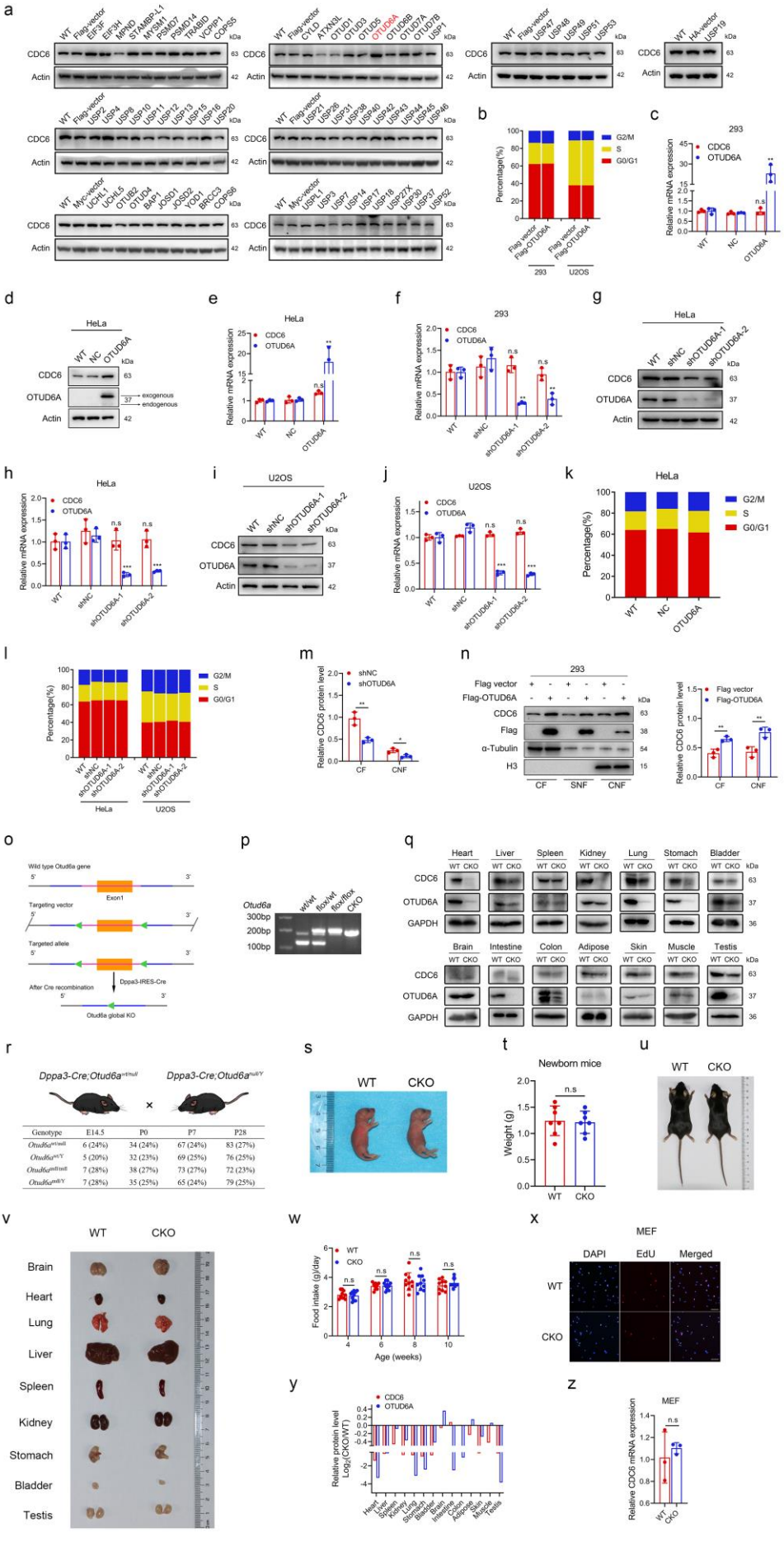
a
WT Flag-vector EIF3F EIF3H MPND STAMBP-L1 MYSM1 PSMD7 PSMD14 TRABID VCPIP1 COPS5
WT Flag-vector CYLD ATXN3L OTUD1 OTUD3 OTUD5 OTUD6A OTUD6B OTUD7A OTUD7B USP1
WT Flag-vector USP47 USP48 USP49 USP51 USP53
WT HA-vector USP19
WT Flag-vector USP2 USP4 USP8 USP10 USP11 USP12 USP13 USP15 USP16 USP20
WT Flag-vector USP21 USP26 USP31 USP38 USP40 USP42 USP43 USP44 USP45 USP46
WT Myc-vector UCHL1 UCHL5 OTUB2 OTUD4 BAP1 JOSD1 JOSD2 YOD1 BRCC3 COPS6
WT Myc-vector USPL1 USP3 USP7 USP14 USP17 USP18 USP27X USP30 USP37 USP52
CDC6
Actin
kDa
b
Percentage(%)
G2/M
S
G0/G1
Flag vector
Flag-OTUD6A
293
U2OS
c
293
CDC6
OTUD6A
Relative mRNA expression
n.s
WT
NC
OTUD6A
d
HeLa
WT
NC
OTUD6A
exogenous
endogenous
e
HeLa
f
293
shNC
shOTUD6A-1
shOTUD6A-2
g
HeLa
h
HeLa
i
U2OS
j
U2OS
k
HeLa
l
HeLa
U2OS
m
shNC
shOTUD6A
Relative CDC6 protein level
CF
CNF
n
293
Flag vector
Flag-OTUD6A
CDC6
Flag
α-Tubulin
H3
CF
SNF
CNF
o
Wild type Otud6a gene
Exon1
Targeting vector
Targeted allele
Dppa3-IRES-Cre
After Cre recombination
Otud6a global KO
p
Otud6a
300bp
200bp
100bp
wt/wt
flox/wt
flox/flox
CKO
q
Heart
Liver
Spleen
Kidney
Lung
Stomach
Bladder
Brain
Intestine
Colon
Adipose
Skin
Muscle
Testis
GAPDH
r
Dppa3-Cre;Otud6a
Genotype
E14.5
P0
P7
P28
s
WT
CKO
t
Newborn mice
Weight (g)
u
v
Brain
Heart
Lung
Liver
Spleen
Kidney
Stomach
Bladder
Testis
w
Food intake (g)/day
Age (weeks)
x
MEF
DAPI
EdU
Merged
y
Relative protein level
Log2(CKO/WT)
z
MEF
Relative CDC6 mRNA expression

Supplementary Fig. 1 OTUD6A upregulates CDC6 protein expression. a, HEK293 (293) cells were transfected with the indicated DUBs individually, and the endogenous CDC6 expression level was measured by Western blotting. **b**, Cell cycle distribution of asynchronous 293 and U2OS cells transiently transfected with indicated vectors. **c**, CDC6 and OTUD6A expression levels were measured in the indicated HeLa cells by qPCR; the levels in WT cells were set as 1. **d, e**, CDC6 and OTUD6A expression levels were measured in the indicated HeLa cells by Western blotting (**d**) and qPCR (**e**); the levels in WT cells were set as 1. **f**, CDC6 and OTUD6A expression levels were measured in the indicated 293 cells by qPCR; the levels in WT cells were set as 1. **g, h**, CDC6 and OTUD6A expression levels were measured in the indicated HeLa cells by Western blotting (**g**) and qPCR (**h**); the levels in WT cells were set as 1. **i**, **j**, CDC6 and OTUD6A expression levels were measured in the indicated U2OS cells by Western blotting (**i**) and qPCR (**j**); the levels in WT cells were set as 1. **k, l**, The cell cycle distribution of asynchronous OTUD6A stably overexpressed HeLa (**k**), as well as asynchronous OTUD6A stably knockdown HeLa and U2OS (**l**) cells were analyzed by flow cytometry. **m**, The relative intensities of the CDC6 bands in CF (CDC6/α-Tubulin) and CNF (CDC6/H3) were quantified from three independent repeated Western blotting analysis. The optical density (OD) of protein bands was analyzed by ImageJ. **n**, Cytoplasmic, soluble nuclear and chromatin-bound nuclear fractions were extracted from the indicated cells using subcellular fractionation assay and detected by Western blotting (left). The relative intensities of the CDC6 bands in CF (CDC6/α-Tubulin) and CNF (CDC6/H3) were quantified from three independent repeated Western blotting

analysis. (right). CF, cytoplasmic fractions; CNF, chromatin-bound nuclear fractions. **o**, The strategy for the generation of global OTUD6A knockout (CKO) mice. Loxp recombination sites (green triangles) were introduced flanking exon 1. **p**, Genotyping of the indicated mice was performed by PCR analysis. **q**, The protein levels of OTUD6A and CDC6 in tissues from OTUD6A WT and CKO littermates (8 weeks old) were measured by Western blotting. **r**, Numbers of mice of each genotype among the progeny of *Dppa3-Cre;Otud6a*$^{wt/null}$ female mice and *Dppa3-Cre;Otud6a*$^{null/Y}$ male mice. **s**, Representative image of the indicated newborn mice. **t**, Quantitative analysis of body weight between newborn WT (n = 7) and CKO (n = 7) mice. **u**, Representative image of 8-week-old WT and CKO mice. **v**, Representative images of the indicated tissues from WT and CKO littermates (8 weeks old) are shown. **w**, Food intake in 4, 6, 8 and 10 week-old CKO and WT mice (g/day) (n=10 in each group). **x**, Representative images of EdU staining are shown. Scale bars, 50 μm. **y**, Relative OTUD6A and CDC6 protein levels shown in Supplementary Fig. 1q from the indicated tissues of 8-week-old WT and CKO mice. **z**, CDC6 and OTUD6A expression levels were measured in WT and CKO mouse-derived mouse embryonic fibroblasts (MEFs) by qPCR; the levels in WT mice were set as 1. All quantitative analyses were based on three independent experiments. The error bars indicate the SDs. *$P < 0.05$, **$P < 0.01$, ***$P < 0.001$, n.s. not significant, based on two-tailed Student's *t* test.

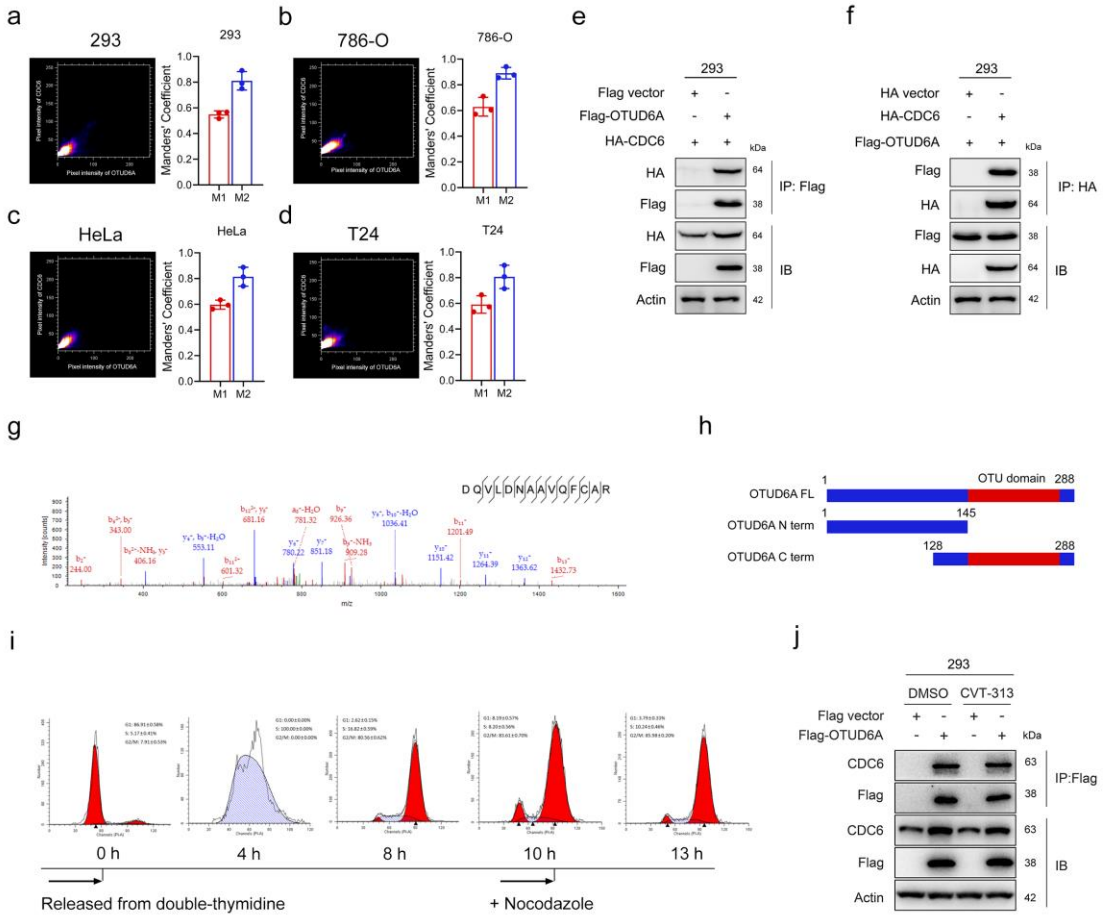

Supplementary Fig. 2 OTUD6A interacts with CDC6. a-d, The colocalization analysis of OTUD6A and CDC6 in 293 (**a**), 786-O (**b**), HeLa (**c**) and T24 (**d**) cells using Manders' coefficient analysis. M1 represents the proportion of overlapping pixel intensity of CDC6 and OTUD6A in CDC6 pixel intensity. M2 represents the proportion of overlapping pixel intensity of CDC6 and OTUD6A in OTUD6A pixel intensity. **e, f**, Flag-OTUD6A and HA-CDC6 were cotransfected into 293 cells for 24 h. Whole-cell lysates were prepared and subjected to immunoprecipitation (IP) with anti-Flag (**e**) or anti-HA (**f**) antibodies. The immunoprecipitates were analysed by Western blotting. **g**, Representative fragmentation spectrum of the identified CDC6 peptides by mass spectrometry. **h**, Schematic illustration of OTUD6A constructs. **i**, Representative flow cytometric plots of the cell cycle distribution at the indicated time points. **j**, 293 cells

transfected with the indicated vector were treated with CVT-313 (2 mM) or DMSO for 24 h. Whole-cell lysates were prepared and subjected to IP with an anti-Flag antibody. The immunoprecipitates were analysed by Western blotting.

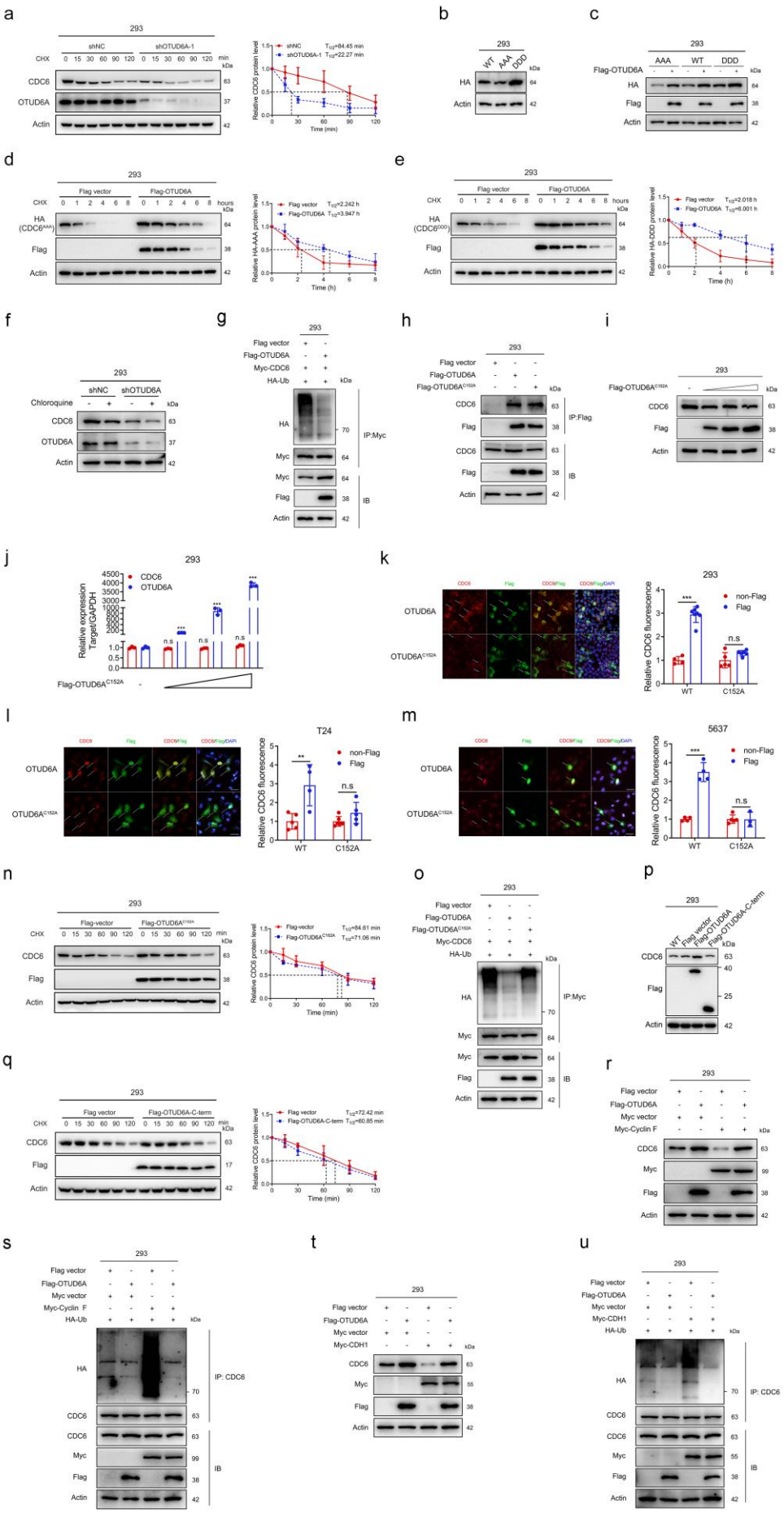
a
293
shNC
shOTUD6A-1
CHX
0 15 30 60 90 120 min
CDC6
OTUD6A
Actin
63
37
42
kDa
Relative CDC6 protein level
shNC T1/2=84.45 min
shOTUD6A-1 T1/2=22.27 min
Time (min)
b
293
WT
AAA
DDD
HA
Actin
64
42
c
293
AAA
WT
DDD
Flag-OTUD6A
HA
Flag
Actin
d
293
Flag vector
Flag-OTUD6A
0 1 2 4 6 8 hours
HA (CDC6AAA)
Flag
Actin
Relative HA-AAA protein level
Flag vector T1/2=2.242 h
Flag-OTUD6A T1/2=3.947 h
Time (h)
e
293
Flag vector
Flag-OTUD6A
HA (CDC6DDD)
Flag
Actin
Flag vector T1/2=2.018 h
Flag-OTUD6A T1/2=6.001 h
Relative HA-DDD protein level
Time (h)
f
293
shNC
shOTUD6A
Chloroquine
CDC6
OTUD6A
Actin
g
293
Flag vector
Flag-OTUD6A
Myc-CDC6
HA-Ub
HA
Myc
Flag
Actin
IP:Myc
IB
h
293
Flag vector
Flag-OTUD6A
Flag-OTUD6AC152A
CDC6
Flag
Actin
IP:Flag
IB
i
293
Flag-OTUD6AC152A
CDC6
Flag
Actin
j
293
CDC6
OTUD6A
Relative expression Target/GAPDH
n.s
Flag-OTUD6AC152A
k
OTUD6A
OTUD6AC152A
293
non-Flag
Flag
Relative CDC6 fluorescence
WT
C152A
l
T24
OTUD6A
OTUD6AC152A
non-Flag
Flag
Relative CDC6 fluorescence
WT
C152A
m
5637
OTUD6A
OTUD6AC152A
non-Flag
Flag
Relative CDC6 fluorescence
WT
C152A
n
293
Flag-vector
Flag-OTUD6AC152A
CDC6
Flag
Actin
Flag-vector T1/2=84.61 min
Flag-OTUD6AC152A T1/2=71.06 min
Time (min)
o
293
Flag vector
Flag-OTUD6A
Flag-OTUD6AC152A
Myc-CDC6
HA-Ub
HA
Myc
Flag
Actin
IP:Myc
IB
p
293
WT
Flag vector
Flag-OTUD6A
Flag-OTUD6A-C-term
CDC6
Flag
Actin
q
293
Flag vector
Flag-OTUD6A-C-term
CDC6
Flag
Actin
Flag vector T1/2=72.42 min
Flag-OTUD6A-C-term T1/2=60.85 min
Time (min)
r
293
Flag vector
Flag-OTUD6A
Myc vector
Myc-Cyclin F
CDC6
Myc
Flag
Actin
s
293
Flag vector
Flag-OTUD6A
Myc vector
Myc-Cyclin F
HA-Ub
HA
CDC6
Myc
Flag
Actin
IP: CDC6
IB
t
293
Flag vector
Flag-OTUD6A
Myc vector
Myc-CDH1
CDC6
Myc
Flag
Actin
u
293
Flag vector
Flag-OTUD6A
Myc vector
Myc-CDH1
HA-Ub
HA
CDC6
Myc
Flag
Actin
IP: CDC6
IB

Supplementary Fig. 3 OTUD6A deubiquitinates CDC6 and promotes CDC6 stability. a, 293 cells with stable OTUD6A knockdown were treated with CHX (20 μg/mL) and harvested at the indicated time points prior to Western blotting (left). The intensities of the CDC6 bands were quantified from three independent repeated Western blotting analysis (right), and the intensity at 0 min was set as 1. **b**, Western blot analysis of lysates from 293 cells transfected with HA-CDC6^{WT}, HA-CDC6^{AAA} and HA-CDC6^{DDD}. **c**, 293 cells transfected with the indicated vectors were harvested and subjected to Western blotting. **d**, **e**, 293 cells were cotransfected with Flag-OTUD6A or Flag vector with HA-CDC6^{AAA} (**d**) or HA-CDC6^{DDD} (**e**) for 24 h. Cells were treated with CHX and harvested at the indicated time points prior to Western blotting (left). The intensities of the CDC6 bands were quantified from three independent repeated Western blotting analysis (right), and the intensity at 0 h was set as 1. **f**, 293 cells transfected with the indicated vectors were treated with chloroquine (20 μM) or DMSO for 6 h. Cell lysates were prepared, and the CDC6 protein level was measured by Western blotting. **g**, 293 cells transfected with the indicated vectors were treated with MG132 for 6 h. Whole-cell lysates were prepared and subjected to IP with an anti-Myc antibody. The immunoprecipitates were analysed by Western blotting. **h**, 293 cells were transfected with the indicated vectors for 24 h. Whole-cell lysates were prepared and subjected to IP with an anti-Flag antibody. The immunoprecipitates were analysed by Western blotting. **i**, **j**, Increasing amounts of Flag-OTUD6A^{C152A} plasmids were transfected into 293 cells, and the protein levels of endogenous CDC6 and exogenous OTUD6A were determined by Western blotting (**i**). The mRNA levels of CDC6 and

OTUD6A were determined by qPCR (**j**), and the levels in Flag vector cells were set as 1. **k-m**, Flag-OTUD6A or Flag-OTUD6A^{C152A} was transfected into 293 (**k**), T24 (**l**) and 5637 (**m**) cells. An additional 24 h later, the cells were fixed and stained as indicated. Representative immunofluorescence images are shown (left). Scale bars, 20 μm. Quantification of the relative fluorescence intensity of CDC6 is shown (right), and the fluorescence intensity of CDC6 in Flag-OTUD6A untransfected cells was set as 1. **n**, 293 cells transfected with the indicated vector were treated with CHX and harvested at the indicated time points prior to Western blotting (left). The intensities of the CDC6 bands were quantified from three independent repeated Western blotting analysis (right), and the intensity at 0 min was set as 1. **o**, 293 cells transfected with the indicated vectors were treated with MG132 for 6 h. Whole-cell lysates were prepared and subjected to IP with an anti-Myc antibody. The immunoprecipitates were analysed by Western blotting. **p**, 293 cells transfected with the indicated plasmids were harvested and subjected to Western blotting. **q**, 293 cells were transfected with indicated vectors for 24 h. Cells were treated with CHX and harvested at the indicated time points prior to Western blotting (left). The intensities of the CDC6 bands were quantified from three independent repeated Western blotting analysis (right), and the intensity at 0 h was set as 1. **r**, 293 cells were cotransfected with Flag-OTUD6A or Flag vector along with Myc-Cyclin F or Myc vector for 24 h, and the indicated protein levels were determined by Western blotting. **s**, 293 cells transfected with the indicated vectors were treated with MG132 for 6 h. Whole-cell lysates were prepared and subjected to IP with an anti-CDC6 antibody. The immunoprecipitates were analysed by Western blotting. **t**, 293

cells were cotransfected with Flag-OTUD6A or Flag vector along with Myc-CDH1 or Myc vector for 24 h, and the indicated protein levels were determined by Western blotting. **u**, 293 cells transfected with the indicated vectors were treated with MG132 for 6 h. Whole-cell lysates were prepared and subjected to IP with an anti-CDC6 antibody. The immunoprecipitates were analysed by Western blotting. All quantitative analyses were based on three independent experiments. The error bars indicate the SDs. $^{**}P < 0.01$, $^{***}P < 0.001$, n.s. not significant, based on two-tailed Student's *t* test.

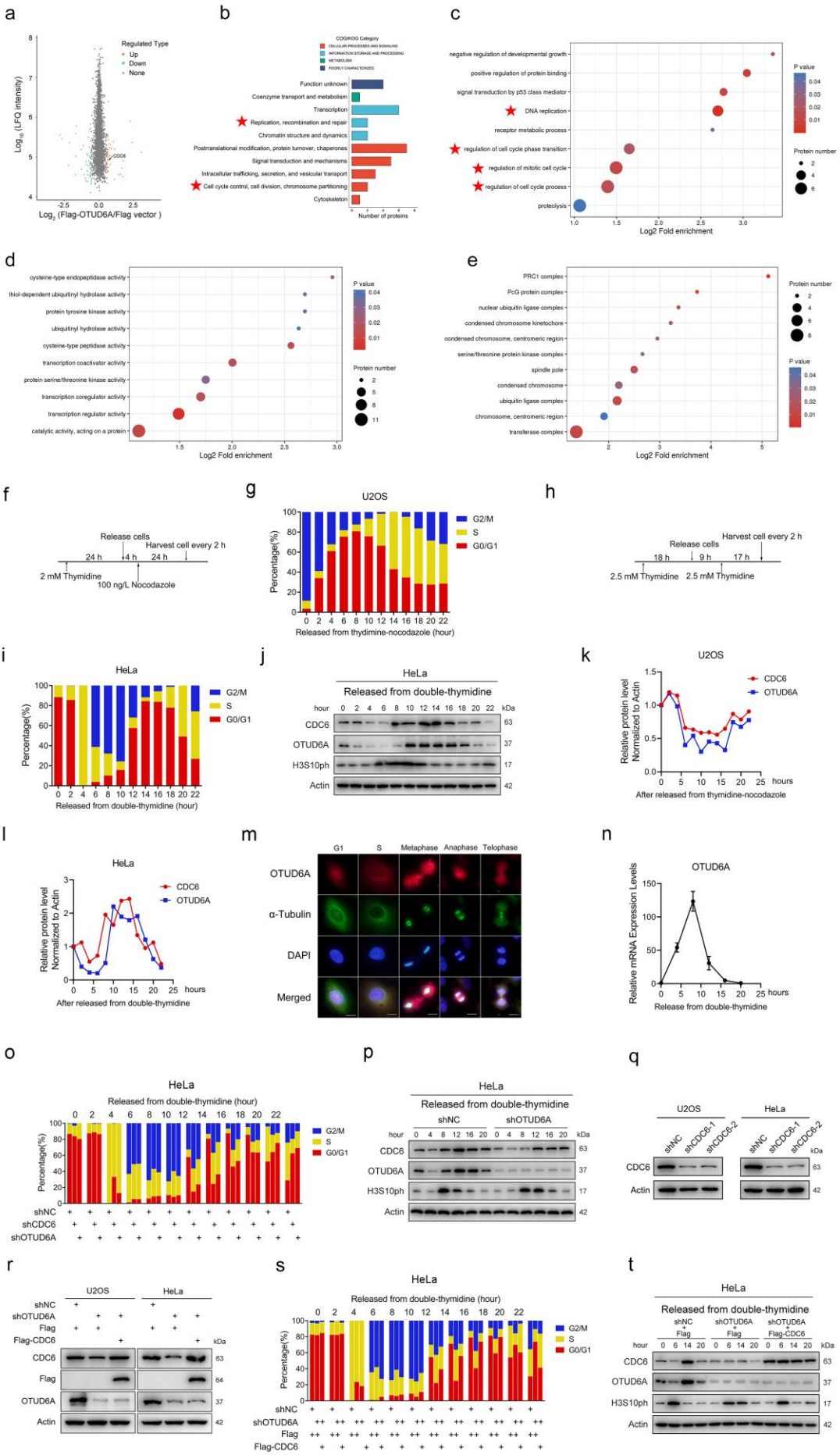
a
Regulated Type
Up
Down
None
CDC6
Log10 (LFQ intensity)
Log2 (Flag-OTUD6A/Flag vector)
b
COG/KOG Category
CELLULAR PROCESSES AND SIGNALING
INFORMATION STORAGE AND PROCESSING
METABOLISM
POORLY CHARACTERIZED
Function unknown
Coenzyme transport and metabolism
Transcription
Replication, recombination and repair
Chromatin structure and dynamics
Posttranslational modification, protein turnover, chaperones
Signal transduction and mechanisms
Intracellular trafficking, secretion, and vesicular transport
Cell cycle control, cell division, chromosome partitioning
Cytoskeleton
Number of proteins
c
negative regulation of developmental growth
positive regulation of protein binding
signal transduction by p53 class mediator
DNA replication
receptor metabolic process
regulation of cell cycle phase transition
regulation of mitotic cell cycle
regulation of cell cycle process
proteolysis
P value
Protein number
Log2 Fold enrichment
d
cysteine-type endopeptidase activity
thiol-dependent ubiquitinyl hydrolase activity
protein tyrosine kinase activity
ubiquitinyl hydrolase activity
cysteine-type peptidase activity
transcription coactivator activity
protein serine/threonine kinase activity
transcription coregulator activity
transcription regulator activity
catalytic activity, acting on a protein
P value
Protein number
Log2 Fold enrichment
e
PRC1 complex
PcG protein complex
nuclear ubiquitin ligase complex
condensed chromosome kinetochore
condensed chromosome, centromeric region
serine/threonine protein kinase complex
spindle pole
condensed chromosome
ubiquitin ligase complex
chromosome, centromeric region
transferase complex
Protein number
P value
Log2 Fold enrichment
f
Release cells
Harvest cell every 2 h
24 h
4 h
24 h
2 mM Thymidine
100 ng/L Nocodazole
g
U2OS
G2/M
S
G0/G1
Percentage(%)
Released from thydimine-nocodazole (hour)
h
Release cells
Harvest cell every 2 h
18 h
9 h
17 h
2.5 mM Thymidine
2.5 mM Thymidine
i
HeLa
G2/M
S
G0/G1
Percentage(%)
Released from double-thymidine (hour)
j
HeLa
Released from double-thymidine
hour
kDa
CDC6
OTUD6A
H3S10ph
Actin
k
U2OS
CDC6
OTUD6A
Relative protein level Normalized to Actin
hours
After released from thymidine-nocodazole
l
HeLa
CDC6
OTUD6A
Relative protein level Normalized to Actin
hours
After released from double-thymidine
m
G1
S
Metaphase
Anaphase
Telophase
OTUD6A
α-Tubulin
DAPI
Merged
n
OTUD6A
Relative mRNA Expression Levels
hours
Release from double-thymidine
o
HeLa
Released from double-thymidine (hour)
G2/M
S
G0/G1
Percentage(%)
shNC
shCDC6
shOTUD6A
p
HeLa
Released from double-thymidine
shNC
shOTUD6A
hour
kDa
CDC6
OTUD6A
H3S10ph
Actin
q
U2OS
HeLa
siNC
shCDC6-1
shCDC6-2
shNC
shCDC6-1
shCDC6-2
kDa
CDC6
Actin
r
U2OS
HeLa
shNC
shOTUD6A
Flag
Flag-CDC6
kDa
CDC6
Flag
OTUD6A
Actin
s
HeLa
Released from double-thymidine (hour)
G2/M
S
G0/G1
Percentage(%)
shNC
shOTUD6A
Flag
Flag-CDC6
t
HeLa
Released from double-thymidine
shNC + Flag
shOTUD6A + Flag
shOTUD6A + Flag-CDC6
hour
kDa
CDC6
OTUD6A
H3S10ph
Actin

Supplementary Fig. 4 OTUD6A fluctuates during the cell cycle and regulates cell cycle progression. **a**, Volcano plot showing the differentially expressed proteins between Flag-OTUD6A and Flag vector groups (fold change > 1.5) based on 4D label-free quantitative proteomics analysis. Significantly downregulated proteins are represented as 'green' dots, and significantly upregulated proteins are represented as 'orange' dots. **b**, EuKaryotic Orthologous Groups (KOG) analysis of the 41 differentially upregulated proteins in Flag-OTUD6A group from 4D label-free quantitative proteomic analysis. **c-e**, Gene Ontology (GO) analysis of the 41 differentially upregulated proteins in Flag-OTUD6A group from 4D label-free quantitative proteomic analysis in the biological process (**c**), molecular function (**d**) and cellular component (**e**) categories. **f**, A diagram of the procedure for cell cycle synchronization with thymidine and nocodazole is shown. **g**, U2OS cells were synchronized in prometaphase and released into fresh medium. Cells were analysed at the indicated time points by flow cytometry. **h**, A diagram of the process for cell cycle synchronization with a double-thymidine block is shown. **i**, **j**, HeLa cells were synchronized in G1/S phase with a double thymidine block and released into fresh medium. The cells were analysed at the indicated time points by flow cytometry (**i**) and Western blotting (**j**). **k, l**, The intensities of the OTUD6A and CDC6 bands in U2OS (**k**) and HeLa (**l**) cells were quantified, and the intensities at 0 h were set as 1. **m**, Representative images of immunofluorescence HeLa cells stained with an anti-OTUD6A antibody (red), α-tubulin antibody (green), and DAPI (blue) are shown. Scale bars, 10 μm. **n**, HeLa cells were synchronized in G1/S phase with a double-thymidine

block and released into fresh medium. The cells were analysed at the indicated time points by qPCR. The levels at 0 h were set as 1. **o, p**, The indicated HeLa cells were synchronized in G1/S phase with a double-thymidine block and released into fresh medium. The cells were analysed at the indicated time points by flow cytometry (**o**) and Western blotting (**p**). **q**, The protein expression levels of CDC6 in the indicated cells were determined by Western blotting. **r**, The protein expression levels of OTUD6A and CDC6 in the indicated U2OS and HeLa cells were determined by Western blotting. **s**, **t**, The indicated HeLa cells were synchronized in G1/S phase with a double-thymidine block and released into fresh medium. The cells were analysed at the indicated time points by flow cytometry (**s**) and Western blotting (**t**). All quantitative analyses were based on three independent experiments. The error bars indicate the SDs.

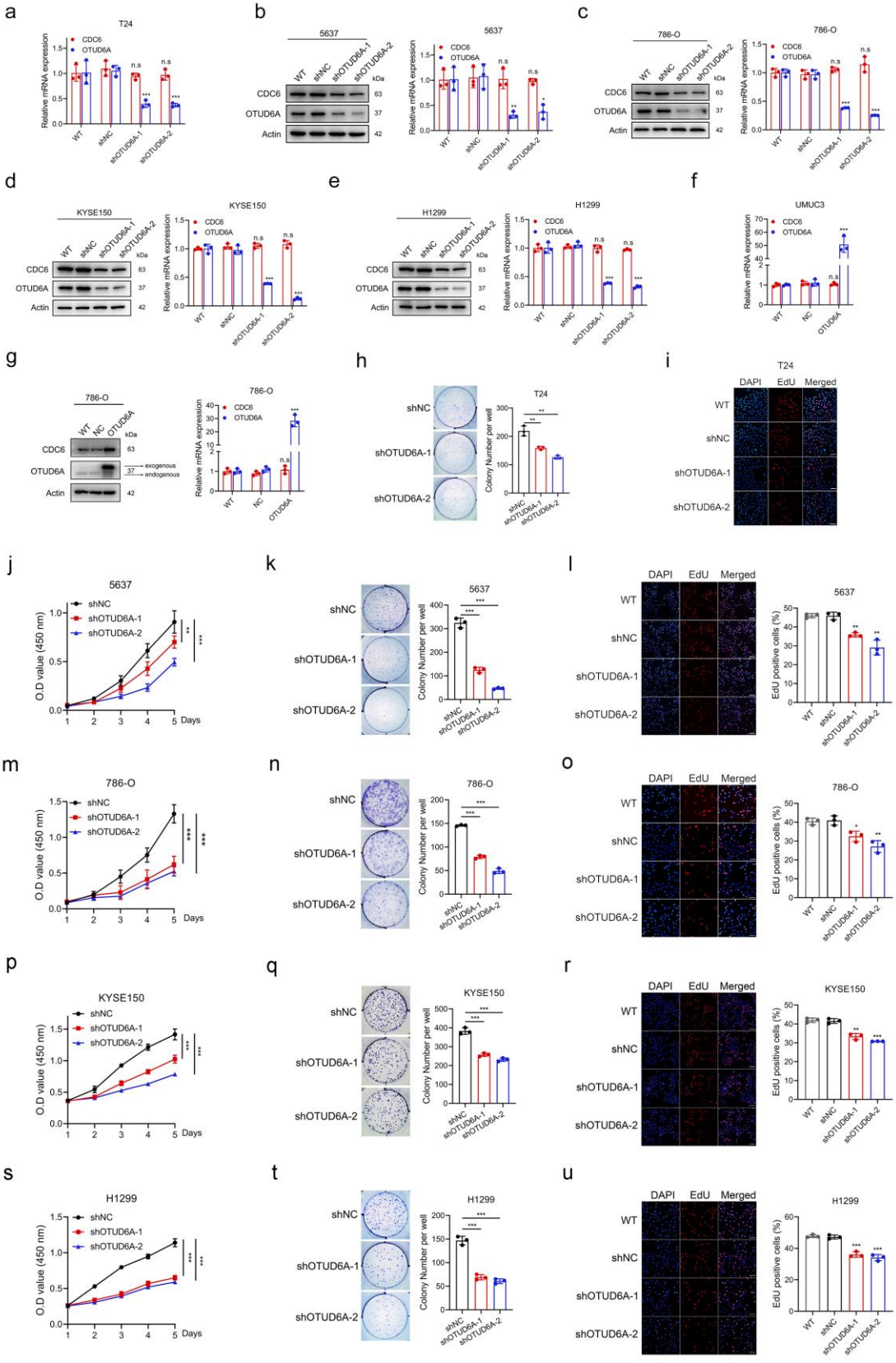

Supplementary Fig. 5 OTUD6A increases the cancer cell proliferation. a, CDC6 and OTUD6A expression levels were measured in T24 cells by qPCR; the levels in WT

cells were set as 1. **b-e**, CDC6 and OTUD6A expression levels were measured in 5637 (**b**), 786-O (**c**), KYSE150 (**d**) and H1299 (**e**) cells by Western blotting (left) and qPCR (right); the levels in WT cells were set as 1. **f**, CDC6 and OTUD6A expression levels were measured in UMUC3 cells by qPCR; the levels in WT cells were set as 1. **g**, CDC6 and OTUD6A expression levels were measured in 786-O cells by Western blotting (left) and qPCR (right); the levels in WT cells were set as 1. **h, i**, The effect of OTUD6A knockdown on T24 cell proliferation was examined by colony formation assays (**h**) and EdU incorporation assays (**i**). Scale bars, 50 μm. **j-l**, The effect of OTUD6A knockdown on 5637 cell proliferation was examined by CCK8 assays (**j**), colony formation assays (**k**) and EdU incorporation assays (**l**). Scale bars, 50 μm. **m-o**, The effect of OTUD6A knockdown on 786-O cell proliferation was examined by CCK8 assays (**m**), colony formation assays (**n**) and EdU incorporation assays (**o**). Scale bars, 50 μm. **p-r**, The effect of OTUD6A knockdown on KYSE150 cell proliferation was examined by CCK8 assays (**p**), colony formation assays (**q**) and EdU incorporation assays (**r**). Scale bars, 50 μm. **s-u**, The effect of OTUD6A knockdown on H1299 cell proliferation was examined by CCK8 assays (**s**), colony formation assays (**t**) and EdU incorporation assays (**u**). Scale bars, 50 μm. All quantitative analyses were based on three independent experiments. The error bars indicate the SDs. *$P < 0.05$, **$P < 0.01$, ***$P < 0.001$, n.s. not significant, based on two-tailed Student's *t* test.

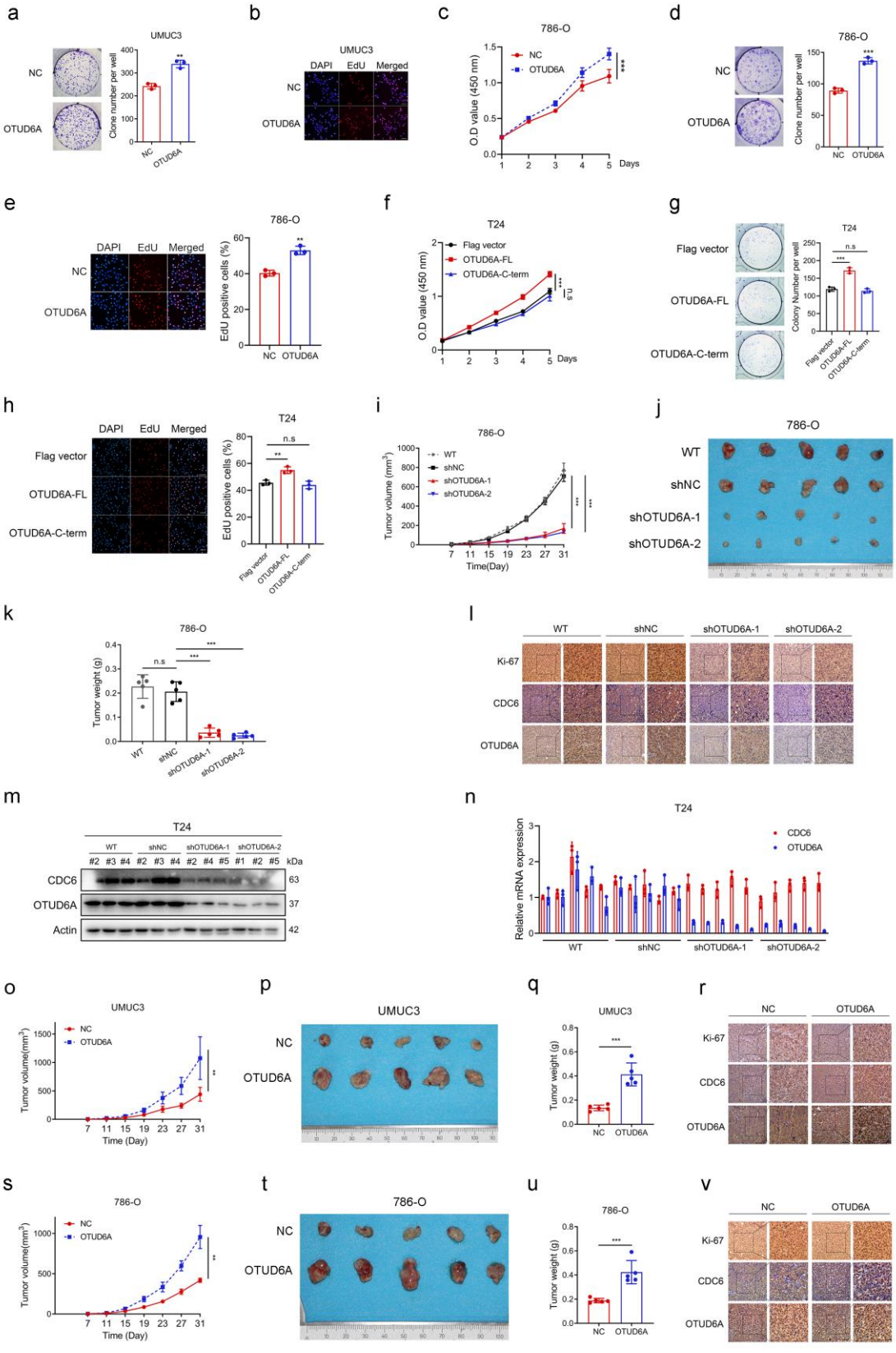

Supplementary Fig. 6 OTUD6A promotes tumour growth. a, b, The effect of OTUD6A overexpression on UMUC3 cell proliferation was examined by colony

formation assays (**a**) and EdU incorporation assays (**b**). Scale bars, 50 μm. **c-e**, The effect of OTUD6A overexpression on 786-O cell proliferation was examined by CCK8 assays (**c**), colony formation assays (**d**) and EdU incorporation assays (**e**). Scale bars, 50 μm. **f-h**, The effect of the C terminus of OTUD6A on T24 cell proliferation was examined by CCK8 assays (**f**), colony formation assays (**g**) and EdU incorporation assays (**h**). Scale bars, 50 μm. **i**, Growth curves of the indicated subcutaneous 786-O tumours are shown. Tumours were measured every 4 days. **j**, An image of subcutaneous tumours formed by the indicated 786-O cells is shown. **k**, The indicated subcutaneous 786-O tumours were weighed. **l**, Representative IHC images indicating Ki-67, CDC6 and OTUD6A expression in the indicated 786-O tumours are shown. Scale bars, 50 μm (left) and 20 μm (right). **m**, **n**, CDC6 and OTUD6A expression levels were measured in the indicated subcutaneous T24 tumours by Western blotting (**m**) and qPCR (**n**). The weight of the first WT tumour was set as 1. **o**, Growth curves of the indicated subcutaneous UMUC3 tumours are shown. Tumours were measured every 4 days. **p**, An image of subcutaneous tumours formed by the indicated UMUC3 cells is shown. **q**, The indicated subcutaneous UMUC3 tumours were weighed. **r**, Representative IHC images indicating Ki-67, CDC6 and OTUD6A expression in the indicated UMUC3 tumours are shown. Scale bars, 50 μm (left) and 20 μm (right). **s**, Growth curves of the indicated subcutaneous 786-O tumours are shown. Tumours were measured every 4 days. **t**, An image of subcutaneous tumours formed by the indicated 786-O cells is shown (right). **u**, The indicated subcutaneous 786-O tumours were weighed. **v**, Representative IHC images indicating Ki-67, CDC6 and OTUD6A expression in the

397 indicated 786-O tumours are shown. Scale bars, 50 μm (left) and 20 μm (right). All
398 quantitative analyses were based on three independent experiments. The error bars
399 indicate the SDs. $^{**}P < 0.01$, $^{***}P < 0.001$, n.s. not significant, based on two-tailed
400 Student's *t* test.

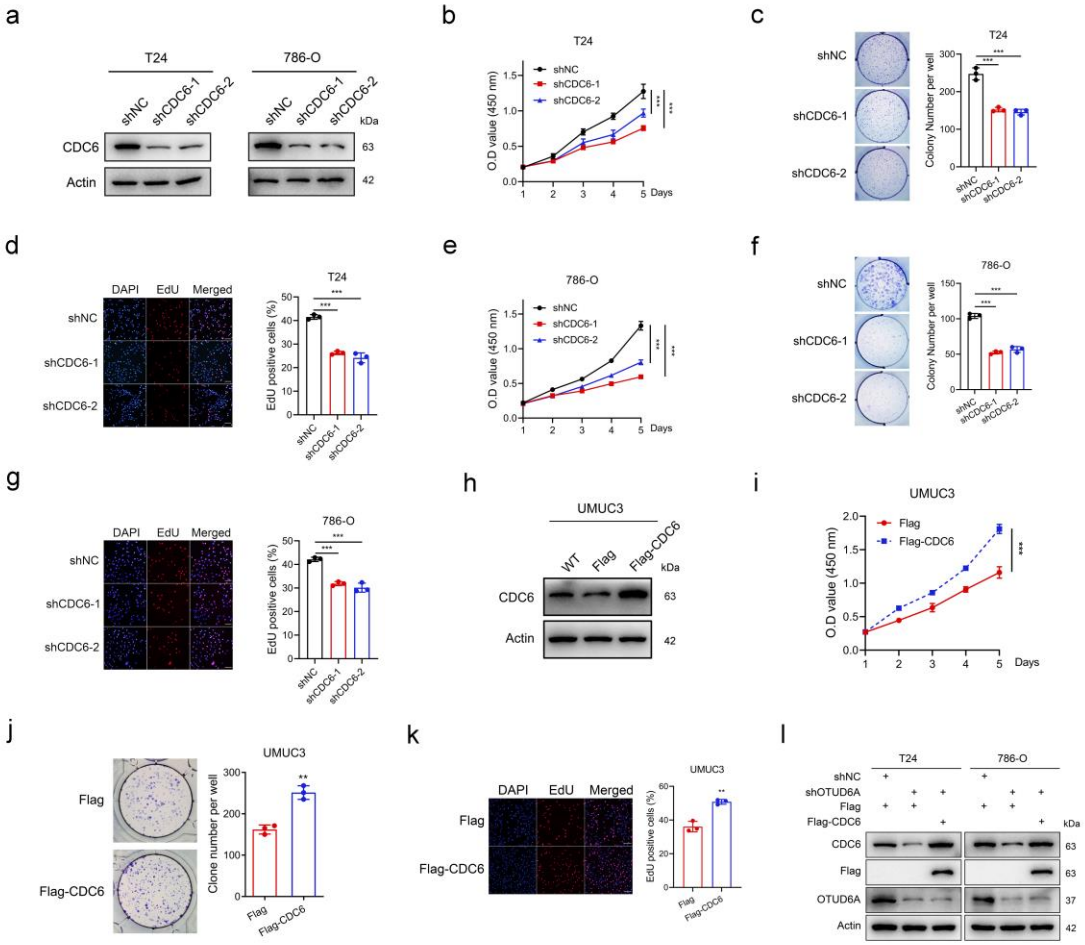

401

402 **Supplementary Fig. 7 CDC6 increases the cancer cell proliferation. a,** The protein
403 expression level of CDC6 in the indicated cells was determined by Western blotting. **b-**
404 **d**, The effect of CDC6 knockdown on T24 cell proliferation was examined by CCK8
405 assays (**b**), colony formation assays (**c**) and EdU incorporation assays (**d**). Scale bars,
406 50 μm. **e-g**, The effect of CDC6 knockdown on 786-O cell proliferation was examined
407 by CCK8 assays (**e**), colony formation assays (**f**) and EdU incorporation assays (**g**).
408 Scale bars, 50 μm. **h**, CDC6 expression levels in UMUC3 cell were measured by
409 Western blotting. **i-k**, The effect of CDC6 overexpression on UMUC3 cell proliferation
410 was examined by CCK8 assays (**i**), colony formation assays (**j**) and EdU incorporation
411 assays (**k**). Scale bars, 50 μm. **l**, The protein expression levels of OTUD6A and CDC6

412 in the indicated T24 and 786-O cells were determined by Western blotting. All
413 quantitative analyses were based on three independent experiments. The error bars
414 indicate the SDs. $^{**}P < 0.01$, $^{***}P < 0.001$, based on two-tailed Student's *t* test.

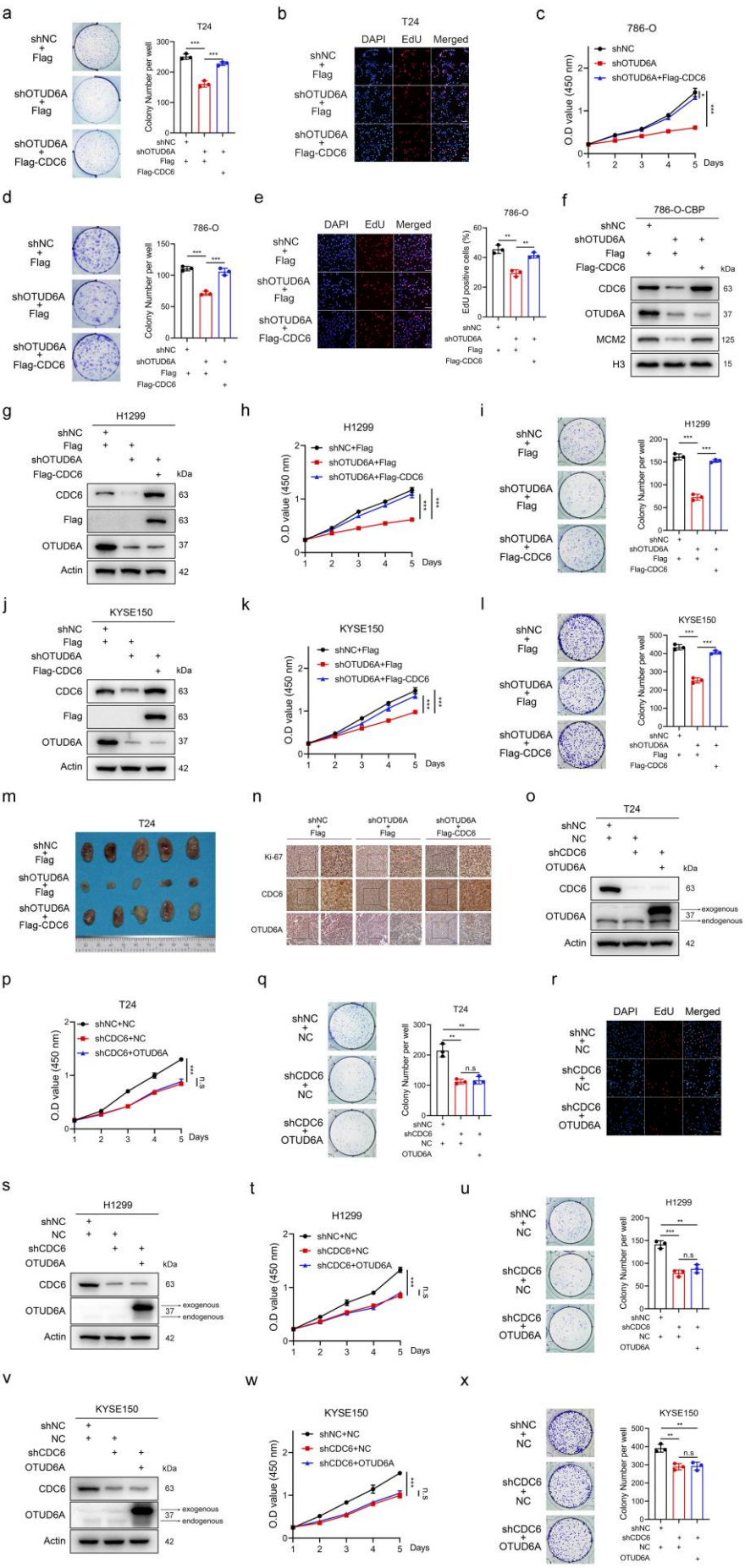
a
shNC + Flag
shOTUD6A + Flag
shOTUD6A + Flag-CDC6
T24
Colony Number per well
b
DAPI
EdU
Merged
T24
c
786-O
shNC
shOTUD6A
shOTUD6A+Flag-CDC6
O.D value (450 nm)
Days
d
786-O
e
786-O
EdU positive cells (%)
f
786-O-CBP
CDC6
OTUD6A
MCM2
H3
kDa
g
H1299
Flag-CDC6
Actin
h
H1299
shNC+Flag
shOTUD6A+Flag
shOTUD6A+Flag-CDC6
i
H1299
j
KYSE150
k
KYSE150
l
KYSE150
m
T24
n
Ki-67
CDC6
OTUD6A
o
T24
shCDC6
exogenous
endogenous
p
T24
shNC+NC
shCDC6+NC
shCDC6+OTUD6A
n.s
q
T24
r
DAPI
EdU
Merged
s
H1299
t
H1299
u
H1299
v
KYSE150
w
KYSE150
x
KYSE150

Supplementary Fig. 8 The OTUD6A-CDC6 axis promotes tumour growth. a, b, Colony formation assays (**a**) and EdU incorporation assays (**b**) were used to examine proliferation in the indicated T24 cells. Scale bars, 50 μm. **c-e**, CCK8 assays (**c**), colony formation assays (**d**) and EdU incorporation assays (**e**) were used to examine proliferation in the indicated 786-O cells. Scale bars, 50 μm. **f**, Chromatin-bound proteins (CBP) were extracted from the indicated 786-O cells and analysed by Western blotting. **g**, The protein levels of OTUD6A and CDC6 in the indicated H1299 cells were determined by Western blotting. **h, i**, CCK8 assays (**h**) and colony formation assays (**i**) were used to examine the proliferation of the indicated H1299 cells. **j**, The protein levels of OTUD6A and CDC6 in the indicated KYSE150 cells were determined by Western blotting. **k, l**, CCK8 assays (**k**) and colony formation assays (**l**) were used to examine the proliferation of the indicated KYSE150 cells. **m**, Images of subcutaneous tumours formed by the indicated T24 cells are shown. **n**, Representative IHC images indicating Ki-67, CDC6 and OTUD6A expression in the indicated T24 tumours are shown. Scale bars, 50 μm (left) and 20 μm (right). **o**, The protein levels of OTUD6A and CDC6 in the indicated T24 cells were determined by Western blotting. **p-r**, CCK8 assays (**p**), colony formation assays (**q**) and EdU incorporation assays (**r**) were used to examine the proliferation of the indicated T24 cells. Scale bars, 50 μm. **s**, The protein levels of OTUD6A and CDC6 in the indicated H1299 cells were determined by Western blotting. **t, u**, CCK8 assays (**t**) and colony formation assays (**u**) were used to examine the proliferation of the indicated H1299 cells. **v**, The protein levels of OTUD6A and CDC6 in the indicated KYSE150 cells were determined by Western blotting. **w, x**, CCK8

assays (**w**) and colony formation assays (**x**) were used to examine the proliferation of the indicated KYSE150 cells. All quantitative analyses were based on three independent experiments. The error bars indicate the SDs. *$P < 0.05$, **$P < 0.01$, ***$P < 0.001$, n.s. not significant, based on two-tailed Student's *t* test.

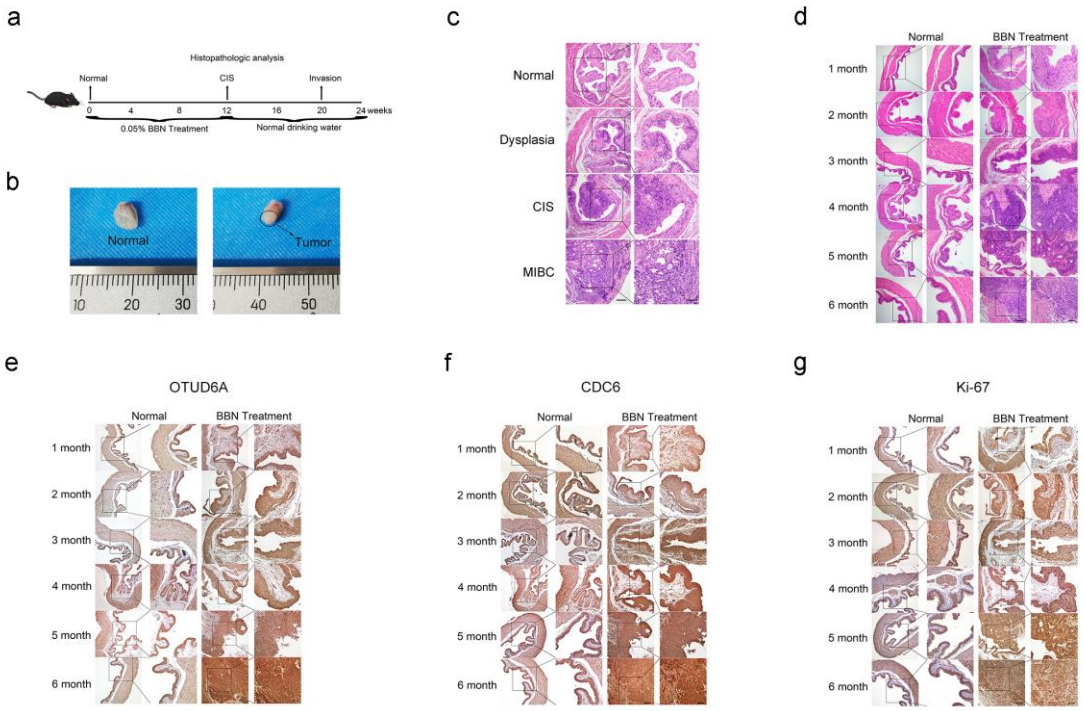

Supplementary Fig. 9 Histopathology of BBN-induced BCa. a, Diagram of the BBN treatment strategy. **b**, Representative images of normal mouse bladders and mouse bladders after 20 weeks of BBN treatment are shown. **c**, Representative images of normal bladder, dysplasia, carcinoma *in situ* (CIS), muscle invasive bladder cancers are indicated. **d-g**, Histological and protein expression changes were observed at different time points during BBN treatment. Representative images of H&E staining (**d**) and IHC staining of OTUD6A (**e**), CDC6 (**f**) and Ki-67 (**g**) are shown. Scale bars, 100 μm (left) and 50 μm (right).

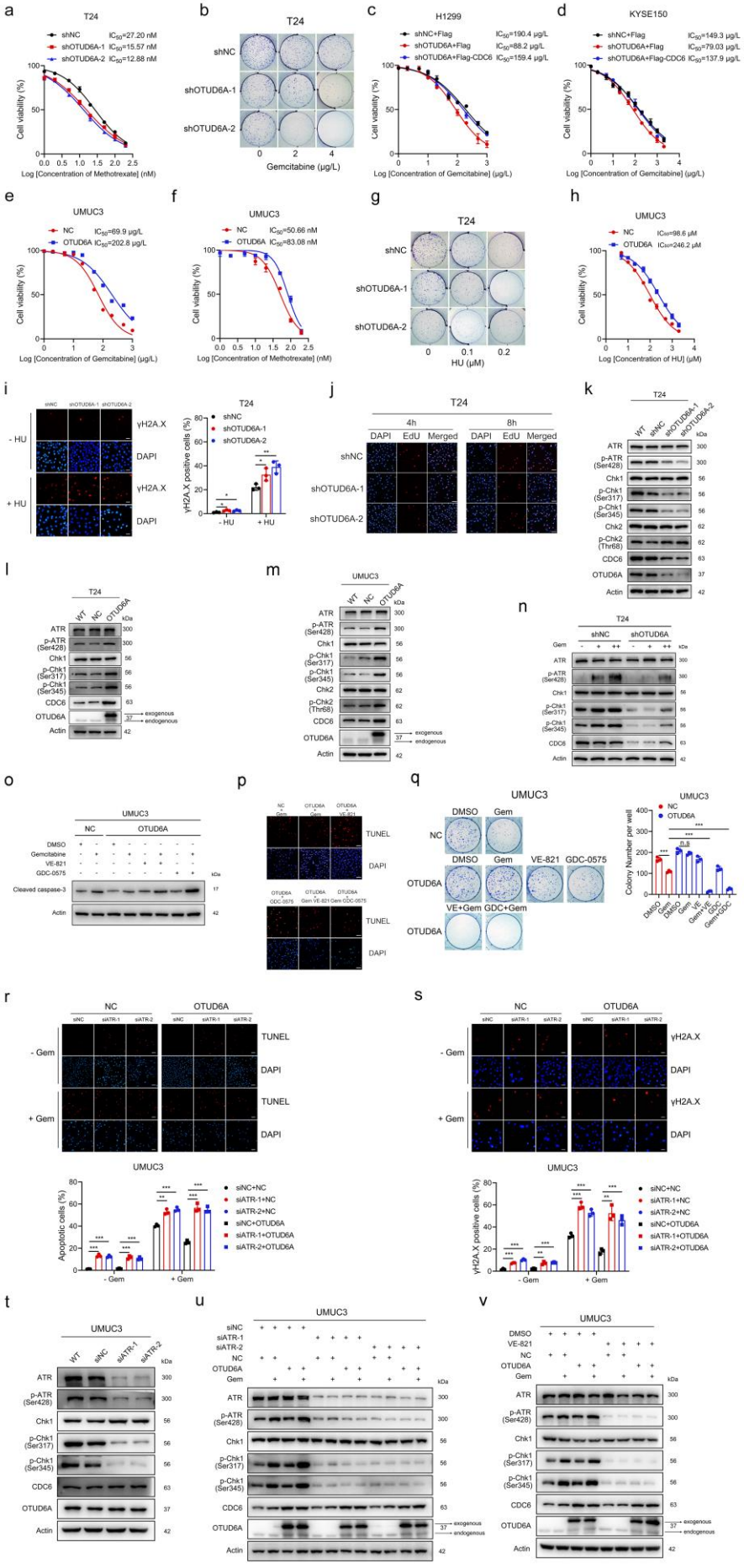
a
T24
shNC IC50=27.20 nM
shOTUD6A-1 IC50=15.57 nM
shOTUD6A-2 IC50=12.88 nM
Cell viability (%)
Log [Concentration of Methotrexate] (nM)
b
T24
shNC
shOTUD6A-1
shOTUD6A-2
Gemcitabine (μg/L)
c
H1299
shNC+Flag IC50=190.4 μg/L
shOTUD6A+Flag IC50=88.2 μg/L
shOTUD6A+Flag-CDC6 IC50=159.4 μg/L
Log [Concentration of Gemcitabine] (μg/L)
d
KYSE150
shNC+Flag IC50=149.3 μg/L
shOTUD6A+Flag IC50=79.03 μg/L
shOTUD6A+Flag-CDC6 IC50=137.9 μg/L
Log [Concentration of Gemcitabine] (μg/L)
e
UMUC3
NC IC50=69.9 μg/L
OTUD6A IC50=202.8 μg/L
Log [Concentration of Gemcitabine] (μg/L)
f
UMUC3
NC IC50=50.66 nM
OTUD6A IC50=83.08 nM
Log [Concentration of Methotrexate] (nM)
g
T24
shNC
shOTUD6A-1
shOTUD6A-2
HU (μM)
h
UMUC3
NC IC50=98.6 μM
OTUD6A IC50=246.2 μM
Log [Concentration of HU] (μM)
i
- HU
+ HU
γH2A.X
DAPI
γH2A.X positive cells (%)
T24
shNC
shOTUD6A-1
shOTUD6A-2
j
T24
4h
8h
DAPI
EdU
Merged
shNC
shOTUD6A-1
shOTUD6A-2
k
T24
WT
shNC
shOTUD6A-1
shOTUD6A-2
ATR
p-ATR (Ser428)
Chk1
p-Chk1 (Ser317)
p-Chk1 (Ser345)
Chk2
p-Chk2 (Thr68)
CDC6
OTUD6A
Actin
kDa
l
T24
WT
NC
OTUD6A
exogenous
endogenous
m
UMUC3
WT
NC
OTUD6A
n
T24
shNC
shOTUD6A
Gem
o
UMUC3
NC
OTUD6A
DMSO
Gemcitabine
VE-821
GDC-0575
Cleaved caspase-3
Actin
p
TUNEL
DAPI
q
UMUC3
DMSO
Gem
VE-821
GDC-0575
VE+Gem
GDC+Gem
NC
OTUD6A
Colony Number per well
r
NC
OTUD6A
siNC
siATR-1
siATR-2
- Gem
+ Gem
TUNEL
DAPI
UMUC3
Apoptotic cells (%)
siNC+NC
siATR-1+NC
siATR-2+NC
siNC+OTUD6A
siATR-1+OTUD6A
siATR-2+OTUD6A
s
γH2A.X
DAPI
UMUC3
γH2A.X positive cells (%)
t
UMUC3
WT
siNC
siATR-1
siATR-2
u
UMUC3
siNC
siATR-1
siATR-2
NC
OTUD6A
Gem
v
UMUC3
DMSO
VE-821
NC
OTUD6A
Gem

Supplementary Fig. 10 OTUD6A regulates chemosensitivity via the ATR-Chk1 pathway. a, The cell viability of the indicated T24 cells was determined after 48 h of continuous exposure to multiple concentrations of methotrexate. The IC_{50} value was defined as the concentration causing a 50% decrease in cell viability. The IC_{50} values were estimated by nonlinear regression using a variable Hill slope model. **b**, Representative images of colony formation assays of the indicated T24 cells treated with different concentrations of gemcitabine are shown. **c, d**, The cell viability of the indicated H1299 (**c**) and KYSE150 (**d**) cells was determined after 48 h of continuous exposure to multiple concentrations of gemcitabine. **e**, **f**, The cell viability of the indicated UMUC3 cells was determined after 48 h of continuous exposure to multiple concentrations of gemcitabine (**e**) and methotrexate (**f**). **g**, Representative images of colony formation assays of the indicated T24 cells treated with different concentrations of hydroxyurea (HU) are shown. **h**, The cell viability of the indicated UMUC3 cells was determined after 48 h of continuous exposure to multiple concentrations of HU. **i**, The γH2A.X protein level was measured by immunofluorescence staining in the indicated T24 cells treated with or without 200 μM HU for 48 h. Scale bars, 20 μm. **j**, Representative images of EdU staining are shown. Scale bars, 50 μm. **k**, The effect of OTUD6A knockdown on the ATR-Chk1 signalling pathway in T24 cells was determined by Western blotting. **l, m**, The effect of OTUD6A overexpression on the ATR-Chk1 signalling pathway in T24 (**l**) and UMUC3 (**m**) cells was determined by Western blotting. **n**, ATR-Chk1 pathway protein levels in OTUD6A-knockdown T24 cells treated with multiple concentrations of gemcitabine for 6 h were determined by

Western blotting. **o**, The effect of ATR and Chk1 inhibitors on regulating the sensitivity of OTUD6A-overexpressing UMUC3 cells to gemcitabine was determined by Western blotting. **p**, Representative images of TUNEL assays of the indicated UMUC3 cells treated with or without gemcitabine, ATR inhibitors and Chk1 inhibitors are shown. Scale bars, 50 μm. **q**, The effects of ATR and Chk1 inhibitors (VE-821 and GDC-0575) on regulating the sensitivity of OTUD6A-overexpressing UMUC3 cells to gemcitabine was determined by colony formation assays. **r**, Apoptosis was measured by TUNEL assays in the indicated UMUC3 cells treated with 100 μg/L gemcitabine for 48 h. Representative images are shown (top). Scale bars, 50 μm. **s**, The γH2A.X protein level was measured by immunofluorescence staining in the indicated UMUC3 cells treated with or without 100 μg/L gemcitabine for 48 h. Representative immunofluorescence images are shown (top). Scale bars, 20 μm. **t**, The effect of ATR knockown on the ATR-Chk1 signalling pathway in UMUC3 cells was determined by Western blotting. **u**, ATR-Chk1 pathway protein levels in the indicated UMUC3 cells treated with 200 μg/L gemcitabine for 6 h were determined by Western blotting. **v**, The effect of ATR inhibitor on regulating the sensitivity of OTUD6A-overexpressing UMUC3 cells to gemcitabine was determined by Western blotting. All quantitative analyses were based on three independent experiments. The error bars indicate the SDs. $*P < 0.05$, $**P < 0.01$, $***P < 0.001$, n.s. not significant, based on two-tailed Student's *t* test.

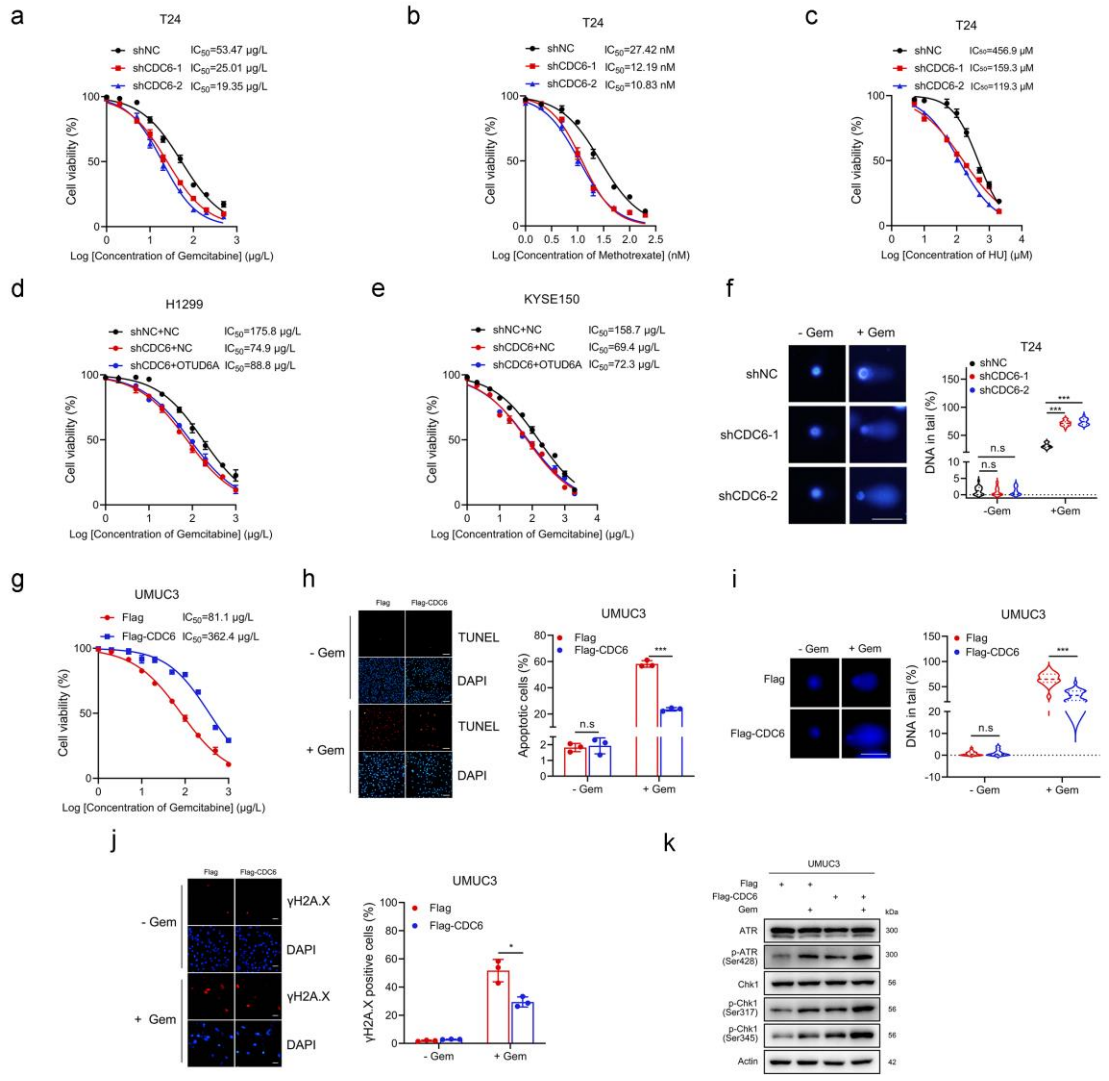

Supplementary Fig. 11 CDC6 decreases sensitivity to chemotherapy via the ATR-Chk1 pathway. a-c, The cell viability of the indicated T24 cells was determined after 48 h of continuous exposure to multiple concentrations of gemcitabine (**a**), methotrexate (**b**) and HU (**c**). **d, e**, The cell viability of the indicated H1299 (**d**) and KYSE150 (**e**) cells was determined after 48 h of continuous exposure to multiple concentrations of gemcitabine. **f**, The amount of DNA strand breaks was quantified by alkaline comet assays in the indicated T24 cells treated with or without 20 μg/L gemcitabine for 48 h. Scale bars, 20 μm. **g**, The cell viability of the indicated UMUC3 cells was determined after 48 h of continuous exposure to multiple concentrations of

gemcitabine. **h**, Apoptosis was measured by TUNEL assays in the indicated UMUC3 cells treated with or without 100 μg/L gemcitabine for 48 h. Representative images are shown (left). Scale bars, 50 μm. **i**, The amount of DNA strand breaks was quantified by alkaline comet assays in the indicated UMUC3 cells treated with or without 100 μg/L gemcitabine for 48 h. Representative images are shown (left). Scale bars, 20 μm. **j**, The γH2A.X protein level was measured by immunofluorescence staining in the indicated UMUC3 cells treated with or without 100 μg/L gemcitabine for 48 h. Representative immunofluorescence images are shown (left). Scale bars, 20 μm. **k**, ATR-Chk1 pathway protein levels in the indicated UMUC3 cells treated with 200 μg/L gemcitabine for 6 h were determined by Western blotting. All quantitative analyses were based on three independent experiments. The error bars indicate the SDs. $*P < 0.05$, $***P < 0.001$, n.s. not significant, based on two-tailed Student's *t* test.

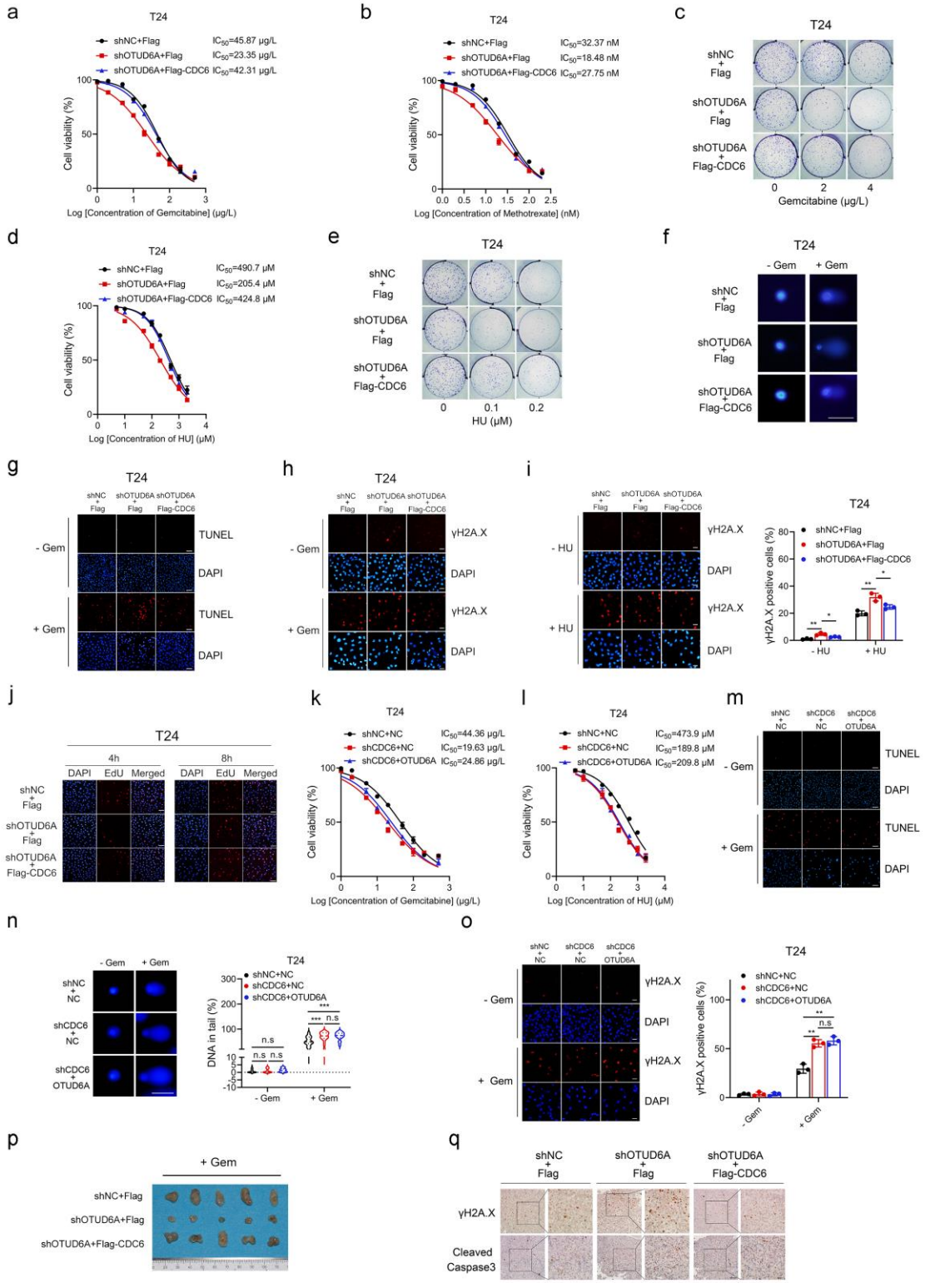

Supplementary Fig. 12 OTUD6A decreases sensitivity to chemotherapy via the CDC6-ATR-Chk1 pathway. a, **b**, The cell viability of the indicated T24 cells was determined after 48 h of continuous exposure to multiple concentrations of gemcitabine

(**a**) and methotrexate (**b**). **c**, Representative images of colony formation assays of the indicated T24 cells treated with different concentrations of gemcitabine are shown. **d**, The cell viability of the indicated T24 cells was determined after 48 h of continuous exposure to multiple concentrations of HU. **e,** Representative images of colony formation assays of the indicated T24 cells treated with different concentrations of HU are shown. **f-h**, Representative images of alkaline comet assays (**f**), TUNEL assays (**g**) and immunofluorescence staining of γH2A.X (**h**) of the indicated T24 cells treated with or without gemcitabine are shown. Scale bars, 50 μm (**g**), 20 μm (**f, h**). **i**, The γH2A.X protein level was measured by immunofluorescence staining in the indicated T24 cells treated with or without 200 μM HU for 48 h. Representative immunofluorescence images are shown (left). Scale bars, 20 μm. **j**, Representative images of EdU staining are shown. Scale bars, 50 μm. **k, l**, The cell viability of the indicated T24 cells was determined after 48 h of continuous exposure to multiple concentrations of gemcitabine (**k**) and HU (**l**). **m**, Representative images of TUNEL assays of the indicated T24 cells treated with or without gemcitabine are shown. Scale bars, 50 μm. **n**, The amount of DNA strand breaks was quantified by alkaline comet assays in the indicated T24 cells treated with or without 20 μg/L gemcitabine for 48 h. Representative images are shown (left). Scale bars, 20 μm. **o**, The γH2A.X protein level was measured by immunofluorescence staining in the indicated T24 cells treated with or without 20 μg/L gemcitabine for 48 h. Representative immunofluorescence images are shown (left). Scale bars, 20 μm. **p**, Images of subcutaneous tumours formed by the indicated T24 cells treated with gemcitabine are shown. **q**, Representative IHC images showing

γH2A.X and cleaved caspase-3 proteins in the indicated subcutaneous T24 tumours are shown. Scale bars, 50 μm (left) and 20 μm (right). All quantitative analyses were based on three independent experiments. The error bars indicate the SDs. *$P < 0.05$, **$P < 0.01$, ***$P < 0.001$, n.s. not significant, based on two-tailed Student's *t* test.

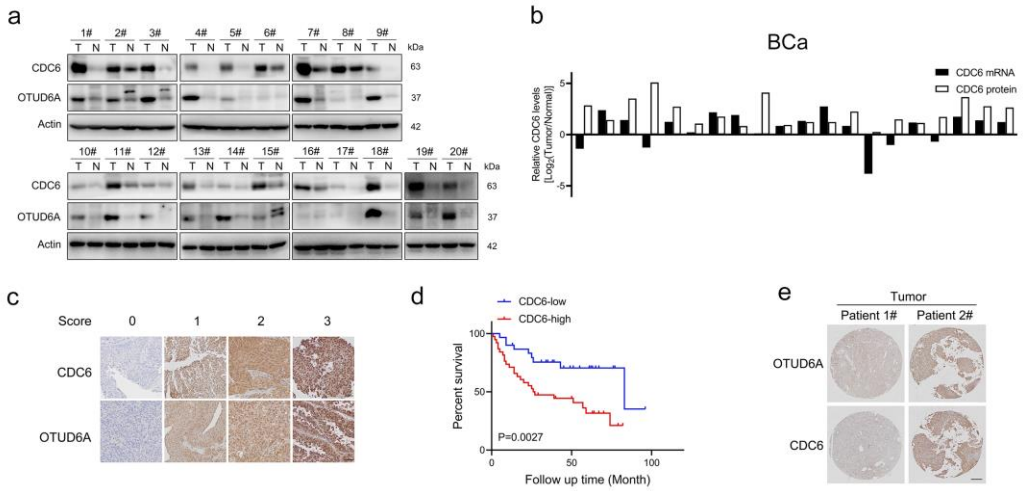

Supplementary Fig. 13 CDC6 protein expression is correlated with the OTUD6A protein level in tumour tissues. a, The protein expression levels of OTUD6A and CDC6 in 20 human BCa tissues and matched adjacent normal bladder tissues were determined by Western blotting. T, BCa tissue; N, Normal bladder tissue. **b**, Relative CDC6 protein and mRNA levels in BCa tissues are shown. **c**, The representative images of score from 0 to 3 for IHC staining intensity are shown. Scale bars, 50 μm. **d**, Kaplan-Meier curves of overall survival for patients with BCa stratified by the CDC6 expression level in the tissue microarray are shown. Data were analysed using the log-rank test. **e**, Representative IHC images showing OTUD6A and CDC6 expression in the renal carcinoma tissue microarray are shown. Scale bar, 500 μm.

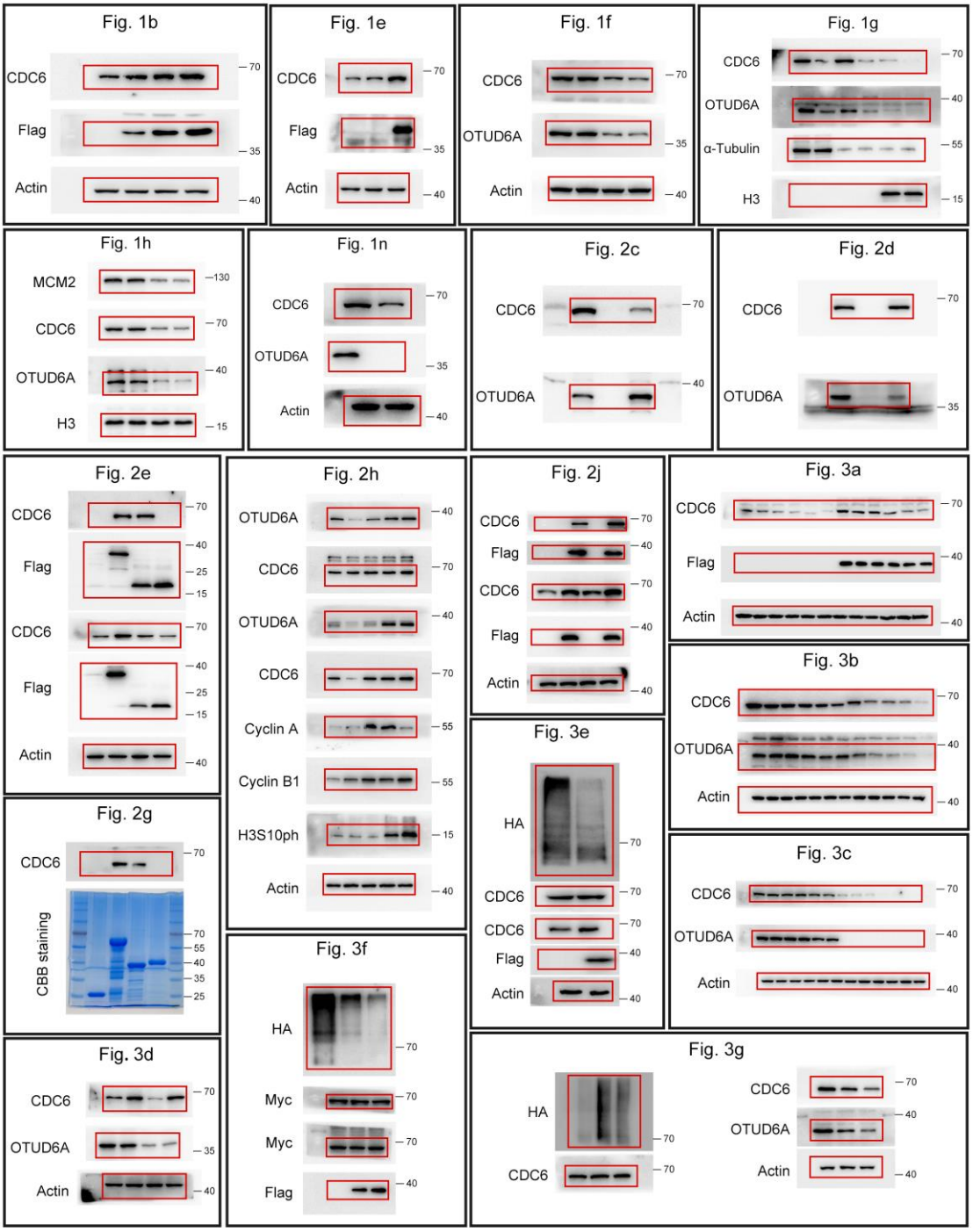

Supplementary Fig. 14 The original WB figures in Fig. 1-3.

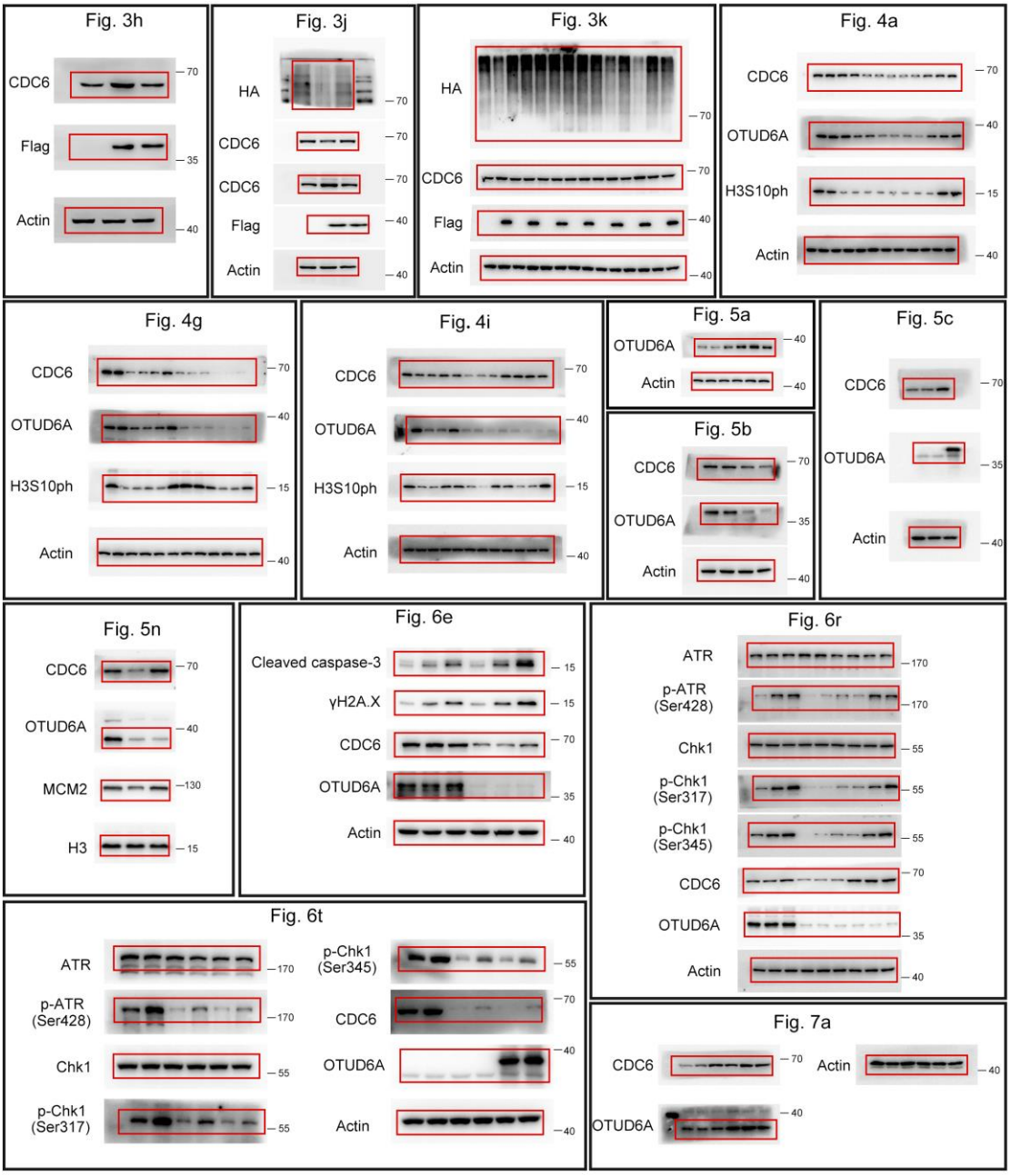

Supplementary Fig. 15 The original WB figures in Fig. 3-7.

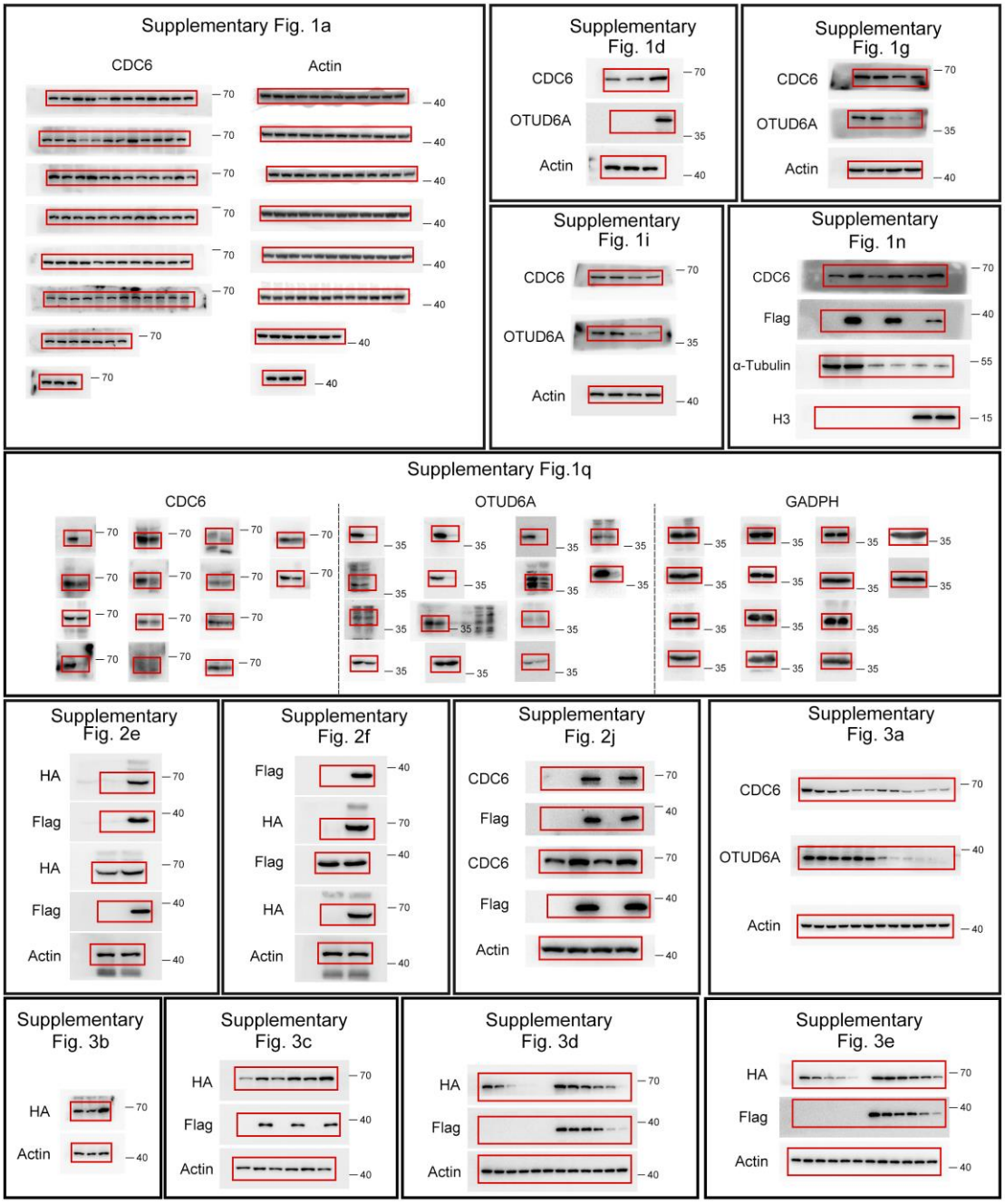

Supplementary Fig. 16 The original WB figures in Supplementary Fig. 1-3.

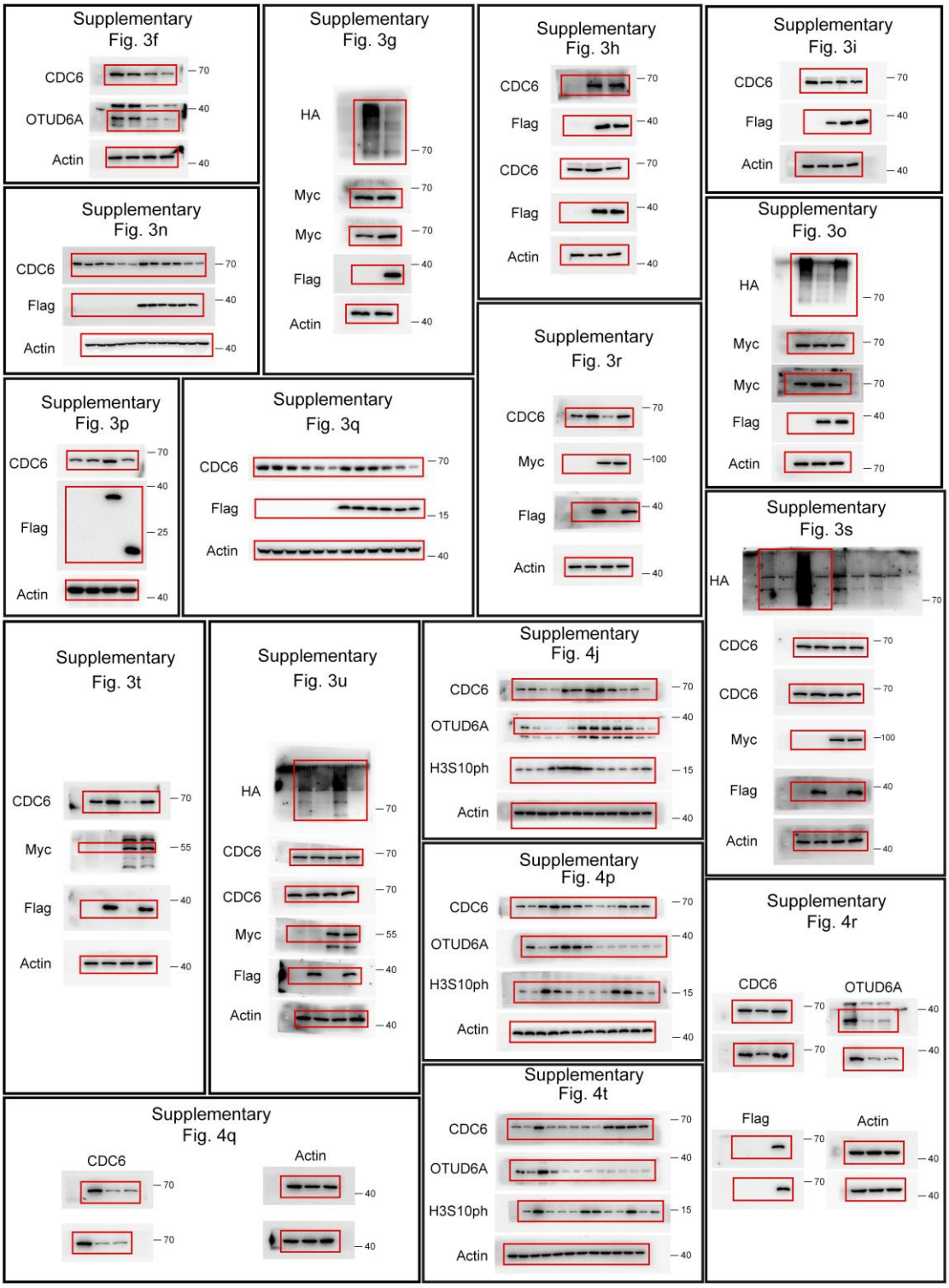

Supplementary Fig. 17 The original WB figures in Supplementary Fig. 3, 4.

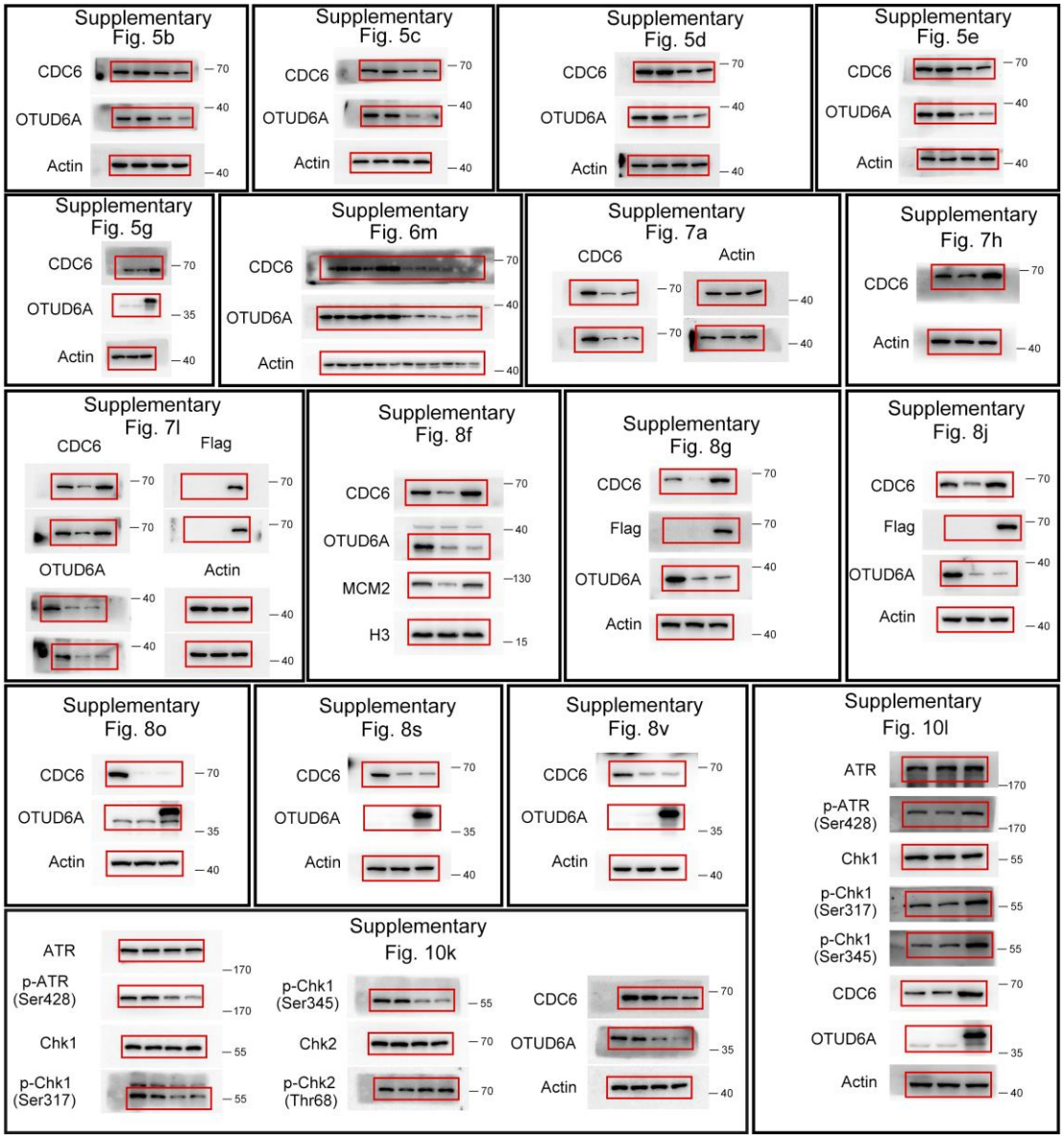

Supplementary Fig. 18 The original WB figures in Supplementary Fig. 5-10.

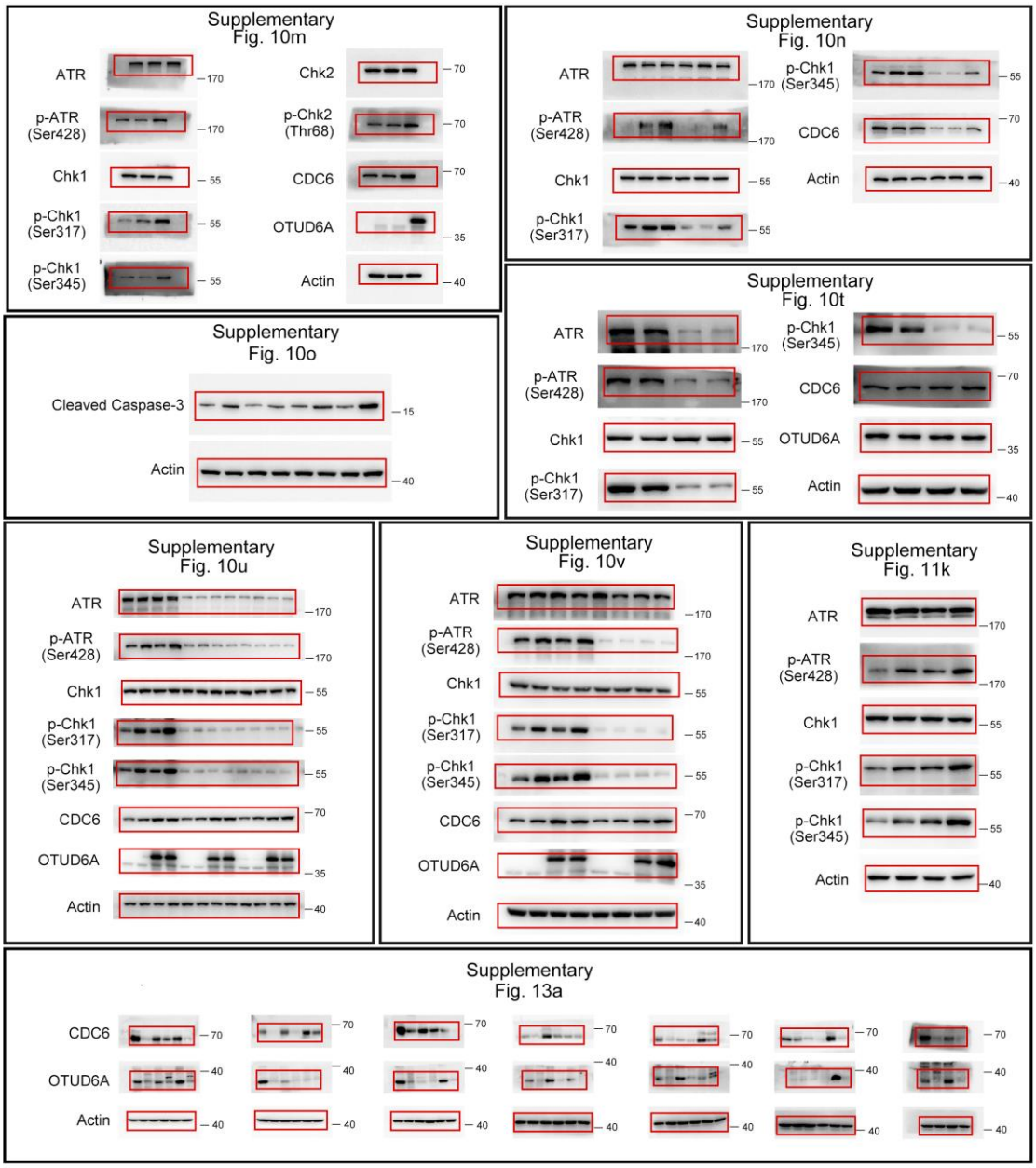

Supplementary Fig. 19 The original WB figures in Supplementary Fig. 10-13.

Supplementary Table 1 Primer sequences used for construction of mutant vectors

Mutated sites	Primers	Sequences
OTUD6A^{C152A}	Forward	TCCCGGCCGACGGCCACGCCATGTACCGCGCCATCCAAGA
OTUD6A^{C152A}	Reverse	TCTTGGATGGCGCGGTACATGGCGTGGCCGTCGGCCGGGA

Supplementary Table 2 qRT-PCR primer sequences

Gene name	Primer	Sequences	Product length (bp)
CDC6	Forward	ACCTATGCAACACTCCCCATT	153
	Reverse	TGGCTAGTTCTCTTTTGCTAGGA	
OTUD6A	Forward	GAAGTTCCAAGACGACAGTAGC	172
	Reverse	CAGGTGCTCCGACATCTCA	
GAPDH	Forward	GGAGCGAGATCCCTCCAAAAT	197
	Reverse	GGCTGTTGTCATACTTCTCATGG	

Supplementary Table 3 Antibodies used in Western blotting, immunofluorescence, immunohistochemistry, chromatin immunoprecipitation and immunoprecipitation

Antibody	Company	Catalog number	Application
anti-Flag-Tag	Sigma Aldrich	F1804	WB, IP, IF
anti-CDC6	Santa Cruz	sc-9964	WB
anti-CDC6	Abcam	ab109315	IF, IHC
anti-CDC6	Abcam	ab188423	IP
anti-CDC6	ProteinTech	66021-1-Ig	IF
anti-OTUD6A	ProteinTech	24486-1-AP	WB, IF
anti-OTUD6A	Invitrogen	PA5-110066	WB, IHC
anti-MCM2	BD Biosciences	610701	WB
anti-γ-tubulin	Santa Cruz	sc-17787	IF
anti-HA-Tag	Abcam	ab18181	WB, IP
anti-Myc-Tag	CST	2276	WB, IP
anti-β-actin	Sigma Aldrich	A5441	WB
anti-Cyclin A	Invitrogen	MA1-154	WB
anti-Cyclin B1	Abcam	ab32053	WB
anti-phospho-Histone H3 (Ser10)	ProteinTech	66863-1-Ig	WB
anti-GAPDH	Abways	AB0037	WB
anti-c-myc	CST	9402	WB
anti-α-Tubulin	Santa Cruz	sc-32293	WB, IF
anti-Histone H3	Abways	CY6587	WB
anti-ATR	CST	13934	WB
anti-p-ATR (Ser428)	CST	2853	WB
anti-Chk1	CST	2360	WB
anti-p-Chk1 (Ser317)	CST	12302	WB
anti-p-Chk1 (Ser345)	CST	2348	WB
anti-Chk2	CST	6334	WB
anti-p-Chk2 (Thr68)	CST	2197	WB
anti-γ-H2A.X	CST	9718	WB, IF, IHC
anti-cleaved caspase-3	Affinity	AF7022	WB
anti-Ki-67	Invitrogen	PA5-19462	IHC, IF
GAPDH	ProteinTech	60004-1-Ig	WB

Supplementary Table 4 Primer sequences used for identifying mice genotypes

Application	Primer	Sequences	Product length（bp）
Otud6a without Cre activity	Forward	TAGGCTGAAAATGGAAATTGTGGG	Flox: 203
	Reverse	TAAGTCATTTCAGCCACACCAACT	WT: 123
Otud6a with Cre activity	Forward	GGGAATGGAGCAGTATCTAAAGGC	187
	Reverse	TAAGTCATTTCAGCCACACCAACT	

Supplementary Table 5 Proteomic analysis of 84 differentially expressed proteins

Protein accession	Gene name	OTUD6A/Flag Ratio	Regulated Type	MW [kDa]	Coverage [%]	Peptides	Unique peptides	Flag	OTUD6A
O00257	CBX4	1.507	Up	61.367	10.4	4	4	0.797913	1.202087
O00401	WASL	0.522	Down	54.826	12.1	3	3	1.314437	0.685563
O00488	ZNF593	1.547	Up	15.199	45.5	4	4	0.785289	1.214711
O60831	PRAF2	0.312	Down	19.258	22.5	3	3	1.524578	0.475422
O75385	ULK1	1.601	Up	112.63	1.9	2	2	0.768824	1.231176
O95905	ECD	1.502	Up	72.757	11.5	5	5	0.79938	1.20062
P11274	BCR	1.557	Up	142.82	2.8	3	2	0.782137	1.217863
P12236	SLC25A6	0.652	Down	32.866	51.3	13	2	1.210928	0.789072
P22492	H1-6	0.412	Down	22.019	15.9	3	2	1.416283	0.583717
P27448	MARK3	3.132	Up	84.428	14.9	7	5	0.484028	1.515972
P31949	S100A11	0.662	Down	11.74	34.3	3	3	1.203152	0.796848
P39060	COL18A1	0.601	Down	178.19	3.2	4	4	1.248833	0.751167
P43121	MCAM	1.78	Up	71.607	5.7	3	3	0.719549	1.280451
P46013	MKI67	1.625	Up	358.69	14.6	28	28	0.761886	1.238114
P49759	CLK1	1.523	Up	57.29	11	4	3	0.792732	1.207268
P49760	CLK2	0.306	Down	60.089	8	3	2	1.53145	0.46855
P54725	RAD23A	0.663	Down	39.609	30.6	8	5	1.202543	0.797457
P57105	SYNJ2BP	0.462	Down	15.928	24.8	3	3	1.368189	0.631811
Q13315	ATM	0.642	Down	350.68	1.4	3	3	1.218302	0.781698
Q13641	TPBG	0.644	Down	46.031	6.7	2	2	1.216179	0.783821
Q14653	IRF3	1.615	Up	47.219	17.1	4	4	0.764901	1.235099
Q16854	DGUOK	0.572	Down	32.055	16.6	2	2	1.27234	0.72766
Q1L5Z9	LONRF2	1.702	Up	83.653	9	4	4	0.740064	1.259936

Q32NB8	PGS1	1.526	Up	62.73	4.5	2	2	0.791817	1.208183
Q3ZAQ7	VMA21	4.831	Up	11.354	24.8	2	2	0.343007	1.656993
Q460N5	PARP14	0.141	Down	202.8	4.1	5	5	1.752982	0.247018
Q53RE8	ANKRD39	2.189	Up	19.651	15.3	2	2	0.62714	1.37286
Q5XKP0	MICOS13	0.623	Down	13.087	35.6	2	2	1.231913	0.768087
Q6UVK1	CSPG4	0.638	Down	250.53	1.7	3	3	1.220767	0.779233
Q712K3	UBE2R2	1.607	Up	27.166	10.1	2	2	0.7672	1.2328
Q71F23	CENPU	1.761	Up	47.521	17.2	5	5	0.724285	1.275715
Q7Z333	SETX	0.326	Down	302.88	0.7	2	2	1.507811	0.492189
Q86T24	ZBTB33	0.222	Down	74.484	5.1	2	2	1.636778	0.363222
Q86UT6	NLRX1	0.312	Down	107.61	2.8	2	2	1.52449	0.47551
Q86WV6	STING1	0.53	Down	42.192	18.7	4	4	1.307197	0.692803
Q8IYU8	MICU2	0.664	Down	49.666	18.9	6	6	1.202021	0.797979
Q8N9B5	JMY	1.553	Up	111.44	3.8	3	3	0.783298	1.216702
Q8N9N5	BANP	0.573	Down	56.494	4.4	2	2	1.271713	0.728287
Q8NFA0	USP32	1.536	Up	181.65	2.1	3	3	0.788791	1.211209
Q8TEY7	USP33	1.566	Up	106.73	2.2	2	2	0.779562	1.220438
Q8WUQ7	CACTIN	0.559	Down	88.701	4.9	2	2	1.283041	0.716959
Q8WV22	NSMCE1	0.645	Down	30.855	15.4	3	3	1.21553	0.78447
Q92558	WASF1	0.157	Down	61.651	7.2	3	3	1.729267	0.270733
Q92575	UBXN4	0.624	Down	56.777	14	4	4	1.231253	0.768747
Q92993	KAT5	2.976	Up	58.581	10.5	4	4	0.503031	1.496969
Q969F9	HPS3	0.666	Down	113.73	8	5	5	1.200587	0.799413
Q96CS2	HAUS1	1.758	Up	31.863	10.1	2	2	0.725232	1.274768
Q96E29	MTERF3	0.65	Down	47.971	6.2	2	2	1.212291	0.787709

Q96EA4	SPDL1	2.69	Up	70.171	9.1	4	4	0.54201	1.45799
Q96EC8	YIPF6	5.361	Up	26.256	8.5	2	2	0.314434	1.685566
Q96GE9	DMAC1	0.659	Down	12.257	32.8	2	2	1.205457	0.794543
Q96N21	TEPSIN	0.532	Down	55.136	5.7	2	2	1.30538	0.69462
Q96QE3	ATAD5	1.548	Up	207.57	1.5	2	2	0.785023	1.214977
Q96QE5	TEFM	0.572	Down	41.676	5.8	2	2	1.272051	0.727949
Q96QR8	PURB	1.575	Up	33.24	10.3	3	3	0.776795	1.223205
Q96S94	CCNL2	1.526	Up	58.147	9.4	3	3	0.791635	1.208365
Q99538	LGMN	8.464	Up	49.411	7.2	2	2	0.211321	1.788679
Q99741	CDC6	1.611	Up	62.72	7.3	3	3	0.765943	1.234057
Q9BTT4	MED10	1.566	Up	15.688	22.2	2	2	0.779547	1.220453
Q9BW62	KATNAL1	1.535	Up	55.392	9.4	3	2	0.789038	1.210962
Q9BXI6	TBC1D10A	1.673	Up	57.117	7.7	4	4	0.748286	1.251714
Q9BYE7	PCGF6	2.199	Up	39.047	8.6	2	2	0.625131	1.374869
Q9C0H2	TTYH3	0.658	Down	57.544	8.6	3	3	1.206472	0.793528
Q9GZN1	ACTR6	1.619	Up	45.81	6.3	2	2	0.763628	1.236372
Q9H082	RAB33B	0.643	Down	25.717	13.1	2	2	1.217582	0.782418
Q9H2D6	TRIOBP	0.475	Down	261.37	1	2	2	1.356213	0.643787
Q9H7B4	SMYD3	0.228	Down	49.097	10.3	3	3	1.628002	0.371998
Q9H9F9	ACTR5	0.508	Down	68.297	14.5	5	5	1.326047	0.673953
Q9HAW4	CLSPN	1.544	Up	151.09	5.5	5	5	0.786286	1.213714
Q9NNX1	TUFT1	1.608	Up	44.263	13.1	3	3	0.76688	1.23312
Q9NP50	SINHCAF	3.4	Up	24.852	11.3	2	2	0.45452	1.54548
Q9NUJ3	TCP11L1	0.416	Down	57.034	9.2	3	3	1.412479	0.587521
Q9NVC6	MED17	2.079	Up	72.889	10	5	5	0.64946	1.35054

Q9NVN8	GNL3L	1.877	Up	65.572	21	9	9	0.695226	1.304774
Q9NVP2	ASF1B	0.551	Down	22.433	15.3	2	2	1.289164	0.710836
Q9NW75	GPATCH2	1.774	Up	58.943	5.7	2	2	0.720973	1.279027
Q9NXX6	NSMCE4A	0.624	Down	44.301	19.2	5	5	1.231685	0.768315
Q9P086	MED11	0.652	Down	13.129	31.6	2	2	1.210515	0.789485
Q9UIM3	FKBPL	0.634	Down	38.176	9.2	3	3	1.223902	0.776098
Q9UJY1	HSPB8	1.556	Up	21.604	12.8	2	2	0.782517	1.217483
Q9ULJ7	ANKRD50	0.661	Down	155.86	2.3	2	2	1.203841	0.796159
Q9Y3B6	EMC9	3.347	Up	23.061	13.9	2	2	0.46007	1.53993
Q9Y3C0	WASHC3	0.587	Down	21.172	16	2	2	1.259958	0.740042
Q9Y3E7	CHMP3	0.583	Down	25.073	9	2	2	1.263793	0.736207